Canonical Dual Finite Element Method For Solving Nonconvex Mechanics and Topology Optimization

Elaf Jaafar Ali

This thesis is submitted in total fulfilment of the requirement for the degree of Doctor of Philosophy

12 February 2018

Abstract

Canonical duality theory (CDT) is a newly developed, potentially powerful methodological theory which can transfer general multi-scale nonconvex/discrete problems in $\mathbb{R}^n$ to a unified convex dual problem in continuous space $\mathbb{R}^m$ with $m \leq n$ and without a duality gap. The associated triality theory provides extremality criteria for both global and local optimal solutions, which can be used to develop powerful algorithms for solving general nonconvex variational problems.

This thesis, first, presents a detailed study of large deformation problems in 2-D structural system. Based on the canonical duality theory, a canonical dual finite element method is applied to find a global minimization to the general nonconvex optimization problem using a new primal-dual semi-definite programming algorithm. Applications are illustrated by numerical examples with different structural designs and different external loads.

Next, a new methodology and algorithm for solving post buckling problems of a large deformed elastic beam is investigated. The total potential energy of this beam is a nonconvex functional, which can be used to model both pre- and post-buckling phenomena. By using the canonical dual finite element method, a new primal-dual semi-definite programming algorithm is presented, which can be used to obtain all possible post-buckled solutions. In order to verify the triality theory, mixed meshes of different dual stress interpolations are applied to obtain the closed dimensions between discretized displacement and discretized stress. Applications are illustrated by several numerical examples with different boundary conditions. We find that the global minimum solution of the nonconvex potential leads to a stable configuration of the buckled beam, the local maximum solution leads to the unbuckled state, and both of these two solutions are numerically stable. However, the local minimum solution leads to an unstable buckled state, which is very sensitive to the external load, thickness of the beam, numerical precision, and the size of finite elements.

Finally, a mathematically rigorous and computationally powerful method for solving 3-D topology optimization problems is demonstrated. This method is based on

CDT developed by Gao in nonconvex mechanics and global optimization. It shows that the so-called NP-hard Knapsack problem in topology optimization can be solved deterministically in polynomial-time via a canonical penalty-duality (CPD) method to obtain precise global optimal 0-1 density distribution at each volume evolution. The relation between this CPD method and Gao's pure complementary energy principle is revealed for the first time. A CPD algorithm is proposed for 3-D topology optimization of linear elastic structures. Its novelty is demonstrated by benchmark problems. Results show that without using any artificial technique, the CPD method can provide mechanically sound optimal design, also it is much more powerful than the well-known BESO and SIMP methods. Finally, computational complexity and conceptual/mathematical mistakes in topology optimization modeling and popular methods are explicitly addressed.

Acknowledgements

At the outset, I am thankful to Almighty Allah, who has been the light in my life during the dimmer moments.

I would like to express my special appreciation and thanks to my principal supervisor, Prof. David Gao, for his strong support, kind consideration, helpful guidance and valuable time throughout my study. His scientific expertise, continuous encouragement and support of my research have been essential for my success.

I thank Dr Ean Ooi at the Department of Civil Engineering for his help throughout my PhD study. I also thank all of the staff in research office for contributing to a friendly work environment.

Finally, thank you to all my family members, my parents, brothers, sisters, daughter and my nephew Yousif, for helping and encouraging me. They are my strength and inspiration.

Dedication

To:

My Parents ...

My brothers, sisters and my dear Yousif ...

My lovely daughter Zahraa ...

Special dedication to the spirit of my sister Dr. Tohfa.

Statement of Authorship

Except where explicit reference is made in the text of the thesis, this thesis contains no material published elsewhere or extracted in whole or in part from a thesis by which I have qualified for or been awarded another degree or diploma. No other person's work has been relied upon or used without due acknowledgement in the main text and bibliography of the thesis.

Signed: ———————————   Signed: ———————————

Date: ———————————   Date: ———————————

Elaf Ali   Prof David Gao

Candidate   Principal Supervisor

Contents

List of publications and conference participation

The following papers were completed during the PhD candidature:

1. Ali, E.J., & Gao, D.Y. (2016). Improved Canonical Dual Finite Element Method and Algorithm for Post Buckling Analysis of Nonlinear Gao Beam, *Canonical Duality Theory: Unified Methodology for Multidisciplinary Study*, Springer, New York, 277-289. doi: 10.1007/978-3-319-58017-3˙14

2. Ali, E.J., & Gao, D.Y. (2016, June). *Canonical Finite Element Method For Solving Nonconvex Variational Problems to Post Buckling Beam Problem*, AIP Conf. Proc. 1776(1), 090045, Pizzo Calabro, Italy. doi: 10.1063/1.4965409

   This paper was presented at the 2nd International Conference and Summer School (NUMTA2016). Numerical Computations: Theory and Algorithms, 19-25 June, 2016. University of Calabria, Pizzo Calabro, Calabria, Italy.

3. Gao, D.Y., & Ali, E.J. (2018). A Novel Canonical Duality Theory for Solving 3-D Topology Optimization Problems, *Emerging Trends in Applied Mathematics and High-Performance Computing*, V.K. Singh, D.Y. Gao, A. Fisher (Eds). Springer International Publishing, Springer, New York. "`https://arxiv.org/abs/1803.02615`".

4. Ali, E.J., & Gao, D.Y. On SDP Method for Solving Canonical Dual Problem in Post Buckling of Large Deformed Elastic Beam, *Communications in Mathematical Sciences*, Date of acceptance is on 19 March 2018. "`https://arxiv.org/pdf/1609.04675.pdf`".

The following work was presented at a conference during the PhD candidature:

1. *On SDP Method for Solving Post Buckling Problems of Nonlinear Gao Beam*, in International Symposium on Control and Optimization for Multidisciplinary

Study (COMS 2017). 6-9 February, 2017. Federation University Australia, Ballarat, Australia.

List of Figures

List of Tables

Chapter 1

Introduction

At the beginning of the last century, duality theory and methods for nonconvex problems were studied by engineers and scientists in mechanics. Traditional finite element methods for solving nonconvex variational problems usually end up with a nonconvex minimization problem in $\mathbb{R}^n$. Due to the lack of global optimality criteria, popular nonlinear programming methods developed from convex optimization cannot be used to find global optimal solutions. It was discovered in [25] that for certain external loads, both global and local minimum solutions to large deformed mechanics problems are usually nonsmooth and cannot be captured by any Newton-type methods. Therefore, most nonconvex optimization problems are considered *NP-hard* (non-deterministic polynomial-time hard) in computer science. Unfortunately, these well-known difficulties are not fully recognized in computational mechanics due to the significant gap between engineering mechanics and global optimization. *Canonical duality theory* provides a potentially powerful methodology which can be used not only for modeling complex systems within a unified framework, but also for solving a large class of challenging problems in nonconvex, nonsmooth, and discrete systems [32].

The canonical duality theory was developed by Gao from his original work with Strang on nonconvex/nonsmooth variational/boundary value problems in finite deformation systems [13]. In order to recover the complementary energy principle in nonconvex problems, they discovered the so-called *complementary gap function*, which leads to a complementary-dual variational principle in finite deformation mechanics. They proved that the positivity of this gap function provides a global optimality condition for nonconvex variational problems. It was realized by Gao seven years later that the negativity of this gap function can be used to identify the biggest local minimal and local maximal solutions. Therefore, a *triality theory*

was first proposed in nonconvex mechanics by Gao in 1996 [16], and a pure complementary energy principle was obtained in 1999 [17]. This principle solved an open problem in nonlinear elasticity [53], which can be used to obtain analytical solutions to general large deformation problems [18, 33, 32]. Based on the canonical duality theory, a canonical dual finite element method has been developed [14] with a successful application for solving nonconvex mechanics problems in phase transitions of solids [26]. A newly published book [41] provides a comprehensive review and applications of the canonical duality theory in multidisciplinary fields of mathematical modeling, nonconvex analysis, global optimization, and computational science. Generally speaking, the canonical duality theory is composed mainly of

1. a *canonical dual transformation*, which can be used to formulate perfect dual problem without a duality gap;

2. a *complementary-dual principle*, which presents a unified analytic solution form for general problems in continuous and discrete systems;

3. a *triality theory*, which can be used to identify both global and local extrema and to develop effective algorithms for solving nonconvex optimization problems.

The study of the canonical duality theory is of interest to operations research, applied mathematics communities and topology optimization.

1.1 Canonical Duality Theory in General Nonconvex Problems

The general nonconvex problem can be defined as (the primal problem $(\mathcal{P})$ in short)

$$(\mathcal{P}): \quad \min_{\mathbf{x} \in \mathcal{X}_a} \left\{ \Pi(\mathbf{x}) = W(\mathbf{x}) - U(\mathbf{x}) \right\}, \tag{1.1}$$

where $W(\mathbf{x})$ is a general nonconvex function, $U(\mathbf{x})$ is a linear Gâteaux differentiable function, and $\mathcal{X}_a \subset \mathbb{R}^n$ is a given feasible space.

1.1.1 Canonical dual transformation

The key idea of the canonical dual transformation is to recover the duality gap by choosing Gâteaux differentiable geometrical operator

$$\boldsymbol{\xi} = \Lambda(\mathbf{x}) : \mathcal{X}_a \rightarrow \mathcal{E}_a, \tag{1.2}$$

which maps each $\mathbf{x} \in \mathcal{X}_a$ into a so-called intermediate space $\mathcal{E}_a$, such that the non-convex function $W(\mathbf{x})$ in the primal problem $(\mathcal{P})$ can be written in the canonical form

$$W(\mathbf{x}) = V(\Lambda(\mathbf{x})). \tag{1.3}$$

The real-valued function $V(\boldsymbol{\xi}) : \mathcal{E}_a \rightarrow \mathbb{R}$ is a *canonical function* of the geometrical measure $\boldsymbol{\xi} = \Lambda(\mathbf{x})$. By the canonical function definition, we have that the duality relation

$$\boldsymbol{\zeta} = \nabla V(\boldsymbol{\xi}) : \mathcal{E}_a \rightarrow \mathcal{E}_a^*,$$

is revertible [19, 41], where $\mathcal{E}_a^*$ is the dual feasible space. Then, the conjugate function $V^* : \mathcal{E}_a^* \rightarrow \mathbb{R}$ can be uniquely defined by the Legendre transformation [19]

$$V^*(\boldsymbol{\zeta}) = \text{sta}\Big\{ \langle \boldsymbol{\xi}; \boldsymbol{\zeta} \rangle - V(\boldsymbol{\xi}) \big| \ \forall \boldsymbol{\xi} \in \mathcal{E}_a \Big\}, \tag{1.4}$$

where sta{ } denotes finding stationary points of the statement in { } and $\langle \boldsymbol{\xi}; \boldsymbol{\zeta} \rangle$ is the canonical dual pair between $\boldsymbol{\xi}$ and its dual variable $\boldsymbol{\zeta}$. Thus, the following canonical duality relations hold on $\mathcal{E}_a \times \mathcal{E}_a^*$

$$\boldsymbol{\zeta} = \nabla V(\boldsymbol{\xi}) \ \Leftrightarrow \ \boldsymbol{\xi} = \nabla V^*(\boldsymbol{\zeta}) \ \Leftrightarrow \ V(\boldsymbol{\xi}) + V^*(\boldsymbol{\zeta}) = \langle \boldsymbol{\xi}; \boldsymbol{\zeta} \rangle. \tag{1.5}$$

By using the canonical transformation (1.3), the problem $(\mathcal{P})$ can be given in the following canonical problem

$$\min_{\mathbf{x} \in \mathcal{X}_a} \{\Pi(\mathbf{x}) = V(\Lambda(\mathbf{x})) - U(\mathbf{x})\}, \tag{1.6}$$

By the chain rule and since $\Lambda(\mathbf{x})$ is Gâteaux differentiable, we can obtain [13]

$$\nabla V(\Lambda(\mathbf{x})) = \Lambda_t(\mathbf{x}) \nabla_{\boldsymbol{\xi}} V(\Lambda(\mathbf{x})), \tag{1.7}$$

where $\Lambda_t(\mathbf{x})$ and $\nabla_{\boldsymbol{\xi}} V(\Lambda(\mathbf{x}))$ are the Gâteaux derivatives of $\Lambda(\mathbf{x})$ and V (with respect to $\boldsymbol{\xi} = \Lambda(\mathbf{x})$), respectively. The stationary condition $\nabla \Pi(\mathbf{x}) = 0$ leads to the

canonical equilibrium equation

$$\Lambda_t^*(\mathbf{x}) \, \nabla_{\boldsymbol{\xi}} V(\Lambda(\mathbf{x})) = \nabla U(\mathbf{x}), \tag{1.8}$$

where $\Lambda_t^*(\mathbf{x})$, the adjoint operator of $\Lambda(\mathbf{x})$, is written by

$$\langle \Lambda_t(\mathbf{x})\mathbf{x}; \boldsymbol{\zeta} \rangle = \langle \mathbf{x}, \Lambda_t^*(\mathbf{x})\boldsymbol{\zeta} \rangle. \tag{1.9}$$

In terms of the canonical duality pair $\langle \boldsymbol{\xi}, \boldsymbol{\zeta} \rangle$, equation (1.8) can be written in the tri-canonical forms

1. geometrical equation: $\boldsymbol{\xi} = \Lambda(\mathbf{x})$,

2. constitutive equation: $\boldsymbol{\zeta} = \nabla V(\boldsymbol{\xi})$,

3. balance equation: $\Lambda_t^*(\mathbf{x})\boldsymbol{\zeta} = \nabla U(\mathbf{x})$.

The nonconvexity of $\Pi(\mathbf{x})$ is mainly due to the geometrically nonlinear of problem (1.6), i.e. the operator $\Lambda(\mathbf{x})$ is nonlinear. Hence, Gao and Strang introduced the following operator decomposition [13]

$$\Lambda(\mathbf{x}) = \Lambda_t(\mathbf{x})\mathbf{x} + \Lambda_c(\mathbf{x}), \tag{1.10}$$

in which the operator $\Lambda_c(\mathbf{x}) = \Lambda(\mathbf{x}) - \Lambda_t(\mathbf{x})\mathbf{x}$ is the complementary operator of Λ_t. This decomposition plays an important role in the canonical duality theory, in which, if $U(\mathbf{x})$ is a linear function, the duality gap existing in classical Lagrangian duality theory can be naturally recovered by the *Gao-Strang complementary gap function* which is defined by

$$G_{ap}(\mathbf{x}, \boldsymbol{\zeta}) = -\langle \Lambda_c(\mathbf{x}); \boldsymbol{\zeta} \rangle \tag{1.11}$$

The following relations (1.12) summarize a fully nonlinear canonical system.

$$
\begin{array}{ccc}
\mathbf{x} \in \mathcal{X}_a \subset \mathcal{X} & \longleftarrow \ \langle \mathbf{x} \, , \, \mathbf{x}^* \rangle \ \longrightarrow & \mathcal{X}^* \supset \mathcal{X}_a^* \ni \mathbf{x}^* \\
\Lambda_t + \Lambda_c = \Lambda \Big\downarrow & & \Big\uparrow \Lambda_t^* = (\Lambda - \Lambda_c)^* \qquad (1.12) \\
\boldsymbol{\xi} \in \mathcal{E}_a \subset \mathcal{E} & \longleftarrow \ \langle \boldsymbol{\xi} \, ; \, \boldsymbol{\zeta} \rangle \ \longrightarrow & \mathcal{E}^* \supset \mathcal{E}_a^* \ni \boldsymbol{\zeta}
\end{array}
$$

According to the canonical transformation (1.3), the nonconvex total potential $\Pi(\mathbf{x})$ can be converted to the following Gao-Strang total complementary energy

$\Xi : \mathcal{X}_a \times \mathcal{E}_a^* \to \mathbb{R}$ [13]

$$\Xi(\mathbf{x}, \boldsymbol{\zeta}) = \langle \Lambda(\mathbf{x}); \boldsymbol{\zeta} \rangle - V^*(\boldsymbol{\zeta}) - U(\mathbf{x}). \tag{1.13}$$

The stationary condition $\nabla \Xi(\mathbf{x}, \boldsymbol{\zeta}) = 0$ leads to the following canonical equations

$$\Lambda(\mathbf{x}) = \nabla V^*(\boldsymbol{\zeta}), \tag{1.14}$$

$$\Lambda_t^*(\mathbf{x}) \, \boldsymbol{\zeta} = \nabla U(\mathbf{x}). \tag{1.15}$$

Thus, by using the so-called Λ-canonical dual transformation [20]

$$U^\Lambda(\boldsymbol{\zeta}) = \operatorname{sta}\{ \langle \Lambda(\mathbf{x}); \boldsymbol{\zeta} \rangle - U(\mathbf{x}) \mid \mathbf{x} \in \mathcal{X}_a \}, \tag{1.16}$$

the canonical dual function of $\Pi(\mathbf{x})$ can be well defined as

$$
\begin{aligned}
\Pi^d(\boldsymbol{\zeta}) &= \operatorname{sta}\{ \Xi(\mathbf{x}, \boldsymbol{\zeta}) \mid \mathbf{x} \in \mathcal{X}_a \} \\
&= U^\Lambda(\boldsymbol{\zeta}) - V^*(\boldsymbol{\zeta}).
\end{aligned} \tag{1.17}
$$

The following theorem details the stationary point and shows that there is no duality gap between the nonconvex function $\Pi(\mathbf{x})$ and its canonical dual $\Pi^d(\boldsymbol{\zeta})$.

Theorem 1 (Gao's Pure Complementary Principle [19])
The function $\Pi^d(\boldsymbol{\zeta}) : \mathcal{E}_a^* \to \mathbb{R}$, is canonically dual to $\Pi(\mathbf{x}) : \mathcal{X}_a \to \mathbb{R}$, in the sense that if $(\bar{\mathbf{x}}, \bar{\boldsymbol{\zeta}})$ is a stationary point of the complementary energy $\Xi(\mathbf{x}, \boldsymbol{\zeta})$, then $\bar{\mathbf{x}}$ is a stationary point of the total potential energy $\Pi(\mathbf{x})$ on $\mathcal{X}_a$, and $\bar{\boldsymbol{\zeta}}$ is a stationary point of the canonical dual function $\Pi^d(\boldsymbol{\zeta})$ on $\mathcal{E}_a^*$, and

$$\Pi(\bar{\mathbf{x}}) = \Xi(\bar{\mathbf{x}}, \bar{\boldsymbol{\zeta}}) = \Pi^d(\bar{\boldsymbol{\zeta}}). \tag{1.18}$$

1.1.2 Complementary-dual principle

Due to the fact that $\Lambda(\epsilon)$ is usually quadratic and by substituting $U(\mathbf{x}) = \langle \mathbf{x}, \mathbf{f}(\boldsymbol{\zeta}) \rangle$ into (1.13), the total complementary function $\Xi(\mathbf{x}, \boldsymbol{\zeta})$ can be rewritten as

$$\Xi(\mathbf{x}, \boldsymbol{\zeta}) = G_{ap}(\mathbf{x}, \boldsymbol{\zeta}) - V^*(\boldsymbol{\zeta}) - \langle \mathbf{x}, \mathbf{f}(\boldsymbol{\zeta}) \rangle, \tag{1.19}$$

where $\langle . , . \rangle$ denotes the bilinear form and $G_{ap}(\mathbf{x}, \boldsymbol{\zeta})$ is the complementary gap function which is defined in [13]

$$G_{ap}(\mathbf{x}, \boldsymbol{\zeta}) = \langle \Lambda(\mathbf{x}); \boldsymbol{\zeta} \rangle = \frac{1}{2} \langle \mathbf{x}, \mathbf{G}(\boldsymbol{\zeta})\mathbf{x} \rangle, \tag{1.20}$$

in which

$$\mathbf{G}(\boldsymbol{\zeta}) = \nabla_{\mathbf{x}}^2 \Xi(\mathbf{x}, \boldsymbol{\zeta}),$$

is the Hessian matrix of $\Xi(\mathbf{x}, \boldsymbol{\zeta})$. Then, by applying the canonical equilibrium equation $\nabla_{\mathbf{x}} \Xi(\mathbf{x}, \boldsymbol{\zeta}) = 0$, we have the following stationary solution

$$\mathbf{x} = \mathbf{G}^{-1}(\boldsymbol{\zeta})\mathbf{f}(\boldsymbol{\zeta}). \tag{1.21}$$

By substituting (1.21) into (1.19), the canonical dual function Π^d in (1.17) can be reformulated as

$$\Pi^d(\boldsymbol{\zeta}) = -G_{ap}^*(\boldsymbol{\zeta}) - V^*(\boldsymbol{\zeta}), \tag{1.22}$$

where $G_{ap}^*(\boldsymbol{\zeta})$ is the so-called *pure complementary gap function* defined in [13]

$$G_{ap}^*(\boldsymbol{\zeta}) = \frac{1}{2} \langle \mathbf{G}^{-1}(\boldsymbol{\zeta})\mathbf{f}(\boldsymbol{\zeta}), \mathbf{f}(\boldsymbol{\zeta}) \rangle.$$

Thus, the stationary point $\mathbf{x}$ in (1.21) is the analytically primal stationary point of $\Pi(\mathbf{x})$, which is dependent on its canonical dual solution, as shown in the following theorem.

Theorem 2 (Analytic Solution [19])
If $\bar{\boldsymbol{\zeta}} \in \mathcal{E}_a^*$ is a stationary point of $\Pi^d(\boldsymbol{\zeta})$, then $\bar{\mathbf{x}} = \mathbf{G}^{-1}(\bar{\boldsymbol{\zeta}})\mathbf{f}(\bar{\boldsymbol{\zeta}})$, is a stationary point of $\Pi(\mathbf{x})$ on $\mathcal{X}_a$, and $\Pi(\bar{\mathbf{x}}) = \Pi^d(\bar{\boldsymbol{\zeta}})$.

1.1.3 Triality theory

The components of triality theory comprise a canonical min-max duality and two pairs of double-min, double-max dualities, which can be used to identify both global and local extrema. This theory implies an intrinsic duality pattern in complex systems and has been applied successfully to solve a wide class of challenging nonconvex/nonsmooth/discrete problems in multidisciplinary fields [22, 30]. The convexity of the canonical function $V : \mathcal{E}_a \to \mathbb{R}$ needs to be assumed so that the extremality conditions of the stationary solutions of the nonconvex problem can be investigated. Let

$$\mathcal{E}_+^* = \{\boldsymbol{\zeta} \in \mathcal{E}_a^* | \ \mathbf{G}(\boldsymbol{\zeta}) \succ 0\}, \tag{1.23}$$

$$\mathcal{E}_-^* = \{\boldsymbol{\zeta} \in \mathcal{E}_a^* | \ \mathbf{G}(\boldsymbol{\zeta}) \prec 0\}, \tag{1.24}$$

where the symbols "$\succ$" and "$\prec$" represent the symmetric positive definite matrix and symmetric negative definite matrix, respectively. So, for any given $\mathbf{x} \in \mathcal{X}_a$ and $\mathbf{x} \neq 0$, the complementary gap function $G_{ap}(\mathbf{x}, \boldsymbol{\zeta})$ is positive if and only if $\boldsymbol{\zeta} \in \mathcal{E}_+^*$, and it is negative if and only if $\boldsymbol{\zeta} \in \mathcal{E}_-^*$.

Theorem 3 (Triality theory [16, 19])

Suppose $(\bar{\mathbf{x}}, \bar{\boldsymbol{\zeta}})$ is a stationary point of $\Xi(\mathbf{x}, \boldsymbol{\zeta})$. If $\bar{\boldsymbol{\zeta}} \in \mathcal{E}_+^*$, then $\bar{\mathbf{x}}$ is a global minimizer of $\Pi(\mathbf{x})$ on $\mathcal{X}_a$ if and only if $\bar{\boldsymbol{\zeta}}$ is a global maximizer of $\Pi^d(\boldsymbol{\zeta})$ on $\mathcal{E}_+^*$, i.e.,

$$\Pi(\bar{\mathbf{x}}) = \min_{\mathbf{x} \in \mathcal{X}_a} \Pi(\mathbf{x}) \quad \Leftrightarrow \quad \max_{\boldsymbol{\zeta} \in \mathcal{E}_+^*} \Pi^d(\boldsymbol{\zeta}) = \Pi^d(\bar{\boldsymbol{\zeta}}). \tag{1.25}$$

If $\bar{\boldsymbol{\zeta}} \in \mathcal{E}_-^*$, then on a neighborhood $\mathcal{X}_o \times \mathcal{E}_o^* \subset \mathcal{X}_a \times \mathcal{E}_a^*$ of $(\bar{\mathbf{x}}, \bar{\boldsymbol{\zeta}})$, we have either $\bar{\mathbf{x}}$ is a local maximizer of $\Pi(\mathbf{x})$ on $\mathcal{X}_o$ if and only if $\bar{\boldsymbol{\zeta}}$ is a local maximizer of $\Pi^d(\boldsymbol{\zeta})$ on $\mathcal{E}_o^*$, i.e.,

$$\Pi(\bar{\mathbf{x}}) = \max_{\mathbf{x} \in \mathcal{X}_o} \Pi(\mathbf{x}) \quad \Leftrightarrow \quad \max_{\boldsymbol{\zeta} \in \mathcal{E}_o^*} \Pi^d(\boldsymbol{\zeta}) = \Pi^d(\bar{\boldsymbol{\zeta}}), \tag{1.26}$$

or (only if $\dim \bar{\mathbf{x}} = \dim \bar{\boldsymbol{\zeta}}$), $\bar{\mathbf{x}}$ is a local minimizer of $\Pi(\mathbf{x})$ on $\mathcal{X}_o$ if and only if $\bar{\boldsymbol{\zeta}}$ is a local minimizer of $\Pi^d(\boldsymbol{\zeta})$ on $\mathcal{E}_o^*$, i.e.,

$$\Pi(\bar{\mathbf{x}}) = \min_{\mathbf{x} \in \mathcal{X}_o} \Pi(\mathbf{x}) \quad \Leftrightarrow \quad \min_{\boldsymbol{\zeta} \in \mathcal{E}_o^*} \Pi^d(\boldsymbol{\zeta}) = \Pi^d(\bar{\boldsymbol{\zeta}}). \tag{1.27}$$

Identifying the global minimizer of the nonconvex total potential energy $\Pi(\mathbf{x})$ is equivalent to identifying the global maximizer of the canonical dual problem $\{\max_{\boldsymbol{\zeta} \in \mathcal{E}_+^*} \Pi^d(\boldsymbol{\zeta})\}$ as shown in the statement (1.25), therefore, this statement is called *canonical min-max duality*. This canonical dual problem is considered a concave maximization problem that can be solved using well-developed convex optimization methods. The weak form of the statement (1.25) was introduced by Gao and Strang in 1989 [13].

Statements (1.26) and (1.27) are called the *canonical double-max duality* and the *canonical double-min duality*, respectively. These two statements can be used to identify the biggest local maximizer and local minimizer of the total potential energy, respectively. It has been proved that the statement (1.27) holds under certain condition that the dimensions of $\bar{\mathbf{x}}$ and $\bar{\boldsymbol{\zeta}}$ are equal in order to get a strong canonical double-min duality, whereas without this additional condition, the double-min duality holds weakly in subspaces of $\mathcal{X}_o \times \mathcal{E}_o^*$ [31, 59, 60]. All these cases will be discussed

7

in Chapter 3.

More detail on this theory with its extensive applications in global optimization and nonconvex mechanics can be found in [19, 27, 32, 37].

1.1.4   Example for canonical duality concept

In this section, a very simple example illustrates the idea of canonical duality with its numerical applications. Let us consider a nonconvex optimization problem in $\mathbb{R}^n$

$$\min_{\mathbf{x} \in \mathbb{R}^n} \Pi(\mathbf{x}) = \frac{1}{2} r_1 \left(\frac{1}{2} |\mathbf{x}|^2 - r_2 \right)^2 - \mathbf{x}^T \mathbf{f}, \tag{1.28}$$

where r_1 and r_2 are given positive parameters. The stationary condition $\nabla \Pi(\mathbf{x}) = 0$ gives the following nonlinear algebraic equation system in $\mathbb{R}^n$

$$r_1 (\frac{1}{2} |\mathbf{x}|^2 - r_2) \mathbf{x} = \mathbf{f}. \tag{1.29}$$

It is very difficult for traditional direct approaches to identify all the roots of problem (1.28) and to determine which root is a global minimizer of $\Pi(\mathbf{x})$. However, by using the canonical dual transformation, this problem can easily be solved completely. Let

$$\boldsymbol{\xi} = \Lambda(\mathbf{x}) = \frac{1}{2} |\mathbf{x}|^2 \in \mathbb{R}.$$

Then, the nonconvex function

$$W(\mathbf{x}) = \frac{1}{2} r_1 (\frac{1}{2} |\mathbf{x}|^2 - r_2)^2,$$

can be written by quadratic canonical form

$$V(\boldsymbol{\xi}) = \frac{1}{2} r_1 (\boldsymbol{\xi} - r_2)^2.$$

Then, its Legendre conjugate is simply given by the following strictly convex quadratic function [19]

$$V^*(\zeta) = \frac{1}{2} r_1^{-1} \zeta^2 + r_2 \zeta.$$

Thus, nonconvex total potential energy $\Pi(\mathbf{x})$ can be converted to the following total complementary function

$$\Xi(\mathbf{x}, \zeta) = \frac{1}{2} |\mathbf{x}|^2 \zeta - \frac{1}{2} r_1^{-1} \zeta^2 - r_2 \, \zeta - \mathbf{x}^T \mathbf{f}. \tag{1.30}$$

The stationary condition $\nabla_{\mathbf{x}}\Xi(\mathbf{x}) = 0$ for a fixed $\zeta \in \mathbb{R}$ leads to the canonical balance equation

$$\zeta\mathbf{x} - \mathbf{f} = 0. \tag{1.31}$$

This canonical balance equation gives the stationary point $\mathbf{x}$

$$\mathbf{x} = \mathbf{f}/\zeta, \quad \zeta \neq 0. \tag{1.32}$$

Substituting this result into the total complementary function Ξ leads to the following canonical dual function

$$\begin{aligned}\Pi^d(\zeta) &= \{\Xi(\mathbf{x},\zeta)|\nabla_{\mathbf{x}}\Xi(\mathbf{x},\zeta) = 0\} \\ &= -\frac{\mathbf{f}^T\mathbf{f}}{2\zeta} - \frac{1}{2}r_1^{-1}\zeta^2 - r_2\zeta, \quad \forall\zeta \neq 0.\end{aligned} \tag{1.33}$$

Then, the stationary condition of this canonical dual function $(\nabla\Pi^d(\zeta) = 0)$ gives the canonical dual algebraic equation

$$(r_1^{-1}\zeta + r_2)\zeta^2 = \frac{1}{2}\mathbf{f}^T\mathbf{f}. \tag{1.34}$$

According to the triality theory, the solutions of this cubic algebraic equation have at most three real roots satisfying

$$\zeta_1 \geq 0 \geq \zeta_2 \geq \zeta_3.$$

From equation (1.32), we have the equivalent stationary points of the nonconvex total potential energy $\Pi(\mathbf{x})$

$$\mathbf{x}_i(\zeta_i) = \mathbf{f}/\zeta_i, \quad \forall\, i = 1, 2, 3.$$

By the canonical min-max duality statement (1.25) of Theorem 3, the stationary point $\mathbf{x}_1(\zeta_1)$ is a global minimizer of $\Pi(\mathbf{x})$ for $\zeta_1 \in \mathcal{E}_+^*$. From statements (1.26) and (1.27), $\mathbf{x}_3(\zeta_3)$ and $\mathbf{x}_2(\zeta_2)$ refer to the local maximizer and local minimizer of $\Pi(\mathbf{x})$, for $\zeta_3, \zeta_2 \in \mathcal{E}_-^*$, respectively.

For further clarification, let $n = 1$, $r_1 = 1$, $r_2 = 3$ and $f = 0.3$. Figure 1.1 illustrates the graphs of both the primal function $\Pi(\mathbf{x})$ and its canonical dual function $\Pi^d(\zeta)$ with their stationary points. Table 1.1 shows the details of all the solutions to problem (1.28), in which $\mathbf{x}_1 = 2.498036$ is a global minimizer of $\Pi(\mathbf{x})$, $\mathbf{x}_3 = -0.100168$ is a local maximizer, and $\mathbf{x}_2 = -2.397869$ is a local minimizer.
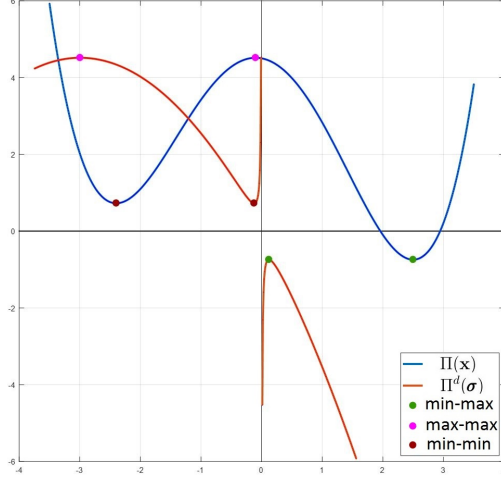
Figure 1.1: *The primal function $\Pi(\mathbf{x})$ with its canonical dual function $\Pi^d(\zeta)$ with $\mathbf{f} = 0.3$*

Table 1.1: *All solutions of $\Pi(\mathbf{x})$ via the triality theory with $f = 0.3$*

Triality theory	ζ_i	State of ζ_i	$\mathbf{x}_i(\zeta_i)$	State of $\mathbf{x}_i(\zeta_i)$	$\Pi^d(\zeta_i) = \Pi(\mathbf{x}_i)$
min-max (1.25), $i = 1$	0.1201	global maximizer	2.4980	global minimizer	-0.742200
min-min (1.27), $i = 2$	-0.1251	local minimizer	-2.3979	local minimizer	0.727187
max-max 1.26), $i = 3$	-2.9950	local maximizer	-0.1002	local maximizer	4.515012

By using the same parameters r_1 and r_2 but with smaller $\mathbf{f} = 0.05$, the canonical dual function $\Pi^d(\zeta)$ will be a finite discontinuous concave function due to a gap located on the interval $(a, b) = (-0.020482, 0.020343)$ as shown in Figure 1.2. From the canonical dual algebraic equation (1.34), we get

$$\zeta^3 + 3\,\zeta^2 - \frac{1}{800} = 0. \tag{1.35}$$

By solving this cubic algebraic equation and by using Theorem 3, we can get all the solutions of the nonconvex function $\Pi(\mathbf{x})$ as reported in Table 1.2, where $\mathbf{x}_1 = 2.45778$ is global minimizer, $\mathbf{x}_2 = -2.441113$ is local minimizer and $\mathbf{x}_3 = -0.016667$ is local maximizer, which correspond to the roots of the canonical function $\Pi^d(\zeta)$; $\zeta_1 = 0.020343$ (global maximizer), $\zeta_2 = -0.020482$ (local minimizer) and $\zeta_3 = -2.999861$ (local maximizer), respectively.
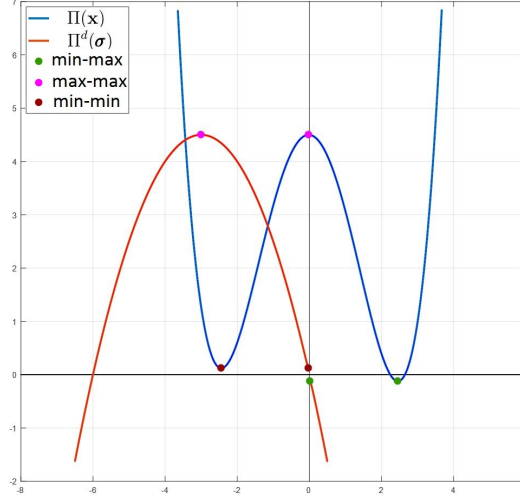
Figure 1.2: *The primal function $\Pi(\mathbf{x})$ with its canonical dual function $\Pi^d(\zeta)$ with* $\mathbf{f} = 0.05$

Table 1.2: *All solutions of $\Pi(\mathbf{x})$ via the triality theory with $f = 0.05$*

Triality theory	ζ_i	State of ζ_i	$\mathbf{x}_i(\zeta_i)$	State of $\mathbf{x}_i(\zeta_i)$	$\Pi^d(\zeta_i) = \Pi(\mathbf{x}_i)$
min-max (1.25), $i = 1$	0.0203	global maximizer	2.4578	global minimizer	-0.122682
min-min (1.27), $i = 2$	-0.0204	local minimizer	-2.4411	local minimizer	0.122265
max-max 1.26), $i = 3$	-2.9999	local maximizer	-0.0167	local maximizer	4.500416

However, the interval (a, b) can be decreased when the value of $\mathbf{f}$ is reduced and it vanishes at $\mathbf{f} = 0$. In the case of $\mathbf{f} = 0$, the graph of $\Pi^d(\zeta)$ is a strictly concave, which corresponds to a symmetric graph $\Pi(\mathbf{x})$, with only one critical point (root ζ_3, local maximizer) and the other two roots $\zeta_1 = \zeta_2 = 0$ located on the boundary of $\mathcal{E}_+^*$. These three roots correspond to a local maximizer ($\mathbf{x}_3 = 0$) and two global minimizers $\mathbf{x}_{1,2} = \pm\sqrt{2r_2}$, respectively, as shown in Figure 1.3.

Generally speaking, the canonical duality equation $\zeta = \nabla V(\boldsymbol{\xi})$ is the so-called the constitutive law. The one-to-one duality equation between each canonical dual pair ensures the existence of the geometrical measure $\boldsymbol{\xi} = \Lambda(\mathbf{x})$ and the canonical form of the functional. In this thesis, several numerical approaches are applied by using the canonical dual transformation method for a large deformation problem.
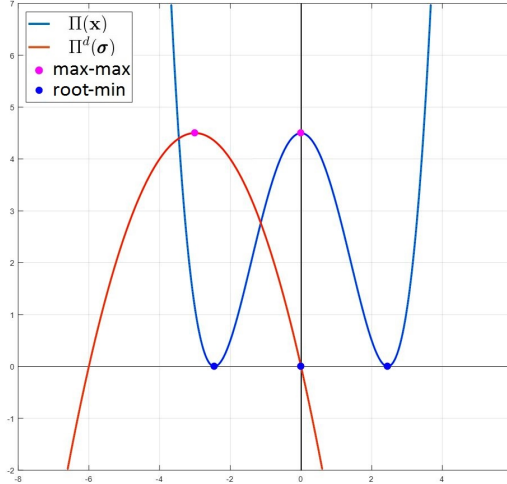
Figure 1.3: *The primal function $\Pi(\mathbf{x})$ with its canonical dual function $\Pi^d(\zeta)$ with $\mathbf{f} = 0$*

1.2 Overview of this thesis

The main goal of this thesis is to solve nonconvex mechanics and topology optimization problems using the newly developed canonical duality theory and to expose its role in establishing connections between nonconvex problems and global optimization. This thesis is structured as follows:

In Chapter 2, a detailed study of a large deformation problems in 2-D structural systems is introduced in order to find a global minimizer of this nonconvex problem. Canonical duality theory provides a potentially useful methodology for solving this challenging problem. In addition to the canonical duality theory, the mixed finite element method is applied with two separate fields, displacement and dual stress fields. Numerical applications are illustrated with different structural designs and different external loads by using a new primal-dual semi-definite programming (PD-SDP) algorithm.

In Chapter 3, we present a new methodology and algorithm for solving post buckling problems of a large deformed elastic beam. The total potential energy of this beam is a nonconvex functional. By using a canonical dual finite element method, a new PD-SDP algorithm is presented, which can be used to obtain all possible post-buckled solutions. Triality theory is verified by creating closed dimensions between discretized displacement and discretized stress by designing mixed meshes of different dual stress interpolations. Applications are illustrated by several numerical examples with different boundary conditions.

In Chapter 4, an evolutionary canonical penalty-duality (CPD) algorithm for solving 3-D benchmark problems in topology optimization is demonstrated. This method is based on the canonical duality theory in nonconvex mechanics and global optimization. It shows that the so-called NP-hard integer programming in topology optimization can be equivalently converted to a concave maximization problem in continuous dual space, which can be solved deterministically via a convex perturbation technique to obtain global optimal 0-1 density distribution without checkerboard patterns. The relation between the canonical penalty-duality method and Gao's pure complementary energy principle is addressed. A comparison is made of two popular methods, bi-directional evolutionary structural optimization (BESO) and solid isotropic material with penalization (SIMP). This chapter ends with a concluding remark devoted to Mathematical mistakes in this popular methods which are explicitly addressed for the first time.

In Chapter 5, we summarize the contributions of this thesis. Some interesting and open problems are also proposed related to our results using canonical duality theory method.

Chapter 2

Canonical Duality Theory in Large Deformation Theory

The minimal nonconvex potential energy of a large deformation problem in nonlinear elasticity can be formulated as follows

$$(\mathcal{P}): \quad \min_{\mathbf{u} \in \mathcal{U}} \Pi(\mathbf{u}) = \int_{\Omega} \Big(W(\nabla \mathbf{u}) - \mathbf{u}.\mathbf{b} \Big) d\Omega - \int_{\Gamma_{\mathbf{t}}} \mathbf{u}.\mathbf{t} \, d\Gamma, \tag{2.1}$$

where $W(\nabla \mathbf{u})$ is a nonconvex stored energy, $\mathcal{U}$ is a kinematically admissible space of deformations over a given design domain $\Omega \subset \mathbb{R}^3$, in which, certain boundary conditions and geometrical constraints are prescribed; $\mathbf{u} : \Omega \to \mathcal{U}$ is a displacement vector field, $\mathbf{b} = \mathbf{b}(x)$ is a given body force vector, $\mathbf{t} = \mathbf{t}(x)$ is a given surface traction on the boundary $\Gamma_t \subset \partial\Omega$, the dot-product $\mathbf{u} \cdot \mathbf{t} = \mathbf{u}^T\mathbf{t}$ and $\mathbf{u}.\mathbf{b} = \mathbf{u}^T\mathbf{b}$.

In mathematical programming and computational sciences, it is fundamentally difficult to solve nonconvex minimization problems $(\mathcal{P})$ by using a traditional convexity methods. Therefore, this has always presented fundamental challenging problems and so, is considered NP-hard in global optimization. The nonconvex minimization problem $(\mathcal{P})$ can be analyzed and solved by using canonical duality theory. The key feature of this theory is that by using a certain canonical strain measure $\mathbf{E} = \Lambda(\mathbf{u})$, general nonconvex/nonsmooth potential variational problems can be equivalently reformulated in finite deformation theory [17]. The finite deformation operator $\Lambda : \mathcal{U}_a \to \mathcal{E}_a$, which is defined from the kinetically admissible space $\mathcal{U}_a \subset \mathcal{U}$ to a closed convex set $\mathcal{E}_a$, can be described as [19]

$$\Lambda(\mathbf{u}) = \frac{1}{2}(\mathbf{F}^T\mathbf{F} - \mathbf{I}), \tag{2.2}$$

where $\mathbf{I}$ is the identity matrix and the deformation gradient $\mathbf{F}$ defined as

$$\mathbf{F} = \mathbf{I} + \nabla\mathbf{u}. \tag{2.3}$$

By substituting (2.3) into (2.2), the finite deformation operator can be written by the following quadratic differential operator

$$\mathbf{E} = \Lambda(\mathbf{u}) = \frac{1}{2}\left[\nabla\mathbf{u} + (\nabla\mathbf{u})^T + (\nabla\mathbf{u})^T\nabla\mathbf{u}\right]. \tag{2.4}$$

The nonconvex stored energy function can be written as

$$W(\nabla\mathbf{u}) = V(\Lambda(\mathbf{u})). \tag{2.5}$$

The canonical dual stress can be uniquely defined by

$$\mathbf{S} = \nabla V(\mathbf{E}) : \mathcal{E}_a \to \mathcal{E}_a^*, \tag{2.6}$$

where $\mathcal{E}_a^*$ is the range of the canonical duality mapping ∇V. A convex differentiable real-valued function

$$V(\mathbf{E}) = \frac{1}{2}\mathbf{E} : \mathbf{H} : \mathbf{E} = \frac{1}{2}\langle\mathbf{E}, \mathbf{H}\mathbf{E}\rangle, \tag{2.7}$$

is said to be canonical on its domain $\mathcal{E}_a$ if the duality relation (2.6) is invertible such that the conjugate function $V^*(\mathbf{S})$ of the canonical function $V(\mathbf{E})$ is defined uniquely by the Legendre transformation [19]

$$V^*(\mathbf{S}) = \{\mathbf{E} : \mathbf{S} - V(\mathbf{E}) \mid \mathbf{S} = \nabla V(\mathbf{E})\}, \tag{2.8}$$

where $\mathbf{E} : \mathbf{S} = \mathbf{E}^T\mathbf{S}$. Then, the following canonical duality relations hold on $\mathcal{E}_a \times \mathcal{E}_a^*$

$$\mathbf{S} = \nabla V(\mathbf{E}) \iff \mathbf{E} = \nabla V^*(\mathbf{S}) \iff V(\mathbf{E}) + V^*(\mathbf{S}) = \mathbf{E} : \mathbf{S}.$$

By replacing $W(\nabla\mathbf{u})$ in the total potential energy $\Pi(\mathbf{u})$ by its canonical form 2.5, the problem (2.1) can be rewritten in the following canonical form

$$(\mathcal{P}) : \quad \min_{\mathbf{u}\in\mathcal{U}} \Pi(\mathbf{u}) = \int_\Omega \left(V(\Lambda(\mathbf{u})) - \mathbf{u}.\mathbf{b}\right)d\Omega - \int_{\Gamma_\mathbf{t}} \mathbf{u}.\mathbf{t}\, d\Gamma, \tag{2.9}$$

By the Fenchel-Young equality

$$V(\Lambda(\mathbf{u})) = \mathbf{E} : \mathbf{S} - V^*(\mathbf{S}) = \Lambda(\mathbf{u}) : \mathbf{S} - V^*(\mathbf{S}),$$

we have the Gao-Strang total complementary energy $\Xi : \mathcal{U}_a \times \mathcal{E}_a^* :\rightarrow \mathbb{R}$ [13]

$$\Xi(\mathbf{u}, \mathbf{S}) = \int_\Omega \left(\mathbf{E} : \mathbf{S} - V^*(\mathbf{S}) - \mathbf{u}.\mathbf{b} \right) d\Omega - \int_{\Gamma_{\mathbf{t}}} \mathbf{u}.\mathbf{t} \; d\Gamma. \tag{2.10}$$

Then, the pure complementary energy can be defined by the following canonical dual transformation [17]

$$\Pi^d(\mathbf{S}) = \{ \Xi(\mathbf{u}, \mathbf{S}) | \; \delta_{\mathbf{u}} \Xi(\mathbf{u}, \mathbf{S}) = 0 \}. \tag{2.11}$$

Let

$$\mathcal{S}_a^+ = \{ \mathbf{S} \in \mathcal{E}_a^* \mid \mathbf{S}(x) \geq 0, \; \forall x \in \Omega \}.$$

The following theorem introduces a global optimal solution to the nonconvex minimization problem $(\mathcal{P})$.

Theorem 4 ([13])
If $(\bar{\mathbf{u}}, \bar{\mathbf{S}})$ is a stationary point of $\Xi(\mathbf{u}, \mathbf{S})$ and $V(\mathbf{E})$ is convex, then for $\bar{\mathbf{S}} \in \mathcal{S}_a^+$, $\bar{\mathbf{u}}$ is a global optimal solution to the problem $(\mathcal{P})$ and

$$\Pi(\bar{\mathbf{u}}) = \min_{\mathbf{u} \in \mathcal{U}_a} \Pi(\mathbf{u}) = \Xi(\bar{\mathbf{u}}, \bar{\mathbf{S}}) = \min_{\mathbf{u} \in \mathcal{U}_a} \max_{\mathbf{S} \in \mathcal{S}_a^+} \Xi(\mathbf{u}, \mathbf{S}) = \max_{\mathbf{S} \in \mathcal{S}_a^+} \min_{\mathbf{u} \in \mathcal{U}_a} \Xi(\mathbf{u}, \mathbf{S}). \tag{2.12}$$

Proof. The following proof was given in Gao and Strang's work [13].
Since the canonical energy $V(\mathbf{E})$ is convex, we have

$$V(\mathbf{E}) - V(\bar{\mathbf{E}}) \geq (\mathbf{E} - \bar{\mathbf{E}}) \nabla V(\bar{\mathbf{E}}) \quad \forall \, \mathbf{E}, \bar{\mathbf{E}} \; \in \; \mathcal{E}_a$$

Let $\bar{\mathbf{E}} = \Lambda(\bar{\mathbf{u}})$, and $\bar{\mathbf{S}} = \nabla V(\Lambda(\bar{\mathbf{u}}))$, this leads to

$$\Pi(\mathbf{u}) - \Pi(\bar{\mathbf{u}}) \geq \int_\Omega \left[\bar{\mathbf{S}}(\Lambda(\mathbf{u}) - \Lambda(\bar{\mathbf{u}})) \right] d\Omega - \int_{\Gamma_{\mathbf{t}}} (\mathbf{u} - \bar{\mathbf{u}}) \mathbf{t} d\Gamma \quad \forall \, \mathbf{u} \; \in \; \mathcal{U}_a.$$

Suppose $\mathbf{u} = \bar{\mathbf{u}} + \delta\mathbf{u}$. By the fact that the geometrical operator $\Lambda(\mathbf{u})$ is a quadratic operator, we have (see [13])

$$\Lambda(\mathbf{u}) = \Lambda(\bar{\mathbf{u}} + \delta\mathbf{u}) = \Lambda(\bar{\mathbf{u}}) + (\nabla\delta\mathbf{u})^T (\nabla\bar{\mathbf{u}}) + \Lambda(\delta\mathbf{u}).$$

Therefore, if $(\bar{\mathbf{u}}, \bar{\mathbf{S}})$ is a stationary point of $\Xi(\mathbf{u}, \mathbf{S})$ and $\mathbf{S} \; \in \; \mathcal{S}_a^+$, we have

$$\Pi(\mathbf{u}) - \Pi(\bar{\mathbf{u}}) = G_{ap}(\delta\mathbf{u}, \bar{\mathbf{S}}) = \int_\Omega \bar{\mathbf{S}}\Lambda(\delta\mathbf{u})d\Omega \geq 0 \quad \forall \, \delta\mathbf{u}.$$

This shows that $\bar{\mathbf{u}}$ is a global minimizer of the total potential energy $\Pi(\mathbf{u})$ over $\mathcal{U}_a$. $\square$

The so-called complementary gap function

$$G_{ap}(\mathbf{u}, \mathbf{S}) = \int_\Omega \mathbf{S}\Lambda(\mathbf{u})d\Omega,$$

is a positive for all $\mathbf{u} \in \mathcal{U}_a$ if and only if $\mathbf{S} \in \mathcal{S}_a^+$. Then we have,

$$\Xi(\mathbf{u}, \bar{\mathbf{S}}) \geq \Xi(\bar{\mathbf{u}}, \bar{\mathbf{S}}) \geq \Xi(\bar{\mathbf{u}}, \mathbf{S}) \ \forall \ (\mathbf{u}, \mathbf{S}) \in \mathcal{U}_a \times \mathcal{S}_a^+.$$

This means, the total complementary energy $\Xi(\mathbf{u}, \mathbf{S})$ is a saddle functional on $\mathcal{U}_a \times \mathcal{S}_a^+$. By applying canonical min-max duality, we obtain the equality relationship (2.12). Theorem 4 shows that the gap function $G_{ap}(\mathbf{u}, \bar{\mathbf{S}}) \geq 0$ achieves a global optimality condition for the problem $(\mathcal{P})$. This gap function has an important role in global optimization (see [28]).

Theorem 5 (Pure complementary energy [19])
Suppose that $(\bar{\mathbf{u}}, \bar{\mathbf{S}})$ is a stationary point of $\Xi(\mathbf{u}, \mathbf{S})$ and $G_{ap}(\bar{\mathbf{u}}, \bar{\mathbf{S}}) \geq 0$. Then $\bar{\mathbf{u}}$ is a global minimizer of $\Pi(\mathbf{u})$ on $\mathcal{U}_a$ if and only if $\bar{\mathbf{S}}$ is a global maximizer of pure complementary energy $\Pi^d(\bar{\mathbf{S}})$, and

$$\Pi(\bar{\mathbf{u}}) = \Xi(\bar{\mathbf{u}}, \bar{\mathbf{S}}) = \Pi^d(\bar{\mathbf{S}}). \tag{2.13}$$

This theorem shows that the canonical min-max duality can be used to find global minimizer of the nonconvex total potential energy $\Pi(\mathbf{u})$ by solving the following canonical dual problem

$$(\mathcal{P}^d): \quad \max\{\Pi^d(\mathbf{S})|\ \mathbf{S} \in \mathcal{S}_a^+\}. \tag{2.14}$$

2.1 Applications for 2-D finite element method

Canonical dual finite element method was first proposed by Gao in 1996 [14]. This section will apply this method for solving large deformed elastic structures. Let us consider a two-dimensional elastic body in x-y directions which is subjected to surface traction $\mathbf{t}$ as shown in Figure 2.1. To generate quadrilateral mesh inside the body domain by using the finite element method, the whole design domain Ω of problem $(\mathcal{P})$ is meshed by dividing it into n rectangular finite elements $\{\Omega_e\}_{e=1}^n$. The domain is mapped into the local coordinate system ξ and η (see Figure 2.2),
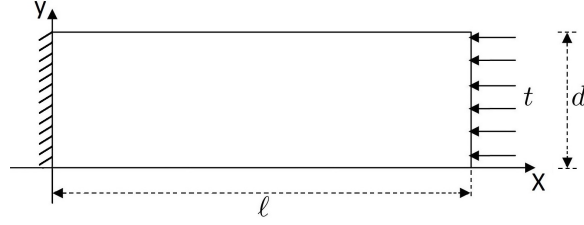
Figure 2.1: *Geometry of the delaminated structure*

then nodal coordinates are transformed back to the global coordinate system x and y, respectively.
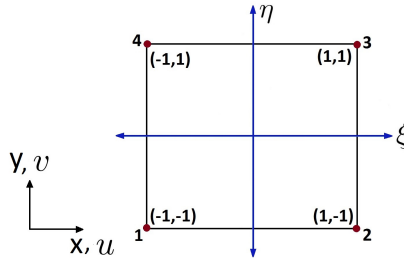
Figure 2.2: *Four node isoparametric quadrilateral element-local coordinate*

The mixed finite element method is proposed to solve the total complementary energy problem (2.10). The spaces $\mathcal{U}_a$ and $\mathcal{S}_a^+$ can be numerically discretized to the finite-dimensional spaces $\mathcal{U}_a^h$ and $\mathcal{S}_+^h$ to determine the displacement field and dual stress field, respectively. The displacement vector $\mathbf{u}$ and the dual stress vector $\mathbf{S}$ can be proposed in separate fields. For the local coordinate system ξ and η, let $\mathbf{p}$ be a nodal deflection vector that relates back to $\mathbf{u}$, and $\mathbf{q}$ is a dual stress vector that relates back to $\mathbf{S}$. Let $\mathbf{p}_e$ and $\mathbf{q}_e$ represent the e-th element Ω_e of $\mathbf{p} \in \mathbb{R}^n$ and $\mathbf{q} \in \mathbb{R}^m$ respectively which can be described in the following forms (see Figure 2.3)

$$\mathbf{p}_e^T = [u_1\ v_1\ u_2\ v_2\ u_3\ v_3\ u_4\ v_4], \tag{2.15}$$

$$\mathbf{q}_e^T = [r_1\ s_1\ t_1\ r_2\ s_2\ t_2\ r_3\ s_3\ t_3\ r_4\ s_4\ t_4], \tag{2.16}$$

where $n = 2d$ and $m = 3d$, and d represents the total number of mesh nodes.

The displacement field and coordinates are interpolated as a four-node isoparametric quadrilateral

$$\mathbf{N} = \begin{bmatrix} N_1 & 0 & N_2 & 0 & N_3 & 0 & N_4 & 0 \\ 0 & N_1 & 0 & N_2 & 0 & N_3 & 0 & N_4 \end{bmatrix} \tag{2.17}$$
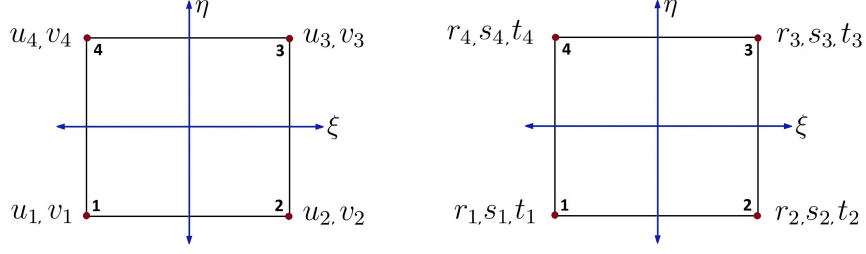
Figure 2.3: *The nodes of $\mathbf{p}_e$ of the deflection vector $\mathbf{p}$ (left) and $\mathbf{q}_e$ of the dual stress vector $\mathbf{q}$ (right) of the e-th element Ω_e*

The explicit forms of the shape functions N_i, $i = 1, ..., 4$ can be defined for the two-dimensional isoparametric quadrilateral elements as the following

$$N_1 = \frac{1}{4}(1 - \xi)(1 - \eta),$$

$$N_2 = \frac{1}{4}(1 + \xi)(1 - \eta),$$

$$N_3 = \frac{1}{4}(1 + \xi)(1 + \eta),$$

$$N_4 = \frac{1}{4}(1 - \xi)(1 + \eta).$$

In geometric interpolation, these shape functions can be used to generate the global coordinates x and y and the displacement interpolation u and v

$$x = \sum_{i=1}^{4} N_i x_i, \qquad y = \sum_{i=1}^{4} N_i y_i. \tag{2.18}$$

$$u = \sum_{i=1}^{4} N_i u_i, \qquad v = \sum_{i=1}^{4} N_i v_i, \tag{2.19}$$

Thus, the deformation field can be formulated by the interpolation matrix $\mathbf{N}$ as the following

$$\mathbf{u}_e^h = (u \ \ v) = \mathbf{N}(\xi, \eta)\mathbf{p}_e, \tag{2.20}$$

On the other hand, the stress field and coordinates are interpolated as a four-node isoparametric quadrilateral

$$\mathbf{M} = \begin{bmatrix} M_1 & 0 & 0 & M_2 & 0 & 0 & M_3 & 0 & 0 & M_4 & 0 & 0 \\ 0 & M_1 & 0 & 0 & M_2 & 0 & 0 & M_3 & 0 & 0 & M_4 & 0 \\ 0 & 0 & M_1 & 0 & 0 & M_2 & 0 & 0 & M_3 & 0 & 0 & M_4 \end{bmatrix}. \tag{2.21}$$

The shape functions M_i, $i = 1, ..., 4$ can be derived by the same explicit forms of N_i as in the following forms

$$M_1 = \frac{1}{4}(1 - \xi)(1 - \eta),$$

$$M_2 = \frac{1}{4}(1 + \xi)(1 - \eta),$$

$$M_3 = \frac{1}{4}(1 + \xi)(1 + \eta),$$

$$M_4 = \frac{1}{4}(1 - \xi)(1 + \eta).$$

Thus, the dual stress field is approximated as

$$\mathbf{S}_e^h = \mathbf{M}(\xi, \eta)\mathbf{q}_e. \tag{2.22}$$

The Green strain tensor can be defined for the large deformation problem by the following quadratic differential operator

$$\mathbf{E} = \mathbf{E}_L + \mathbf{E}_{NL}, \tag{2.23}$$

in which $\mathbf{E}_L$ and $\mathbf{E}_{NL}$ are the linear and nonlinear components of $\mathbf{E}$, respectively:

$$\mathbf{E}_L = \frac{1}{2}\left[\nabla\mathbf{u} + (\nabla\mathbf{u})^T\right], \tag{2.24}$$

$$\mathbf{E}_{NL} = \frac{1}{2}\left[(\nabla\mathbf{u})^T\nabla\mathbf{u}\right]. \tag{2.25}$$

The linear Green strain tensor $\mathbf{E}_L$ can be expressed by the linear partial differential vector

$$\mathbf{E}_L = \begin{bmatrix} \frac{\partial u}{\partial x} \\ \frac{\partial v}{\partial y} \\ \frac{\partial u}{\partial y} + \frac{\partial v}{\partial x} \end{bmatrix}, \tag{2.26}$$

and, the nonlinear Green strain tensor $\mathbf{E}_{NL}$ can be expressed by the quadratic partial differential vector

$$\mathbf{E}_{NL} = \frac{1}{2}\begin{bmatrix} (\frac{\partial u}{\partial x})^2 + (\frac{\partial v}{\partial x})^2 \\ (\frac{\partial u}{\partial y})^2 + (\frac{\partial v}{\partial y})^2 \\ 2(\frac{\partial u}{\partial x}\frac{\partial u}{\partial y} + \frac{\partial v}{\partial x}\frac{\partial v}{\partial y}) \end{bmatrix}. \tag{2.27}$$

Thus, the total elastic strain energy of the system can be stated as the following:

$$\int_\Omega \mathbf{E}^T\mathbf{S}d\Omega = \int_\Omega \left((\mathbf{E}_L)^T\mathbf{S} + (\mathbf{E}_{NL})^T\mathbf{S}\right)d\Omega. \tag{2.28}$$

Typically, the linear elasticity term in independent fields $\mathbf{u}$ and $\mathbf{S}$ takes the form

$$
\begin{aligned}
\int_\Omega (\mathbf{E}_L)^T \mathbf{S} \, d\Omega &= \int_\Omega \Big(\mathbf{B}(\xi, \eta).\mathbf{p} \Big)^T \Big(\mathbf{M}(\xi, \eta).\mathbf{q} \Big) \, d\Omega \\
&= \int_\Omega \mathbf{p}^T \mathbf{B}^T(\xi, \eta) \mathbf{M}(\xi, \eta) \mathbf{q} \, d\Omega \\
&= \mathbf{p}^T \mathbf{Q} \, \mathbf{q},
\end{aligned}
\tag{2.29}
$$

where $\mathbf{B}(\xi, \eta)$ is the strain displacement matrix

$$
\mathbf{B}(\xi, \eta) = \begin{bmatrix}
\frac{\partial N_1}{\partial x} & 0 & \frac{\partial N_2}{\partial x} & 0 & \frac{\partial N_3}{\partial x} & 0 & \frac{\partial N_4}{\partial x} & 0 \\
0 & \frac{\partial N_1}{\partial y} & 0 & \frac{\partial N_2}{\partial y} & 0 & \frac{\partial N_3}{\partial y} & 0 & \frac{\partial N_4}{\partial y} \\
\frac{\partial N_1}{\partial y} & \frac{\partial N_1}{\partial x} & \frac{\partial N_2}{\partial y} & \frac{\partial N_2}{\partial x} & \frac{\partial N_3}{\partial y} & \frac{\partial N_3}{\partial x} & \frac{\partial N_4}{\partial y} & \frac{\partial N_4}{\partial x}
\end{bmatrix},
$$

and the matrix $\mathbf{Q}$ is composed by assembling the following element matrices

$$
\mathbf{Q}_e = \int_{-1}^{1} \int_{-1}^{1} \mathbf{B}^T(\xi, \eta) \, \mathbf{M}(\xi, \eta) \, |\mathbf{J}| d\xi d\eta,
\tag{2.30}
$$

where $\mathbf{Q}_e \in \mathbb{R}^8 \times \mathbb{R}^{12}$ and $|\mathbf{J}|$ is a determinant of the Jacobian matrix $\mathbf{J}$

$$
\mathbf{J} = \begin{bmatrix}
\frac{\partial x}{\partial \xi} & \frac{\partial y}{\partial \xi} \\
\frac{\partial x}{\partial \eta} & \frac{\partial y}{\partial \eta}
\end{bmatrix}.
\tag{2.31}
$$

By substituting x and y in (2.18) into (2.31), the Jacobian matrix can be converted to the following discretized form

$$
\mathbf{J} = \begin{bmatrix}
N_{,\xi}^T \cdot \bar{\mathbf{x}} & N_{,\xi}^T \cdot \bar{\mathbf{y}} \\
N_{,\eta}^T \cdot \bar{\mathbf{x}} & N_{,\eta}^T \cdot \bar{\mathbf{y}}
\end{bmatrix},
\tag{2.32}
$$

where

$$
\bar{\mathbf{x}}^T = \begin{bmatrix} x_1 & x_2 & x_3 & x_4 \end{bmatrix},
$$

and

$$
\bar{\mathbf{y}}^T = \begin{bmatrix} y_1 & y_2 & y_3 & y_4 \end{bmatrix},
$$

are the global coordinates of each rectangular element Ω_e. $\bar{\mathbf{N}}_{,\xi}^T$ and $\bar{\mathbf{N}}_{,\eta}^T$ are the derivatives of

$$
\bar{\mathbf{N}}^T = \begin{bmatrix} N_1 & N_2 & N_3 & N_4 \end{bmatrix},
$$

with respect to the local coordinates ξ and η, respectively, which can be written as

21

the following forms

$$
\begin{aligned}
\bar{\mathbf{N}}_{,\xi}^T &= \begin{bmatrix} \dfrac{\partial N_1}{\partial \xi} & \dfrac{\partial N_2}{\partial \xi} & \dfrac{\partial N_3}{\partial \xi} & \dfrac{\partial N_4}{\partial \xi} \end{bmatrix} \\
&= \frac{1}{4}\left[-(1-\eta)\ \ (1-\eta)\ \ (1+\eta)\ \ -(1+\eta)\right],
\end{aligned}
\tag{2.33}
$$

and

$$
\begin{aligned}
\bar{\mathbf{N}}_{,\eta}^T &= \begin{bmatrix} \dfrac{\partial N_1}{\partial \eta} & \dfrac{\partial N_2}{\partial \eta} & \dfrac{\partial N_3}{\partial \eta} & \dfrac{\partial N_4}{\partial \eta} \end{bmatrix} \\
&= \frac{1}{4}\left[-(1-\xi)\ \ -(1+\xi)\ \ (1+\xi)\ \ (1-\xi)\right].
\end{aligned}
\tag{2.34}
$$

Thus, the Jacobian determinant $|\mathbf{J}|$ can be easily obtained in the following discretized form

$$
|\mathbf{J}| = (\bar{\mathbf{N}}_{,\xi}^T \cdot \bar{\mathbf{x}})(\ \bar{\mathbf{N}}_{,\eta}^T \cdot \bar{\mathbf{y}}) - (\bar{\mathbf{N}}_{,\eta}^T \cdot \bar{\mathbf{x}})(\ \bar{\mathbf{N}}_{,\xi}^T \cdot \bar{\mathbf{y}}).
\tag{2.35}
$$

For the large deformation behavior in nonlinear elasticity, the nonlinear strain energy $\mathbf{E}_{NL}$ in (2.27) can be reformulated as

$$
\mathbf{E}_{NL} = \frac{1}{2}\mathbf{p}^T\widehat{\mathbf{B}}(\xi, \eta)\ \mathbf{p},
\tag{2.36}
$$

where the matrix $\widehat{\mathbf{B}}(\xi, \eta) \in \mathbb{R}^{8 \times 3 \times 8}$ can be expressed in the following way

$$
\widehat{\mathbf{B}}^T = \begin{bmatrix} \widehat{\mathbf{B}}_1 & \widehat{\mathbf{B}}_2 & \widehat{\mathbf{B}}_3 \end{bmatrix},
$$

in which $\widehat{\mathbf{B}}_1$, $\widehat{\mathbf{B}}_2$ and $\widehat{\mathbf{B}}_3$ are the matrices obtained by using the shape functions of

the displacement field:

$$
\widehat{\mathbf{B}}_1 =
\begin{bmatrix}
(N_{1,x})^2 & 0 & N_{1,x}N_{2,x} & 0 & N_{1,x}N_{3,x} & 0 & N_{1,x}N_{4,x} & 0 \\
& (N_{1,x})^2 & 0 & N_{1,x}N_{2,x} & 0 & N_{1,x}N_{3,x} & 0 & N_{1,x}N_{4,x} \\
& & (N_{2,x})^2 & 0 & N_{2,x}N_{3,x} & 0 & N_{2,x}N_{4,x} & 0 \\
& & & (N_{2,x})^2 & 0 & N_{2,x}N_{3,x} & 0 & N_{2,x}N_{4,x} \\
& & & & (N_{3,x})^2 & 0 & N_{3,x}N_{4,x} & 0 \\
& & & & & (N_{3,x})^2 & 0 & N_{3,x}N_{4,x} \\
& & & & & & (N_{4,x})^2 & 0 \\
Sym & & & & & & & (N_{4,x})^2
\end{bmatrix}
, \ (2.37)
$$

$$
\widehat{\mathbf{B}}_2 =
\begin{bmatrix}
(N_{1,y})^2 & 0 & N_{1,y}N_{2,y} & 0 & N_{1,y}N_{3,y} & 0 & N_{1,y}N_{4,y} & 0 \\
& (N_{1,y})^2 & 0 & N_{1,y}N_{2,y} & 0 & N_{1,y}N_{3,y} & 0 & N_{1,y}N_{4,y} \\
& & (N_{2,y})^2 & 0 & N_{2,y}N_{3,y} & 0 & N_{2,y}N_{4,y} & 0 \\
& & & (N_{2,y})^2 & 0 & N_{2,y}N_{3,y} & 0 & N_{2,y}N_{4,y} \\
& & & & (N_{3,y})^2 & 0 & N_{3,y}N_{4,y} & 0 \\
& & & & & (N_{3,y})^2 & 0 & N_{3,y}N_{4,y} \\
& & & & & & (N_{4,y})^2 & 0 \\
Sym & & & & & & & (N_{4,y})^2
\end{bmatrix}
, \ (2.38)
$$

and,

$$
\widehat{\mathbf{B}}_3 = 2
\begin{bmatrix}
N_{1,x}N_{1,y} & 0 & N_{1,x}N_{2,y} & 0 & N_{1,x}N_{3,y} & 0 & N_{1,x}N_{4,y} & 0 \\
0 & N_{1,x}N_{1,y} & 0 & N_{1,x}N_{2,y} & 0 & N_{1,x}N_{3,y} & 0 & N_{1,x}N_{4,y} \\
N_{2,x}N_{1,y} & 0 & N_{2,x}N_{2,y} & 0 & N_{2,x}N_{3,y} & 0 & N_{2,x}N_{4,y} & 0 \\
0 & N_{2,x}N_{1,y} & 0 & N_{2,x}N_{2,y} & 0 & N_{2,x}N_{3,y} & 0 & N_{2,x}N_{4,y} \\
N_{3,x}N_{1,y} & 0 & N_{3,x}N_{2,y} & & N_{3,x}N_{3,y} & 0 & N_{3,x}N_{4,y} & 0 \\
0 & N_{3,x}N_{1,y} & 0 & N_{3,x}N_{2,y} & 0 & N_{3,x}N_{3,y} & 0 & N_{3,x}N_{4,y} \\
N_{4,x}N_{1,y} & 0 & N_{4,x}N_{2,y} & 0 & N_{4,x}N_{3,y} & 0 & N_{4,x}N_{4,y} & 0 \\
0 & N_{4,x}N_{1,y} & 0 & N_{4,x}N_{2,y} & 0 & N_{4,x}N_{3,y} & 0 & N_{4,x}N_{4,y}
\end{bmatrix}
\tag{2.39}
$$

where, for any ith node the $N_{i,x}$ and $N_{i,y}$ represent $\frac{\partial N_i}{\partial x}$ and $\frac{\partial N_i}{\partial y}$, respectively. Thus, the derivative of the shape function N_i for the global coordinates x and y can be written as

$$
\begin{bmatrix}
\frac{\partial N_i}{\partial x} \\
\frac{\partial N_i}{\partial y}
\end{bmatrix}
=
\begin{bmatrix}
\frac{\partial N_i}{\partial \xi}\frac{\partial \xi}{\partial x} + \frac{\partial N_i}{\partial \eta}\frac{\partial \eta}{\partial x} \\
\frac{\partial N_i}{\partial \xi}\frac{\partial \xi}{\partial y} + \frac{\partial N_i}{\partial \eta}\frac{\partial \eta}{\partial y}
\end{bmatrix}
\tag{2.40}
$$

$$
=
\begin{bmatrix}
\frac{\partial \xi}{\partial x} & \frac{\partial \eta}{\partial x} \\
\frac{\partial \xi}{\partial y} & \frac{\partial \eta}{\partial y}
\end{bmatrix}
\begin{bmatrix}
\frac{\partial N_i}{\partial \xi} \\
\frac{\partial N_i}{\partial \eta}
\end{bmatrix}.
\tag{2.41}
$$

It is easy to see that the matrix in (2.41) represents the inverse Jacobian matrix

$$
\mathbf{J}^{-1} =
\begin{bmatrix}
\frac{\partial \xi}{\partial x} & \frac{\partial \eta}{\partial x} \\
\frac{\partial \xi}{\partial y} & \frac{\partial \eta}{\partial y}
\end{bmatrix}.
\tag{2.42}
$$

The inverse Jacobian matrix can be also obtained by using (2.32) in order to compute

the derivative of N_i for x and y as in the following discretized form

$$
\begin{aligned}
\begin{bmatrix} \frac{\partial N_i}{\partial x} \\ \frac{\partial N_i}{\partial y} \end{bmatrix}
&= \mathbf{J}^{-1} \begin{bmatrix} \frac{\partial N_i}{\partial \xi} \\ \frac{\partial N_i}{\partial \eta} \end{bmatrix} \\
&= \begin{bmatrix} \bar{\mathbf{N}}_{,\xi}^T \cdot \bar{\mathbf{x}} & \bar{\mathbf{N}}_{,\xi}^T \cdot \bar{\mathbf{y}} \\ \bar{\mathbf{N}}_{,\eta}^T \cdot \bar{\mathbf{x}} & \bar{\mathbf{N}}_{,\eta}^T \cdot \bar{\mathbf{y}} \end{bmatrix}^{-1} \begin{bmatrix} N_{i,\xi} \\ N_{i,\eta} \end{bmatrix} \\
&= \frac{1}{|\mathbf{J}|} \begin{bmatrix} \left(\bar{\mathbf{N}}_{,\eta}^T \bar{\mathbf{y}}\right) N_{i,\xi} - \left(\bar{\mathbf{N}}_{,\xi}^T \bar{\mathbf{y}}\right) N_{i,\eta} \\ -\left(\bar{\mathbf{N}}_{,\eta}^T \bar{\mathbf{x}}\right) N_{i,\xi} + \left(\bar{\mathbf{N}}_{,\xi}^T \bar{\mathbf{x}}\right) N_{i,\eta} \end{bmatrix},
\end{aligned}
\tag{2.43}
$$

where $|\mathbf{J}|$ is computed in (2.35). Thus, the nonlinear elasticity term in (2.28) can be expressed in discretized form as the following

$$
\begin{aligned}
\int_\Omega (\mathbf{E}_{NL})^T \mathbf{S} \, d\Omega &= \int_\Omega \frac{1}{2} \left(\mathbf{p}^T \widehat{\mathbf{B}}^T(\xi, \eta) \, \mathbf{p} \right) \left(\mathbf{M}(\xi, \eta) \, \mathbf{q} \right) d\Omega \\
&= \int_\Omega \frac{1}{2} \mathbf{p}^T \left(\widehat{\mathbf{B}}^T(\xi, \eta) \mathbf{M}(\xi, \eta) \, \mathbf{q} \right) \mathbf{p} \, d\Omega \\
&= \frac{1}{2} \mathbf{p}^T \bar{\mathbf{G}}(\mathbf{q}) \, \mathbf{p},
\end{aligned}
\tag{2.44}
$$

where $\bar{\mathbf{G}}(\mathbf{q})$ is obtained by assembling the following matrices

$$
\mathbf{G}_e(\mathbf{q}) = \int_{-1}^{1} \int_{-1}^{1} \widehat{\mathbf{B}}^T \, \mathbf{M}(\xi, \eta) \, \mathbf{q} \, |\mathbf{J}| d\xi d\eta,
\tag{2.45}
$$

in which $\mathbf{G}_e(\mathbf{q}) \in \mathbb{R}^8 \times \mathbb{R}^8$. It is clear that, both $\widehat{\mathbf{B}}_1$ and $\widehat{\mathbf{B}}_2$ are symmetric matrices whereas $\widehat{\mathbf{B}}_3$ is not symmetric, therefore, $\bar{\mathbf{G}}(\mathbf{q})$ is also not symmetric. Due to the fact that

$$
\mathbf{p}^T \bar{\mathbf{G}}(\mathbf{q}) \, \mathbf{p} = \mathbf{p}^T \left[\frac{\bar{\mathbf{G}}(\mathbf{q}) + \bar{\mathbf{G}}^T(\mathbf{q})}{2} \right] \mathbf{p},
\tag{2.46}
$$

the $\bar{\mathbf{G}}(\mathbf{q})$ in equation (2.44) can be replaced by the following symmetric matrix

$$
\mathbf{G}(\mathbf{q}) = \left[\frac{\bar{\mathbf{G}}(\mathbf{q}) + \bar{\mathbf{G}}^T(\mathbf{q})}{2} \right].
\tag{2.47}
$$

Thus, the nonlinear elasticity term can be rewritten as

$$
\begin{aligned}
\int_\Omega \mathbf{E}_{NL}^T \mathbf{S} \, d\Omega &= \frac{1}{2} \mathbf{p}^T \mathbf{G}(\mathbf{q}) \, \mathbf{p} \\
&= G_{ap}(\mathbf{u}(\mathbf{p}), \mathbf{S}(\mathbf{q})),
\end{aligned}
\tag{2.48}
$$

where $G_{ap}(\mathbf{u}(\mathbf{p}), \mathbf{S}(\mathbf{q}))$ is so-called complementary gap function.

By the Legendre transformation, the canonical complementary energy in this problem can be obtained by

$$V^*(\mathbf{S}) = \frac{1}{2}\mathbf{S}^T\mathbf{H}^{-1}\mathbf{S}, \tag{2.49}$$

where the constitutive matrix $\mathbf{H}$ is defined for the plane stress by the following matrix

$$\mathbf{H} = \frac{E}{1-\mu^2} \begin{bmatrix} 1 & \mu & 0 \\ \mu & 1 & 0 \\ 0 & 0 & \frac{1-\mu}{2} \end{bmatrix}, \tag{2.50}$$

in which E is the Young's modulus and μ is the Poisson's ratio. Then we have

$$\begin{aligned} \int_\Omega V^*(\mathbf{S})d\Omega &= \int_\Omega \frac{1}{2}\mathbf{S}^T\mathbf{H}^{-1}\mathbf{S}d\Omega \\ &= \int_\Omega \frac{1}{2}\mathbf{q}^T\mathbf{M}^T(\xi,\eta)\mathbf{H}^{-1}\mathbf{M}(\xi,\eta)\mathbf{q}d\Omega \\ &= \frac{1}{2}\mathbf{q}^T\mathbf{K}\mathbf{q}, \tag{2.51} \end{aligned}$$

where $\mathbf{K}$ is obtained by assembling the following matrices $\mathbf{K}_e \in \mathbb{R}^{12} \times \mathbb{R}^{12}$

$$\mathbf{K}_e = \int_{-1}^{1}\int_{-1}^{1} \mathbf{M}^T(\xi,\eta)\mathbf{H}^{-1}\mathbf{M}(\xi,\eta) \, |\mathbf{J}|d\xi d\eta. \tag{2.52}$$

A whole vector of the body force $\mathbf{b}$, denoted by $\bar{\mathbf{b}}$, is defined by assembling vectors

$$\mathbf{b}_e = \int_{-1}^{1}\int_{-1}^{1} \mathbf{b}.\mathbf{N}(\xi,\eta) \, |\mathbf{J}|d\xi d\eta.$$

Since the surface traction $\mathbf{t}$ is only along the body surface, we can use a linear shape function to construct a whole vector of $\mathbf{t}$, denoted by $\bar{\mathbf{t}}$, by assembling vectors

$$\mathbf{t}_e = \begin{cases} \int_{-1}^{1} \frac{l_e}{2} \mathbf{t} \, \tilde{\mathbf{N}}(\tilde{\xi}) \, d\tilde{\xi} & \text{if } x \in \Gamma_\mathbf{t} \\ \\ 0 & \text{otherwise,} \end{cases} \tag{2.53}$$

where $\tilde{\xi} = \frac{2x}{l_e} - 1$ is the local coordinate, $l_e = b - a$ is the length of the element surface which is subjected by surface traction $\mathbf{t}$ over interval $[a, b]$, and the linear

shape function $\tilde{\mathbf{N}}(\tilde{\xi})$ is defined as

$$\tilde{\mathbf{N}}(\tilde{\xi}) = \begin{bmatrix} \tilde{N}_1 \\ 0 \\ \tilde{N}_2 \\ 0 \end{bmatrix},$$

where

$$\tilde{N}_1(\tilde{\xi}) = \frac{1}{2}(1 - \tilde{\xi}),$$

and

$$\tilde{N}_2(\tilde{\xi}) = \frac{1}{2}(1 + \tilde{\xi}).$$

In the present work we focus on a horizontal uniformly distributed loading, in which $\mathbf{t}^T = (t_x, t_y) = (t_x, 0)$, where t_x and t_y represent the x-direction and y-direction of the surface traction $\mathbf{t}$, respectively.

Thus, in terms of $\mathbf{p}$ and $\mathbf{q}$ and on the discretized feasible deformation space $\mathcal{U}_a^h$, the Gao-Strang total potential energy can be written in the following discretized canonical mixed form

$$
\begin{aligned}
\Xi^h(\mathbf{p}, \mathbf{q}) &= \sum_e \left(\frac{1}{2}\mathbf{p}_e^T \, \mathbf{G}_e(\mathbf{q}_e) \, \mathbf{p}_e - \frac{1}{2}\mathbf{q}_e^T \, \mathbf{K}_e \, \mathbf{q}_e - \mathbf{p}_e^T \boldsymbol{\tau}_e(\mathbf{q}_e) \right) \\
&= \frac{1}{2}\mathbf{p}^T \, \mathbf{G}(\mathbf{q}) \, \mathbf{p} - \frac{1}{2}\mathbf{q}^T \, \mathbf{K} \, \mathbf{q} - \mathbf{p}^T \boldsymbol{\tau}(\mathbf{q}),
\end{aligned}
\tag{2.54}
$$

where,

$$\boldsymbol{\tau}(\mathbf{q}) = \bar{\mathbf{f}} + \bar{\mathbf{t}} - \mathbf{Q}\,\mathbf{q}.$$

Finally, with the positive definite matrix $\mathbf{G}(\mathbf{q})$, the problem $(\mathcal{P})$ can be expressed via Theorem 5 in the following discrete problem

$$
\begin{aligned}
\max_{\mathbf{q}\in\mathbb{R}^m} \min_{\mathbf{p}\in\mathbb{R}^n} \Xi(\mathbf{p}, \mathbf{q}) &= \frac{1}{2}\mathbf{p}^T\mathbf{G}(\mathbf{q})\,\mathbf{p} - \frac{1}{2}\mathbf{q}^T\mathbf{K}\mathbf{q} - \mathbf{p}^T\boldsymbol{\tau}(\mathbf{q}), \\
s.t. \quad \mathbf{G}(\mathbf{q}) &\succeq 0.
\end{aligned}
\tag{2.55}
$$

The critical condition $\delta\Xi(\mathbf{p}, \mathbf{q}) = 0$, leads to the following canonical equilibrium equations

$$\mathbf{G}(\mathbf{q})\,\mathbf{p} - \boldsymbol{\tau}(\mathbf{q}) = 0, \tag{2.56}$$

$$\frac{1}{2}\mathbf{p}^T \, \mathbf{G}_{,\mathbf{q}}(\mathbf{q})\,\mathbf{p} - \mathbf{K}\,\mathbf{q} + \mathbf{Q}\,\mathbf{p} = 0, \tag{2.57}$$

where $\mathbf{G}_{,\mathbf{q}}(\mathbf{q})$ is the Hessian matrix of the discretized Gao-Strang gap function.

Theorem 6 ([14])

For any given finite-element discretization of problem $(\mathcal{P})$, if:

- *the complementary gap function $G_{ap}(\mathbf{u}(\mathbf{p}), \mathbf{S}(\mathbf{q})) \geq 0, \forall \mathbf{p} \in \mathbb{R}^n$ and $\mathbf{q} \in \mathbb{R}^m$, and*

- *the following rank condition holds,*

$$rank\ G_{ap} = n < m, \tag{2.58}$$

then problem (2.55) has at least one solution $(\mathbf{p}, \mathbf{q})$, and it has a unique solution if the gap function is strictly positive.

By this theorem, if the gap function G_{ap} possesses a right sign and the rank condition (2.58) is true, then the sequence $\{\mathbf{p}^k, \mathbf{q}^k\}$ will converge to the global minimal solution $(\mathbf{p}, \mathbf{q})$ of the primal problem $(\mathcal{P})$ (see [14]). It is easy to see that the rank condition (2.58) in problem (2.55) holds, due to the fact that the size of the configure vector $\mathbf{p}_e$ of $\mathbf{p}$ is less than the size of configure vector $\mathbf{q}_e$ of $\mathbf{q}$, as shown in (2.15) and (2.16).

2.2   Semi-definite programming algorithm

Semi-definite programming (SDP) was the most exciting and active research area in mathematical programming during the 1990s. SDP is a subfield of convex optimization and is concerned with the optimization of a linear objective function over the intersection of the cone of positive semidefinite matrices [43, 72].

In order to solve problem (2.55), it will be converted to an SDP problem which can be efficiently solved by interior point methods. By the fact that $\Xi(\mathbf{p}, \mathbf{q})$ is a saddle function on $\mathcal{U}_a^h \times \mathbf{S}^+$, where $\mathbf{S}^+ = \{\mathbf{q} \in \mathbb{R}^m \mid \mathbf{G}(\mathbf{q}) \succeq 0\}$, we have

$$\min_{\mathbf{p} \in \mathcal{U}_a^h} \Pi_p^h(\mathbf{p}) = \min_{\mathbf{p} \in \mathcal{U}_a^h} \max_{\mathbf{q} \in \mathbf{S}^+} \Xi(\mathbf{p}, \mathbf{q}) = \max_{\mathbf{q} \in \mathbf{S}^+} \min_{\mathbf{p} \in \mathcal{U}_a^h} \Xi(\mathbf{p}, \mathbf{q}). \tag{2.59}$$

in which $rank(\mathbf{p}) < rank(\mathbf{q})$. Thus, the problem $(\mathcal{P})$ can be proposed as the following problem

$$
\begin{aligned}
\max_{\mathbf{q} \in \mathbb{R}^m} \min_{\mathbf{p} \in \mathbb{R}^n} \Xi(\mathbf{p}, \mathbf{q}) &= \frac{1}{2}\mathbf{p}^T \mathbf{G}(\mathbf{q})\, \mathbf{p} - \frac{1}{2}\mathbf{q}^T \mathbf{K}\mathbf{q} - \mathbf{p}^T \boldsymbol{\tau}(\mathbf{q}), \\
s.t. \quad \mathbf{G}(\mathbf{q}) &\succeq 0, \tag{2.60}
\end{aligned}
$$

28

where the symbol "$\succeq$" represents the symmetric positive semi-definite matrix. By applying equilibrium equation (2.56) and for any given $\mathbf{q} \in \mathbf{S}^+$, the solution to $\min_{\mathbf{p} \in \mathcal{U}_a^h} \Xi(\mathbf{p}, \mathbf{q})$ leads to

$$\mathbf{p} = \mathbf{p}(\mathbf{q}) = \mathbf{G}^{-1}(\mathbf{q}) \, \boldsymbol{\tau}(\mathbf{q}). \tag{2.61}$$

Therefore, the stress field $\mathbf{q}$ can be found by the following problem

$$
\begin{aligned}
\max_{\mathbf{q}} \; \Xi(\mathbf{p}(\mathbf{q}), \mathbf{q}) &= \Theta(\mathbf{q}) - \frac{1}{2}\mathbf{q}^T \mathbf{K} \, \mathbf{q} \\
\text{s.t.} \qquad \mathbf{G}(\mathbf{q}) &\succeq 0,
\end{aligned}
\tag{2.62}
$$

where the function $\Theta(\mathbf{q})$ is defined by

$$\Theta(\mathbf{q}) = \frac{1}{2}\mathbf{p}^T(\mathbf{q})\mathbf{G}(\mathbf{q})\,\mathbf{p}(\mathbf{q}) - \mathbf{p}^T(\mathbf{q})\boldsymbol{\tau}(\mathbf{q}).$$

Clearly, by using the canonical min-max duality, if $\mathbf{q}^* \in \mathbf{S}^+$ is a global maximizer of problem (3.45), then $\mathbf{p}^* = \mathbf{p}(\mathbf{q}^*)$ must be a global minimizer of $\Pi_p^h(\mathbf{p})$. Furthermore, problem (3.45) is equivalent to:

$$\max_{\mathbf{q}, z} \; z \quad \text{s.t.} \quad \mathbf{G}(\mathbf{q}) \succeq 0, \quad z \leq \Theta(\mathbf{q}) - \frac{1}{2}\mathbf{q}^T \mathbf{K} \, \mathbf{q}. \tag{2.63}$$

By the fact that $\mathbf{K} \succeq 0$, the Schur complement lemma for the second inequality constraint in (2.63) implies (see [72])

$$\begin{bmatrix} 2\mathbf{K}^{-1} & \mathbf{q} \\ \mathbf{q}^T & \Theta(\mathbf{q}) - z \end{bmatrix} \succeq 0. \tag{2.64}$$

Thus, problem (2.63) can be relaxed to the following SDP problem

$$\max_{\mathbf{q}, z} \; z \quad \text{s.t.} \quad \mathbf{G}(\mathbf{q}) \succeq 0, \quad \begin{bmatrix} 2\mathbf{K}^{-1} & \mathbf{q} \\ \mathbf{q}^T & \Theta(\mathbf{q}) - z \end{bmatrix} \succeq 0. \tag{2.65}$$

The following algorithm for the primal-dual semidefinite programming (PD-SDP) solves a large deformation problem for nonconvex minimization problems

PD-SDP Algorithm:

1. Initial primal solution $\mathbf{p}^{(0)}$ and error allowance $\epsilon > 0$ are given. Let the iteration number $k = 1$.

2. Compute the dual solutions $\{\mathbf{q}^{(k)}\}$ by applying the SDP solver for problem

(2.65).

3. Compute the primal solution $\mathbf{p}^{(k)} = \mathbf{G}^{-1}(\mathbf{q}^{(k)})\boldsymbol{\tau}(\mathbf{q})$.

4. Convergence test; if $\|\mathbf{p}^{(k)} - \mathbf{p}^{(k-1)}\|/\|\mathbf{p}^{(k)}\| \leq \epsilon$, stop with the optimal solution $\mathbf{p}^* = \mathbf{p}^{(k)}$. Otherwise, let $k = k + 1$ and go to step 2.

The SDP solver used in this algorithm is a popular software package named SeDuMi.

2.3   Numerical solutions

The PD-SDP algorithm is implemented in two different types of structures as shown in Figures 2.1 and 2.5 to conduct large deformation finite-element methods. In the following examples, the elastic modulus and Poisson's ratio are considered as $E = 25000 \text{ N/mm}^2$ and $\mu = 0.15$, respectively. Two different load cases are applied, case-a and case-b, in which the load of the case-b is twice that of case-a, and body force is neglected.

2.3.1   Regular rectangular structure

We present, in this section, a regular rectangular structure which is fixed at $x = 0$ and free at the other sides, as shown in Figure 2.1. The length and width of this structure are 2.8m and 0.4m, respectively. The mesh domain is made up of 28 elements with 40 nodes, i.e. $d = 40$. Figure 2.4 shows the results after undergoing a horizontal uniformly distributed load on the right of the regular rectangular structure. The red circles in this Figure represent to the original nodes of the structure while the black dots represent to the place of these nodes after undergoing. We found that all the eigenvalues of matrix $\mathbf{G}$ are positive in this example. Thus, matrix $\mathbf{G}$ is a positive definite matrix, therefore, the solution to problem (2.55) is a unique solution (see Theorem 6).

2.3.2   Rectangular structure with two semicircle gaps

A rectangular structure with two semicircle gaps is fixed at $x = 0$ and free at the other sides, as shown in Figure 2.5. The length and width of this structure are 2.4m and 0.4m, respectively. The number of mesh elements is 48 and the number of nodes is $d = 69$. The result of the structure after undergoing a horizontal uniformly distributed
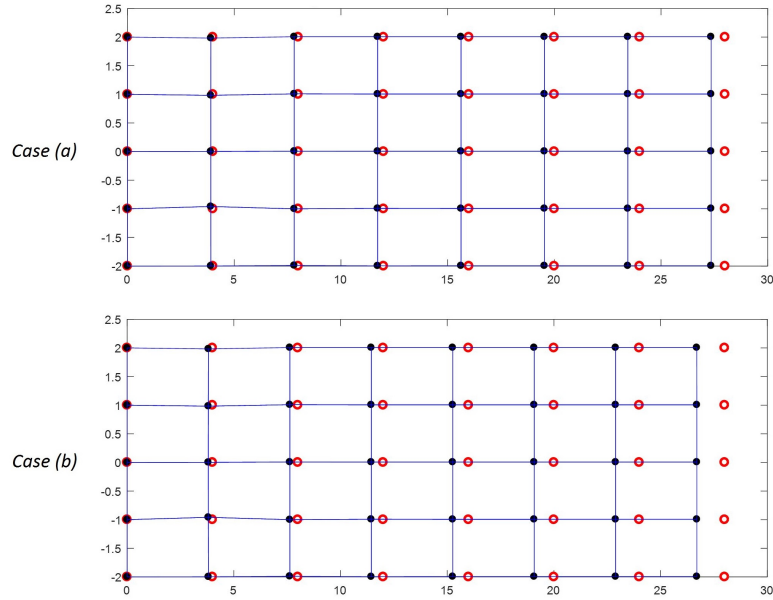
Figure 2.4: *Regular rectangular structure after undergoing a horizontal uniformly distributed load*

loading is shown in Figure 2.6. Once again, we found that all the eigenvalues of matrix **G** are positive, therefore the solution of this example is unique.
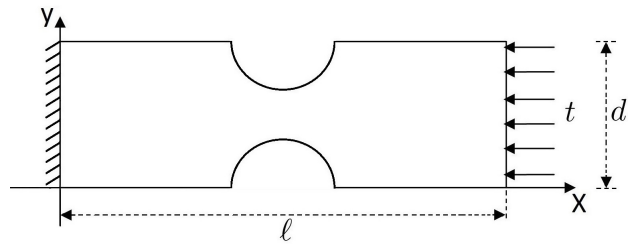
Figure 2.5: *Structure with two semicircle gaps*
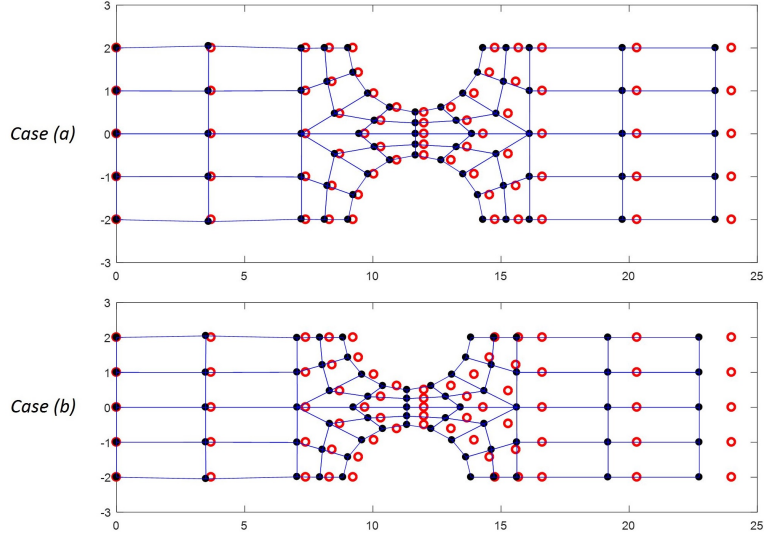
Figure 2.6: *Rectangular structure with two semicircle gaps after undergoing a horizontal uniformly distributed load*

2.4 Summary

This work presents a detailed study of a large deformation problem in 2-D structure. It is a fundamentally difficult to find a global minimization of nonconvex problems, and none of the classical numerical methods can be used to solve a large class of problem ($\mathcal{P}$). Canonical duality theory provides a potentially useful methodology for solving this challenging nonconvex minimization problem ($\mathcal{P}$). Beside the canonical duality theory, the mixed finite element method is applied with two separate fields, displacement and dual stress fields, in order to find the global minimizer of the total potential energy problem. Numerical applications are illustrated with different structural designs and different external loads. We found that the gap function G_{ap} of problem (2.55) is strictly positive, and therefore, Theorem 6 holds in our applications with a unique solution.

32

Chapter 3

Post-Buckling of a Large Deformed Elastic Beam

It is known that the total potential energy for the post-buckling of large deformed structures must be nonconvex to allow multiple local minimum solutions for all possible buckled status [15]. The canonical duality theory and its associated triality theory provide extremality criteria for both global and local optimal solutions and present a canonical dual finite element method for solving general nonconvex variational problems. Recently, it was discovered [8, 71] that by using Gao-Strang's complementary-dual principle and mixed finite element discretization, the nonconvex variational problem of a post-buckled nonlinear Gao beam can have at most three smooth solutions: a global minimizer representing a stable buckled state, a local maximizer for an unbuckled state, and a local minimizer for an unstable buckled state.

The main goal of this chapter is to develop a new canonical primal-dual algorithm for solving the post-buckling problem with special attention to the local unstable buckled configuration of a large deformed beam. The Gao-Strang total complementary energy associated with this model is a nonconvex functional and is reformulated as a global optimization problem to study the post-buckling responses of the beams. Based on the canonical duality theory and the associated triality theorem, a new primal-dual semi-definite program (PD-SDP) algorithm is proposed for solving this challenging problem to obtain all possible solutions. Applications are illustrated by different boundary value problems. Moreover, to verify the triality theory on the post-buckling problem of a large elastic deformation of beam, which is governed by a fourth order nonlinear differential equation, mixed meshes of different dual stress interpolations are used to obtain a closed dimensions between the discretized dis-

placement and discretized stress (see Section 3.5). Numerical results show that the proposed algorithm produces stable solutions for the global minimizer and local maximizer. However, the local minimizer is very sensitive to numerical discretization and external loads.

3.1 Nonconvex problem and canonical duality theory

Let us consider an elastic beam subjected to a vertical distributed lateral load $q(x)$ and compressive external axial force F at the right end as shown in Figure 3.1. Gao
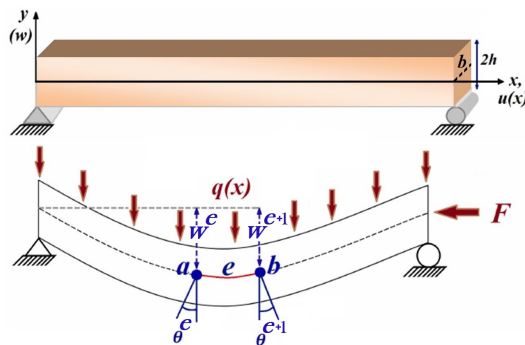
Figure 3.1: *Simply supported beam model - pre and post buckling analysis*

discovered in 1996 [15] that the well-known von Karman nonlinear plate model in one-dimension is equivalent to a linear differential equation and therefore, it cannot be used to study post-buckling phenomena. The main reason for this "paradox" is due to the fact that the stress in the lateral direction of a large deformed plate was ignored by von Karman. Therefore, the von Karman equation works only for thin-plates and cannot be used as a beam model. For a relatively thick beam such that $h/L \sim w(x) \in O(1)$, the deformation in the lateral direction cannot be ignored. Based on the finite deformation theory for Hooke's material and the Euler-Bernoulli hypothesis (i.e. straight lines normal to the mid-surface remain straight and normal to the mid-surface after deformation), a nonlinear beam model was proposed by Gao [15]:

$$EIw_{,xxxx} - \alpha Ew_{,x}^2 w_{,xx} + E\lambda w_{,xx} - f(x) = 0, \ \forall x \in [0, L] \tag{3.1}$$

where E is the elastic modulus of material, $I = 2h^3/3$ is the second moment of area of the beam's cross-section, w is the transverse displacement field of the beam, $\alpha = 3h(1 - \mu^2) > 0$ with μ as the Poisson's ratio, $\lambda = (1 + \mu)(1 - \mu^2)F/E > 0$ is

34

an integral constant, $f(x) = (1 - \mu^2)q(x)$ depends mainly on the distributed lateral load $q(x)$, $2h$ and L represent the height and length of the beam, respectively. The axial displacement $u(x)$ is governed by the following differential equation [15]:

$$u_{,x} = -\frac{1}{2}(1 + \mu)w_{,x}^2 - \frac{\lambda}{2h(1 + \mu)} , \qquad (3.2)$$

which shows that if $u(x) \sim w_{,x}(x) \in O(\epsilon)$, then $u_{,x}(x) \sim w_{,xx}(x) \in O(\epsilon^2)$.

The total potential energy of this beam model is $\Pi(w) : \mathcal{U}_a \to \mathbb{R}$ defined by

$$\Pi(w) = \int_0^L \left(\frac{1}{2}EIw_{,xx}^2 + \frac{1}{12}E\alpha w_{,x}^4 - \frac{1}{2}E\lambda w_{,x}^2 - f(x) \, w \right) dx, \qquad (3.3)$$

where $\mathcal{U}_a$ is the kinematically admissible space, in which certain necessary boundary conditions are given. Thus, for the given external loads $f(x)$ and end load λ, the primal variational problem is to find $\bar{w} \in \mathcal{U}_a$ such that

$$(\mathcal{P}): \quad \Pi(\bar{w}) = \inf \{\Pi(w)|w \in \mathcal{U}_a\}. \qquad (3.4)$$

It is easy to prove that the stationary condition $\delta\Pi(w) = 0$ leads to the governing equation (3.1).

If the nonlinear term in (3.1) is ignored and $f = 0$, then this nonlinear Gao beam is degeneralized to the well-known Euler-Bernoulli beam equation[1]:

$$EIw_{,xxxx} + \lambda Ew_{,xx} = 0. \qquad (3.5)$$

It is known that this linear beam will be buckled if the axial load λ reaches the Euler buckling load λ_{cr} defined by

$$\lambda_{cr} = \inf_{w \in \mathcal{U}_a} \frac{\int_0^L EIw_{,xx}^2 dx}{\int_0^L Ew_{,x}^2 dx}. \qquad (3.6)$$

Clearly, in the pre-buckling state, i.e. before the axial load λ reaches the Euler buckling load λ_{cr}, we have

$$\Pi_{EB}(w) = \int_0^L EIw_{,xx}^2 dx - \lambda \int_0^L Ew_{,x}^2 dx > 0 \quad \forall w \in \mathcal{U}_a, \ \lambda < \lambda_{cr}. \qquad (3.7)$$

---

[1]Strictly speaking, instead of λ, the axial load in the Euler-Bernoulli beam should be $F = \lambda E/[(1 + \mu)(1 - \mu^2)]$.

In this case, $\Pi_{EB}(w)$ and $\Pi(w)$ are strictly convex on $\mathcal{U}_a$, therefore, both the Euler-Bernoulli beam (3.5) and the nonlinear Gao beam (3.1) can have only one solution (see Lemma 2.1. and Theorem 2.1 in [57]).

Dually, in the post-buckling state, i.e. $\lambda > \lambda_{cr}$, the total potential energy for the Euler-Bernoulli beam is strictly concave and

$$\inf \left\{ \Pi_{EB}(w) \mid w \in \mathcal{U}_a, \ \lambda > \lambda_{cr} \right\} = -\infty,$$

which means that the Euler-Bernoulli beam is crushed. This shows that the Euler-Bernoulli beam cannot be used for studying post-buckling problems. However, for the nonlinear Gao beam, it was proved recently by Machalová and Netuka (see Remark 2.2, [57]) that there exists a constant $\lambda_{cr}^G \geq \lambda_{cr}$ such that the total potential energy $\Pi(w)$ is a nonconvex (double-well) functional if $\lambda > \lambda_{cr}^G$, which allows at most three critical points, i.e. the strong solutions to the nonlinear equation (3.1) at each material point $x \in [0, L]$: two minimizers corresponding to the two possible buckled states, one local maximizer corresponding to the possible unbuckled state [24]. Clearly, these solutions are sensitive to both the axial load λ and the distributed lateral force field $f(x)$. By equation (3.2) we know that the axial deformation could be relatively large, while the nonconvexity of the total potential shows that this nonlinear beam model can be used for studying both pre and post-buckling problems [8, 71]. Recently, the Gao beam model has been generalized for many real-world applications in engineering and sciences [1, 2, 3, 49, 52, 55, 56, 58].

Although the nonlinear Gao beam can be used for modeling natural phenomena, the nonconvexity of this beam model leads to some fundamental challenges in mathematics and computational science. Generally speaking, traditional numerical methods and nonlinear optimization techniques can be used only for solving convex minimization problems. Due to the lack of a global optimality criterion to identify a global minimizer at each iteration, most of nonconvex optimization problems cannot be solved deterministically, therefore, they are considered to be NP-hard in global optimization and computer science [28].

It was shown in [19] that by introducing a canonical strain measure

$$\epsilon = \Lambda(w) = \frac{1}{2} w_{,x}^2, \tag{3.8}$$

and a convex canonical function

$$V(\epsilon) = \frac{1}{3} E\alpha\epsilon^2 - E\lambda\epsilon,$$

the nonconvex (double-well) potential

$$W(w_{,x}) = \frac{1}{12}E\alpha w_{,x}^4 - \frac{1}{2}E\lambda w_{,x}^2$$

in Π can be written in the canonical form

$$W(w_{,x}) = V(\Lambda(w)).$$

Thus, the canonical dual stress can be uniquely defined by

$$\sigma = \partial V(\epsilon) = \frac{2E\alpha}{3}\epsilon - E\lambda. \qquad (3.9)$$

By the Legendre transformation we have the canonical complementary energy

$$\begin{aligned} V^*(\sigma) &= \epsilon\sigma - V(\epsilon) \\ &= \frac{3}{4E\alpha}(\sigma + E\lambda)^2. \end{aligned} \qquad (3.10)$$

Thus, replacing $W(w_{,x})$ with

$$V(\Lambda(w)) = \Lambda(w)\sigma - V^*(\sigma),$$

the Gao-Strang total complementary energy $\Xi : \mathcal{U}_a \times \mathcal{S}_a \to \mathbb{R}$ [13] in nonlinear elasticity can be defined as

$$\begin{aligned} \Xi(w,\sigma) &= \int_0^L \left(\frac{1}{2}EIw_{,xx}^2 + \frac{1}{2}\sigma w_{,x}^2 - \frac{3}{4E\alpha}(\sigma + E\lambda)^2 - f(x)w \right) dx \\ &= G(w,\sigma) - \int_0^L \left(V^*(\sigma) - f(x)w \right) dx, \end{aligned} \qquad (3.11)$$

where

$$\mathcal{S}_a = \{\sigma \in C[0,L] | \ \sigma(x) \geq -\lambda E \ \ \forall x \in [0,L]\},$$

and

$$G(w,\sigma) = \int_0^L \left(\frac{1}{2}EIw_{,xx}^2 + \frac{1}{2}\sigma w_{,x}^2 \right) dx \qquad (3.12)$$

is the generalized Gao-Strang complementary gap function [13].

Theorem 7 (Complementary-duality Principle [19])
For any given external loads $f(x)$ and end load λ, the pair $(\bar{w}, \bar{\sigma})$ is a critical point of $\Xi(w,\sigma)$ if and only if $\bar{w}$ is a critical point of $\Pi(w)$ and $\Pi(\bar{w}) = \Xi(\bar{w}, \bar{\sigma})$.

37

Proof. The criticality condition $\delta\Xi(\bar{w}, \bar{\sigma}) = 0$ leads to the following canonical equations:

$$EI\bar{w}_{,xxxx} - \bar{\sigma}\bar{w}_{,xx} = f(x), \tag{3.13}$$

$$\frac{1}{2}\bar{w}_{,x}^2 = \frac{3}{2E\alpha}(\bar{\sigma} + E\lambda), \tag{3.14}$$

which are equivalent to equation (3.1). The equality

$$\Pi(\bar{w}) = \Xi(\bar{w}, \bar{\sigma}),$$

follows directly from the Fenchel-Young equality

$$V(\Lambda(\bar{w})) + V^*(\bar{\sigma}) = \Lambda(\bar{w})\bar{\sigma},$$

due to the convexity of the canonical function $V(\epsilon)$. □

Theorem 8 (Triality Theory [19])
Let $(\bar{w}, \bar{\sigma})$ be a critical point of $\Xi(w, \sigma)$.
If $G(\bar{w}, \bar{\sigma}) \geq 0$, then $\bar{w}$ is a global minimizer of $\Pi(w)$ on $\mathcal{U}_a$ and

$$\Pi(\bar{w}) = \min_{w \in \mathcal{U}_a} \Pi(w) = \min_{w \in \mathcal{U}_a} \max_{\sigma \in \mathcal{S}_a} \Xi(w, \sigma). \tag{3.15}$$

If $G(\bar{w}, \bar{\sigma}) < 0$, then on a neighborhood $\mathcal{U}_o \times \mathcal{S}_o$ of $(\bar{w}, \bar{\sigma})$, we have either

$$\Pi(\bar{w}) = \min_{w \in \mathcal{U}_o} \Pi(w) = \min_{w \in \mathcal{U}_o} \max_{\sigma \in \mathcal{S}_o} \Xi(w, \sigma) = \Xi(\bar{w}, \bar{\sigma}), \tag{3.16}$$

or

$$\Pi(\bar{w}) = \max_{w \in \mathcal{U}_o} \Pi(w) = \max_{w \in \mathcal{U}_o} \max_{\sigma \in \mathcal{S}_o} \Xi(w, \sigma) = \Xi(\bar{w}, \bar{\sigma}). \tag{3.17}$$

Proof. For the positive gap function, $\Xi(w, \sigma)$ is a saddle functional and the total potential $\Pi(w)$ is convex on $\mathcal{U}_a$ [13]. In this case, statement (3.15) follows directly from Gao and Strang's theory for general large deformation problems [13], whereas for the negative gap function, $\Xi(w, \sigma)$ is a bi-concave functional. In this case, the total potential $\Pi(w)$ is nonconvex on $\mathcal{U}_a$, which could have both local minimum and local maximum solutions. Due to the fact that

$$\max_{\sigma \in \mathcal{S}_o} \Xi(w, \sigma) = \max_{w \in \mathcal{U}_o} \Pi(w),$$

statements (3.16) and (3.17) can be proved easily by the general triality theory [19].
□

The *triality theory* was first discovered in the post-buckling analysis of the large deformed beam theory [17]. Generalization to nonconvex/discrete optimization problems was given in 2000 [27]. Detailed information relating to this theory with its extensive applications in global optimization and nonconvex mechanics can be found in the monograph [19] and recent review articles [27, 32, 37].

3.2   Mixed finite element method

By using the finite element method, the domain of the beam is discretized into m elements $[0, L] = \bigcup_{e=1}^{m} \Omega^e$. In each element $\Omega^e = [x^e, x^{e+1}]$, the deflection, rotating angular and dual stress for node x^e are marked as w^e, θ^e and σ^e, respectively, and similar for node x^{e+1}. Then, we have the nodal displacement vector w_e of the e-th element

$$w_e^T = [w^e \ \ \theta^e \ \ w^{e+1} \ \ \theta^{e+1}], \tag{3.18}$$

and the nodal dual stress element σ_e

$$\sigma_e^T = [\sigma^e \ \ \sigma^{e+1}]. \tag{3.19}$$

In each element, we use mixed finite element interpolations for both $w(x)$ and $\sigma(x)$, i.e. $\forall x \in \Omega^e$,

$$w_e^h(x) = N_w^T(x) w_e, \tag{3.20}$$

and

$$\sigma_e^h(x) = N_\sigma^T(x) \sigma_e. \tag{3.21}$$

Thus, the spaces $\mathcal{U}_a$ and $\mathcal{S}_a$ can be numerically discretized to finite-dimensional spaces $\mathcal{U}_a^h$ and $\mathcal{S}_a^h$, respectively. The shape functions are based on the piecewise-cubic polynomial for $w(x)$,

$$N_w = \begin{bmatrix} \frac{1}{4}(1-\xi)^2(2+\xi) \\ \frac{L_e}{8}(1-\xi)^2(1+\xi) \\ \frac{1}{4}(1+\xi)^2(2-\xi) \\ \frac{L_e}{8}(1+\xi)^2(\xi-1) \end{bmatrix}, \tag{3.22}$$

and piecewise-linear for $\sigma(x)$,

$$N_\sigma = \frac{1}{2}\begin{bmatrix} (1-\xi) \\ (1+\xi) \end{bmatrix}, \tag{3.23}$$

where $\xi = 2x/L_e - 1$ with L_e being the length of the e-th beam element. Thus, on the discretized feasible deformation space $\mathcal{U}_a^h$, the Gao-Strang total complementary energy can be expressed in the following discretized form

$$
\begin{aligned}
\Xi^h(\mathbf{w}, \boldsymbol{\sigma}) &= \sum_{e=1}^{m} \left(\frac{1}{2} w_e^T\, G^e(\sigma_e)\, w_e - \frac{1}{2} \sigma_e^T\, K_e\, \sigma_e - \lambda_e^T\, \sigma_e - f_e^T\, w_e - c_e \right) \\
&= \frac{1}{2} \mathbf{w}^T\, \mathbf{G}(\boldsymbol{\sigma})\, \mathbf{w} - \frac{1}{2} \boldsymbol{\sigma}^T\, \mathbf{K}\, \boldsymbol{\sigma} - \boldsymbol{\lambda}^T\, \boldsymbol{\sigma} - \mathbf{f}^T\, \mathbf{w} - c,
\end{aligned}
\tag{3.24}
$$

where $\mathbf{w} \in \mathcal{U}_a^h \subset \mathbb{R}^{2(m+1)}$ and $\boldsymbol{\sigma} \in \mathcal{S}_a^h \subset \mathbb{R}^{m+1}$ are the nodal deflection and dual stress vectors, respectively. We let

$$
\mathcal{S}_a^h = \{ \boldsymbol{\sigma} \in \mathbb{R}^{m+1} |\ \ \det \mathbf{G}(\boldsymbol{\sigma}) \neq 0 \}.
\tag{3.25}
$$

The Hessian matrix of the gap function $\mathbf{G}(\boldsymbol{\sigma}) \in \mathbb{R}^{2(m+1)} \times \mathbb{R}^{2(m+1)}$ is obtained by assembling the following symmetric matrices $G^e(\sigma_e)$:

$$
\begin{aligned}
G^e(\sigma_e) &= \int_{\Omega_e} \left(EI\, N_w''\, (N_w'')^T + (N_\sigma)^T\, \sigma_e\, N_w'\, (N_w')^T \right) dx \\
&= \int_{-1}^{1} \frac{L_e}{2} \left(EI\, N_w''\, (N_w'')^T + (N_\sigma)^T\, \sigma_e\, N_w'\, (N_w')^T \right) d\xi \\
&= \frac{EIL_e}{2} \int_{-1}^{1} N_w''\, (N_w'')^T d\xi + \frac{L_e}{2} \int_{-1}^{1} (N_\sigma)^T\, \sigma_e\, N_w'\, (N_w')^T d\xi \\
&= G_1^e + G_2^e(\sigma_e),
\end{aligned}
\tag{3.26}
$$

where,

$$
\begin{aligned}
G_1^e &= \frac{EIL_e}{2} \int_{-1}^{1} N_w''\, (N_w'')^T d\xi \\
&= \begin{bmatrix}
\frac{12EI}{L_e^3} & \frac{6EI}{L_e^2} & -\frac{12EI}{L_e^3} & \frac{6EI}{L_e^2} \\
\frac{6EI}{L_e^2} & \frac{4EI}{L_e} & -\frac{6EI}{L_e^2} & \frac{2EI}{L_e} \\
-\frac{12EI}{L_e^3} & -\frac{6EI}{L_e^2} & \frac{12EI}{L_e^3} & -\frac{6EI}{L_e^2} \\
\frac{6EI}{L_e^2} & \frac{2EI}{L_e} & -\frac{6EI}{L_e^2} & \frac{4EI}{L_e}
\end{bmatrix},
\end{aligned}
\tag{3.27}
$$

40

and G_2^e is defined by the two stress ends σ^e and σ^{e+1} of the beam element

$$G_2^e(\sigma_e) = \left[g_{ij}^e \right]_{4\times4} = \frac{L_e}{2} \int_{-1}^{1} (N_\sigma)^T \sigma^e N_w' (N_w')^T d\xi \tag{3.28a}$$

$$= \begin{bmatrix} \frac{3(\sigma^e+\sigma^{e+1})}{5Le} & \frac{\sigma^{e+1}}{10} & -g_{11}^e & \frac{\sigma^e}{10} \\ g_{12}^e & L_e(\frac{\sigma^e}{10} + \frac{\sigma^{e+1}}{30}) & -g_{12}^e & -\frac{L_e(\sigma^e+\sigma^{e+1})}{60} \\ -g_{11}^e & -g_{12}^e & g_{11}^e & -g_{14}^e \\ g_{14}^e & g_{24}^e & -g_{14}^e & L_e(\frac{\sigma^e}{30} + \frac{\sigma^{e+1}}{10}) \end{bmatrix}. \tag{3.28b}$$

The matrix $\mathbf{K} \in \mathbb{R}^{m+1} \times \mathbb{R}^{m+1}$ is obtained by assembling the following positive-definite matrices K_e

$$K_e = \int_{\Omega_e} \left(\frac{3}{2E\alpha} N_\sigma N_\sigma^T \right) dx \tag{3.29a}$$

$$= \int_{-1}^{1} \left(\frac{3L_e}{4E\alpha} N_\sigma N_\sigma^T \right) d\xi \tag{3.29b}$$

$$= \frac{L_e}{E\alpha} \begin{bmatrix} \frac{1}{2} & \frac{1}{4} \\ \frac{1}{4} & \frac{1}{2} \end{bmatrix}. \tag{3.29c}$$

The vector $\boldsymbol{\lambda} = \{\lambda_e\} \in \mathbb{R}^{m+1}$ is defined by assembling the following λ_e

$$\lambda_e = \int_{\Omega_e} \left(\frac{3}{2\alpha} \lambda N_\sigma \right) dx \tag{3.30a}$$

$$= \int_{-1}^{1} \left(\frac{3L_e}{4\alpha} \lambda N_\sigma \right) d\xi \tag{3.30b}$$

$$= \frac{\lambda L_e}{a} \begin{bmatrix} \frac{3}{4} \\ \frac{3}{4} \end{bmatrix}. \tag{3.30c}$$

Also, $\mathbf{f} = \{f_e\} \in \mathbb{R}^{2(m+1)}$ is defined by assembling the following f_e

$$f_e = \int_{\Omega_e} f(x) N_w \, dx = \int_{-1}^{1} \frac{L_e}{2} f(\xi) N_w d\xi , \tag{3.31}$$

and $c = \sum_{e=1}^{m} c_e \in \mathbb{R}$ is defined as

$$
\begin{aligned}
c_e &= \int_{\Omega_e} \left(\frac{3E}{4\alpha} \lambda^2 \right) dx = \int_{-1}^{1} \left(\frac{3EL_e}{8\alpha} \lambda^2 \right) d\xi \\
&= \frac{3}{4\alpha} EL_e \lambda^2.
\end{aligned}
\tag{3.32}
$$

By the critical condition $\delta \Xi^h(\mathbf{w}, \boldsymbol{\sigma}) = 0$, canonical equations (3.13) and (3.14) have the following discretized forms

$$
\mathbf{G}(\boldsymbol{\sigma}) \, \mathbf{w} - \mathbf{f} = 0,
\tag{3.33}
$$

$$
\frac{1}{2} \mathbf{w}^T \, \mathbf{H} \, \mathbf{w} - \mathbf{K} \, \boldsymbol{\sigma} - \boldsymbol{\lambda} = 0,
\tag{3.34}
$$

where $\mathbf{H} = \mathbf{G}_{,\boldsymbol{\sigma}}(\boldsymbol{\sigma})$ stands for gradient of $\mathbf{G}(\boldsymbol{\sigma})$ with respect to the vector $\boldsymbol{\sigma}$ and

$$
\mathbf{w}^T \mathbf{H} \mathbf{w} =
\begin{bmatrix}
\mathbf{w}^T \mathbf{G}_{,\boldsymbol{\sigma}_1}(\boldsymbol{\sigma}) \mathbf{w} \\
\mathbf{w}^T \mathbf{G}_{,\boldsymbol{\sigma}_2}(\boldsymbol{\sigma}) \mathbf{w} \\
\cdot \\
\cdot \\
\cdot \\
\mathbf{w}^T \mathbf{G}_{,\boldsymbol{\sigma}_{m+1}}(\boldsymbol{\sigma}) \mathbf{w}
\end{bmatrix}
\in \mathbb{R}^{m+1},
$$

in which $\boldsymbol{\sigma}^T = [\boldsymbol{\sigma}_1, \boldsymbol{\sigma}_2, ..., \boldsymbol{\sigma}_{m+1}]$.

For any given $\mathbf{w} \in \mathcal{U}_a^h$, we know that $\Xi(\mathbf{w}, *) : \mathcal{S}_a^h \to \mathbb{R}$ is concave and the discretized total potential energy can be obtained by

$$
\begin{aligned}
\Pi_p^h(\mathbf{w}) &= \max\{\Xi(\mathbf{w}, \boldsymbol{\sigma}) | \ \boldsymbol{\sigma} \in \mathcal{S}_a^h\} \\
&= \{\Xi(\mathbf{w}, \boldsymbol{\sigma}) | \ \boldsymbol{\sigma} = \mathbf{K}^{-1}(\frac{1}{2} \mathbf{w}^T \, \mathbf{H} \, \mathbf{w} - \boldsymbol{\lambda})\}.
\end{aligned}
\tag{3.35}
$$

However, the convexity $\Xi(*, \boldsymbol{\sigma}) : \mathcal{U}_a^h \to \mathbb{R}$ will depend on $\boldsymbol{\sigma} \in \mathcal{S}_a^h$. The discretized pure complementary energy $\Pi_d^h : \mathcal{S}_a^h \to \mathbb{R}$ can be obtained by the following canonical dual transformation

$$
\begin{aligned}
\Pi_d^h(\boldsymbol{\sigma}) &= \operatorname{sta} \{\Xi(\mathbf{w}, \boldsymbol{\sigma}) | \ \mathbf{w} \in \mathcal{U}_a^h\} \\
&= \{\Xi(\mathbf{w}, \boldsymbol{\sigma}) | \ \mathbf{w} = \mathbf{G}^{-1}(\boldsymbol{\sigma})\mathbf{f}\} \\
&= -\frac{1}{2} \mathbf{f}^T \, \mathbf{G}^{-1}(\boldsymbol{\sigma}) \, \mathbf{f} - \frac{1}{2} \boldsymbol{\sigma}^T \, \mathbf{K} \, \boldsymbol{\sigma} - \boldsymbol{\lambda}^T \, \boldsymbol{\sigma} - c
\end{aligned}
\tag{3.36}
$$

where sta $\{g(\mathbf{w})|\mathbf{w} \in \mathcal{U}_a^h\}$ stands for finding the stationary value of $g(\mathbf{w})$ on $\mathcal{U}_a^h$. Clearly, its convexity depends on $\mathbf{G}(\boldsymbol{\sigma})$. Let

$$\mathcal{S}_a^+ = \{\boldsymbol{\sigma} \in \mathcal{S}_a^h \mid \mathbf{G}(\boldsymbol{\sigma}) \succ 0\}, \tag{3.37}$$

$$\mathcal{S}_a^- = \{\boldsymbol{\sigma} \in \mathcal{S}_a^h \mid \mathbf{G}(\boldsymbol{\sigma}) \prec 0\}. \tag{3.38}$$

Theorem 9 ([19])

Suppose $(\bar{\mathbf{w}}, \bar{\boldsymbol{\sigma}})$ is a stationary point of $\Xi^h(\mathbf{w}, \boldsymbol{\sigma})$, then $\Pi_p^h(\bar{\mathbf{w}}) = \Xi^h(\bar{\mathbf{w}}, \bar{\boldsymbol{\sigma}}) = \Pi_d^h(\bar{\boldsymbol{\sigma}})$. Moreover, if $\bar{\boldsymbol{\sigma}} \in \mathcal{S}_a^+$, then we have
   Canonical Min-Max Duality:

$$\Pi_p^h(\bar{\mathbf{w}}) = \min_{\mathbf{w} \in \mathcal{U}_a^h} \Pi_p^h(\mathbf{w}) \quad \Leftrightarrow \quad \max_{\boldsymbol{\sigma} \in \mathcal{S}_a^+} \Pi_d^h(\boldsymbol{\sigma}) = \Pi_d^h(\bar{\boldsymbol{\sigma}}). \tag{3.39}$$

If $\bar{\boldsymbol{\sigma}} \in \mathcal{S}_a^-$, then on a neighborhood $\mathcal{U}_o \times \mathcal{S}_o \subset \mathcal{U}_a^h \times \mathcal{S}_a^-$ of $(\bar{\mathbf{w}}, \bar{\boldsymbol{\sigma}})$ we have
   Canonical Double-max Duality:

$$\Pi_p^h(\bar{\mathbf{w}}) = \max_{\mathbf{w} \in \mathcal{U}_o} \Pi_p^h(\mathbf{w}) \quad \Leftrightarrow \quad \max_{\boldsymbol{\sigma} \in \mathcal{S}_o} \Pi_d^h(\boldsymbol{\sigma}) = \Pi_d^h(\bar{\boldsymbol{\sigma}}). \tag{3.40}$$

Canonical Double-min Duality (if $\dim \mathcal{U}_a^h = \dim \mathcal{S}_a^h$):

$$\Pi_p^h(\bar{\mathbf{w}}) = \min_{\mathbf{w} \in \mathcal{U}_o} \Pi_p^h(\mathbf{w}) \quad \Leftrightarrow \quad \min_{\boldsymbol{\sigma} \in \mathcal{S}_o} \Pi_d^h(\boldsymbol{\sigma}) = \Pi_d^h(\bar{\boldsymbol{\sigma}}). \tag{3.41}$$

The canonical min-max duality can be used to find the global minimizer of the nonconvex problem by using the canonical dual problem

$$(\mathcal{P}^d): \quad \max\{\Pi_d^h(\boldsymbol{\sigma}) \mid \boldsymbol{\sigma} \in \mathcal{S}_a^+\}, \tag{3.42}$$

which is a concave maximization problem and can be solved easily by well-developed convex analysis and optimization techniques. The canonical double-max and double-min duality statements can be used to find the biggest local maximizer and a local minimizer of the nonconvex primal problem, respectively. It was proved in [7, 31, 60] that both canonical min-max and double-max duality statements hold strongly regardless of the dimensions of $\mathcal{U}_a^h$ and $\mathcal{S}_a^h$, while the canonical double-min duality statement (3.41) holds weakly if $\dim \mathcal{U}_a^h \neq \dim \mathcal{S}_a^h$, but strongly if $\dim \mathcal{U}_a^h = \dim \mathcal{S}_a^h$. All these cases are within our reach in Sections 3.4 and 3.5.

3.3 Semi-definite programming algorithm

It is easy to understand that the nonconvex post-buckling problem could have multiple global minimizers for certain external loads, say $q(x) = 0$. In this case, we have $\det \mathbf{G}(\boldsymbol{\sigma}) = 0$ and $\mathcal{S}_a^h = \emptyset$. In order to deal with this case, this section presents a SDP (Semi-Definite Programming, see [43] and [72]) reformulation to solve the canonical dual problem (3.42). The SDP algorithm is applied to obtain all post-buckled solutions of a large deformed elastic beam.

By the fact that $\Xi(\mathbf{w}, \boldsymbol{\sigma})$ is a saddle function on $\mathcal{U}_a^h \times \mathcal{S}_a^+$, we have

$$\min_{\mathbf{w} \in \mathcal{U}_a^h} \Pi_p^h(\mathbf{w}) = \min_{\mathbf{w} \in \mathcal{U}_a^h} \max_{\boldsymbol{\sigma} \in \mathcal{S}_a^+} \Xi(\mathbf{w}, \boldsymbol{\sigma}) = \max_{\boldsymbol{\sigma} \in \mathcal{S}_a^+} \min_{\mathbf{w} \in \mathcal{U}_a^h} \Xi(\mathbf{w}, \boldsymbol{\sigma}). \tag{3.43}$$

For any given $\boldsymbol{\sigma} \in \mathcal{S}_a^+$, the solution to $\min_{\mathbf{w} \in \mathcal{U}_a^h} \Xi(\mathbf{w}, \boldsymbol{\sigma})$ leads to

$$\mathbf{w} = \mathbf{w}(\boldsymbol{\sigma}) = \mathbf{G}^{-1}(\boldsymbol{\sigma})\mathbf{f} \tag{3.44}$$

Thus, the stress fields $\boldsymbol{\sigma}$ can be found by the following problem

$$\begin{aligned}
\max_{\boldsymbol{\sigma}} \Xi(\mathbf{w}(\boldsymbol{\sigma}), \boldsymbol{\sigma}) &= \frac{1}{2}\mathbf{w}(\boldsymbol{\sigma})^T \mathbf{G}(\boldsymbol{\sigma})\mathbf{w}(\boldsymbol{\sigma}) - \frac{1}{2}\boldsymbol{\sigma}^T \mathbf{K} \, \boldsymbol{\sigma} - \boldsymbol{\lambda}^T \boldsymbol{\sigma} - \mathbf{f}^T \mathbf{w}(\boldsymbol{\sigma}) - c \\
&\equiv \max_{\boldsymbol{\sigma}} \Pi_d^h(\boldsymbol{\sigma}) \\
\text{s.t. } \mathbf{G}(\boldsymbol{\sigma}) &\succeq 0.
\end{aligned} \tag{3.45}$$

By canonical min-max duality we know that if $\boldsymbol{\sigma}^* \in \mathcal{S}_a^+$ is a global maximizer of problem (3.45), then $\mathbf{w}^* = \mathbf{w}(\boldsymbol{\sigma}^*)$ should be a global minimizer of $\Pi_p^h(\mathbf{w})$. Furthermore, the problem (3.45) is the same as:

$$\max_{\boldsymbol{\sigma}, t} t \quad \text{s.t.} \quad \mathbf{G}(\boldsymbol{\sigma}) \succeq 0, \quad t \le \phi(\boldsymbol{\sigma}) - \frac{1}{2}\boldsymbol{\sigma}^T \mathbf{K} \, \boldsymbol{\sigma} \tag{3.46}$$

where

$$\phi(\boldsymbol{\sigma}) = \frac{1}{2}\mathbf{w}(\boldsymbol{\sigma})^T \mathbf{G}(\boldsymbol{\sigma})\mathbf{w}(\boldsymbol{\sigma}) - \boldsymbol{\lambda}^T \boldsymbol{\sigma} - \mathbf{f}^T \mathbf{w}(\boldsymbol{\sigma}) - c.$$

By the fact that $\mathbf{K} \succ 0$, the Schur complement lemma (see [72]) for the second inequality constraint in (3.46) implies

$$\begin{bmatrix} 2\mathbf{K}^{-1} & \boldsymbol{\sigma} \\ \boldsymbol{\sigma}^T & \phi(\boldsymbol{\sigma}) - t \end{bmatrix} \succeq 0. \tag{3.47}$$

Thus, the problem (3.46) can be relaxed to the following SDP problem

$$\max_{\boldsymbol{\sigma},t} \ t \quad \text{s.t.} \quad \mathbf{G}(\boldsymbol{\sigma}) \succeq 0, \quad \begin{bmatrix} 2\mathbf{K}^{-1} & \boldsymbol{\sigma} \\ \boldsymbol{\sigma}^T & \phi(\boldsymbol{\sigma}) - t \end{bmatrix} \succeq 0. \tag{3.48}$$

By the same way, the SDP relaxation for the canonical double-max duality statement

$$\max_{\mathbf{w} \in \mathcal{U}_a^h} \Pi_p^h(\mathbf{w}) = \max_{\mathbf{w},\boldsymbol{\sigma}} \Xi(\mathbf{w}, \boldsymbol{\sigma}) = \max \Pi_d^h(\boldsymbol{\sigma}) \quad \text{s.t.} \quad \boldsymbol{\sigma} \in \mathcal{S}_a^- \tag{3.49}$$

should be equivalent to

$$\max_{\boldsymbol{\sigma},t} \ t \quad \text{s.t.} \quad -\mathbf{G}(\boldsymbol{\sigma}) \succ 0, \quad \begin{bmatrix} 2\mathbf{K}^{-1} & \boldsymbol{\sigma} \\ \boldsymbol{\sigma}^T & \phi(\boldsymbol{\sigma}) - t \end{bmatrix} \succeq 0, \tag{3.50}$$

which leads to a local maximum solution to the post-buckling problem.

Now, let $(\mathbf{w}^*, \boldsymbol{\sigma}^*)$ be a local minimizer of the canonical double-min problem

$$\min_{\mathbf{w}} \Pi_p^h(\mathbf{w}) = \min_{\mathbf{w}} \max_{\boldsymbol{\sigma}} \Xi(\mathbf{w}, \boldsymbol{\sigma}) = \min_{\boldsymbol{\sigma}} \Pi_d^h(\boldsymbol{\sigma}), \ \text{s.t.} \ \boldsymbol{\sigma} \in \mathcal{S}_a^-.$$

By equation (3.44), the local minimizer is equivalent to the following problem

$$\min_{\boldsymbol{\sigma}} \left\{ \Xi(\mathbf{w}(\boldsymbol{\sigma}), \boldsymbol{\sigma}) \equiv \Pi_d^h(\boldsymbol{\sigma}) \right\} \quad \text{s.t.} \quad \mathbf{G}(\boldsymbol{\sigma}) \prec 0. \tag{3.51}$$

This problem is the same as:

$$\begin{aligned} \min_{\boldsymbol{\sigma},t} \quad & t \\ \text{s.t.} \quad & \mathbf{G}(\boldsymbol{\sigma}) \prec 0, \\ & t \geq -\frac{1}{2}\mathbf{f}^T \mathbf{G}^{-1}(\boldsymbol{\sigma}) \mathbf{f} - \frac{1}{2}\boldsymbol{\sigma}^T \mathbf{K} \boldsymbol{\sigma} - \boldsymbol{\lambda}^T \boldsymbol{\sigma} - c. \end{aligned} \tag{3.52}$$

In order to apply the Schur complement lemma to the second inequality in (3.52), we need to linearize the complementary energy

$$V^*(\boldsymbol{\sigma}) = \frac{1}{2}\boldsymbol{\sigma}^T \mathbf{K} \boldsymbol{\sigma}.$$

By using equation (3.29a), the complementary energy $V^*(\boldsymbol{\sigma})$ can be expressed by

using finite element mesh in the following discretized form

$$\frac{1}{2}\sigma_e^T K_e \sigma_e = \frac{1}{2}\sigma_e^T \left[\int_{\Omega_e} \frac{3}{2E\alpha} N_\sigma N_\sigma^T dx \right] \sigma_e$$

$$= \frac{3}{4E\alpha} \int_{\Omega_e} \sigma_e^T N_\sigma (N_\sigma^T \sigma_e) dx, \qquad (3.53)$$

then from (3.21), we get

$$\frac{1}{2}\sigma_e^T K_e \sigma_e = \frac{3}{4E\alpha} \int_{\Omega_e} \sigma_e^T N_\sigma \sigma_e^h dx. \qquad (3.54)$$

By substituting (3.8) into (3.9) and then substituting (3.9) into (3.54), we have

$$\frac{1}{2}\sigma_e^T K_e \sigma_e = \frac{3}{4E\alpha} \int_{\Omega_e} (N_\sigma^T \sigma_e)^T \left[\frac{E\alpha}{3} w_e^T N_w' (N_w')^T w_e - E\lambda \right] dx$$

$$= \frac{1}{2}w_e^T \left[\int_{\Omega_e} \frac{1}{2} N_\sigma^T \sigma_e N_w' (N_w')^T dx \right] w_e - \frac{1}{2} \left[\int_{\Omega_e} \frac{3\lambda}{2\alpha} N_\sigma^T dx \right] \sigma_e. (3.55)$$

Finally from (3.30a), the discretized form of the complementary energy $V^*(\sigma)$ can be rewritten as

$$\frac{1}{2}\sigma_e^T K_e \sigma_e = \frac{1}{2}w_e^T M^e(\sigma_e) w_e - \frac{1}{2}\lambda_e^T \sigma_e. \qquad (3.56)$$

In which, the matrix $M^e(\sigma_e)$ is defined as

$$M^e(\sigma_e) = \int_{\Omega_e} \frac{1}{2} \left((N_\sigma)^T \sigma_e N_w' (N_w')^T \right) dx$$

$$= \int_{-1}^{1} \frac{L_e}{4} \left((N_\sigma)^T \sigma_e N_w' (N_w')^T \right) d\xi$$

$$= \begin{bmatrix} \frac{3}{10L_e}(\sigma^e + \sigma^{e+1}) & \frac{1}{20}\sigma^{e+1} & -M_{1,1}^e & \frac{1}{20}\sigma^e \\ M_{12}^e & \frac{L_e}{60}(3\sigma^e + \sigma^{e+1}) & -M_{12}^e & \frac{-L_e}{120}(\sigma^e + \sigma^{e+1}) \\ M_{13}^e & M_{23}^e & M_{11}^e & -M_{14}^e \\ M_{14}^e & M_{24}^e & M_{34}^e & \frac{L_e}{60}(\sigma^e + 3\sigma^{e+1}) \end{bmatrix}$$

$$= \frac{1}{2}G_2^e(\sigma_e). \qquad (3.57)$$

Thus, by using linearization of the complementary energy, a reformulated pure com-

plementary energy can be given as

$$\widehat{\Pi}^d(\boldsymbol{\sigma}, \mathbf{w}) = -\frac{1}{2}\mathbf{f}^T \, \mathbf{G}^{-1}(\boldsymbol{\sigma}) \, \mathbf{f} - \frac{1}{2}\mathbf{w}^T \, \mathbf{M}(\boldsymbol{\sigma}) \, \mathbf{w} - \frac{1}{2}\boldsymbol{\lambda}^T \, \boldsymbol{\sigma} - c, \qquad (3.58)$$

in which the stiffness matrix $\mathbf{M}(\boldsymbol{\sigma})$ in the strain energy

$$V(\mathbf{w}) = \frac{1}{2}\mathbf{w}^T \, \mathbf{M}(\boldsymbol{\sigma}) \, \mathbf{w} = V^*(\boldsymbol{\sigma}),$$

can be obtained by assembling the symmetric matrices $M^e(\sigma_e)$. Then, by using $\widehat{\Pi}^d(\boldsymbol{\sigma}, \mathbf{w})$, problem (3.52) can be relaxed to

$$\min_{\boldsymbol{\sigma}, t} \ t \quad \text{s.t.} \quad \mathbf{G}(\boldsymbol{\sigma}) \prec 0, \quad \frac{1}{2}\mathbf{f}^T \, \mathbf{G}^{-1}(\boldsymbol{\sigma}) \, \mathbf{f} + \hat{\phi}(\boldsymbol{\sigma}, \mathbf{w}) + t \geq 0, \qquad (3.59)$$

where

$$\hat{\phi}(\boldsymbol{\sigma}, \mathbf{w}) = \frac{1}{2}\mathbf{w}^T \, \mathbf{M}(\boldsymbol{\sigma}) \, \mathbf{w} + \frac{1}{2}\boldsymbol{\lambda}^T \, \boldsymbol{\sigma} + c.$$

The primal variable $\mathbf{w}$ in this problem can be computed by the dual solution $\boldsymbol{\sigma}$ in the primal-dual iteration. Thus, by using the Schur complement lemma this problem can be relaxed to the following SDP problem

$$\min_{\boldsymbol{\sigma}, t} \ t \quad \text{s.t.} \quad - \mathbf{G}(\boldsymbol{\sigma}) \succ 0, \quad \begin{bmatrix} -2\mathbf{G}(\boldsymbol{\sigma}) & \mathbf{f} \\ \mathbf{f}^T & \hat{\phi}(\boldsymbol{\sigma}, \mathbf{w}) + t \end{bmatrix} \succeq 0, \qquad (3.60)$$

Clearly, if the stress $\boldsymbol{\sigma}^*$ is a local minimizer on $\mathcal{S}_a^-$ of problem (3.60), the canonical double-min duality shows that $\mathbf{w}^* = \mathbf{w}(\boldsymbol{\sigma}^*)$ should be a local minimizer of $\Pi_p^h(\mathbf{w})$.

Consequently, the primal-dual semi-definite programming (PD-SDP) algorithm for solving all possible post-buckling problems can be proposed as the following.

PD-SDP Algorithm:

1. Given initial primal solution $\mathbf{w}^{(0)}$ and error allowance $\epsilon > 0$, let $k = 1$;

2. Compute the dual solutions $\{\boldsymbol{\sigma}^{(k)}\}$ by applying the SDP solver for problems (3.48), (3.50) and (3.60), respectively.

3. Compute the primal solution $\mathbf{w}^{(k)} = [\mathbf{G}(\boldsymbol{\sigma}^{(k)})]^{-1}\mathbf{f}$.

4. For check convergence; if $\|\mathbf{w}^{(k)} - \mathbf{w}^{(k-1)}\|/\|\mathbf{w}^{(k)}\| \leq \epsilon$, stop with the optimal solution $\mathbf{w}^* = \mathbf{w}^{(k)}$. Otherwise, let $k = k + 1$ and go to step 2.

The SDP solver used in this algorithm is a popular software package named SeDuMi, which is based on the interior point method [73].

3.4 Large deformation with piecewise-linear dual stress interpolation

3.4.1 Numerical examples

We present in this section two different types of beams by using piecewise-linear dual stress (PLS) interpolation, shown in (3.23). Geometrical data were kept fixed for all computations; elastic modulus $E = 1000Pa$, Poisson's ratio $\mu = 0.3$ and beam length $L = 1$m. The lateral load $q(x)$ is assumed to be either a uniformly distributed load such that $f(x) = (1 - \mu^2)q(x) = 0.1N/$m or a concentrated force on the center of the beam in which $f(x) = 0.1N$. A different number of elements with the same beam length, different compressive load λ with different values of beam height are applied in this section.

(a) Simply supported beam

(b) Clamped beam
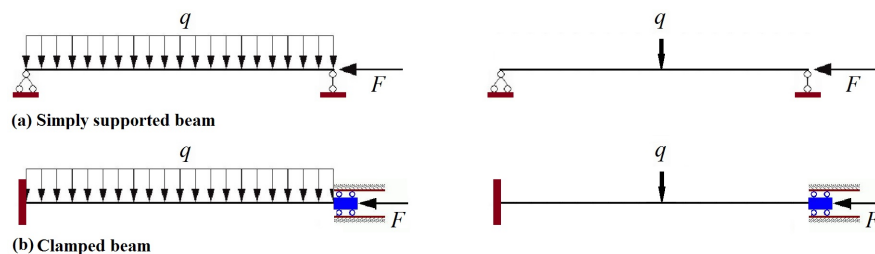
Figure 3.2: *Types of beams - uniformly distributed load (left), concentrated force (right)*

3.4.1.1 Simply supported beam

A simply supported beam model is fixed in both directions at $x = 0$ and fixed only in the y-direction at $x = L$, as shown in Figure 3.2-a, with the boundary conditions

$$w(0) = w''(0) = w(L) = w''(L) = 0.$$

If the beam height is 0.1 (i.e. $h = 0.05$m), the critical load is $\lambda_{cr} = 0.00097$m^2 (see equation (3.6)). For a different number of beam elements, the approximate deflections of this beam with $\lambda = 0.01$m$^2 > \lambda_{cr}$ under a uniformly distributed load are illustrated in Figure 3.3. In the graphs, red represents the global minimum, green represents the
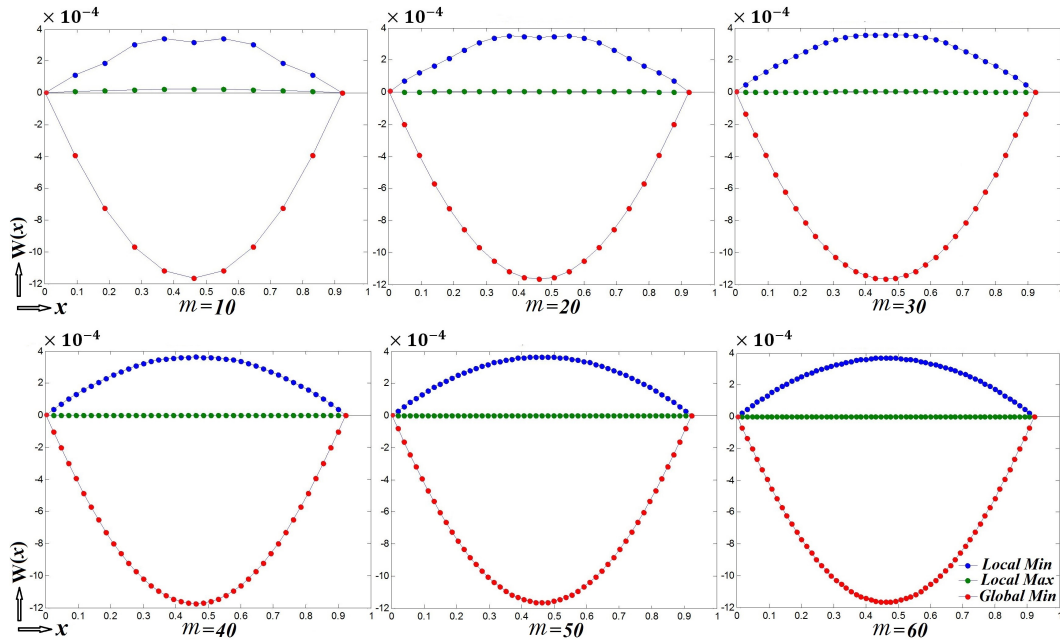
Figure 3.3: *Simply supported beam under a uniformly distributed load with $\lambda = 0.01\text{m}^2$ ($h = 0.05\text{m}$)*

local maximum and blue represents the local minimum of $\Pi(w)$. Figure 3.3 shows that the two post-buckled configurations, global minimum and local maximum, look alike with all of the different number of beam elements. In contrast to the local minimum, few differences appear in the local unstable buckled configuration. The curve charts with 40, 50 and 60 elements seem very similar and more stable than the curve charts that contain 10, 20 and 30 elements. Once again, Figure 3.4 shows that, with a different number of elements at $\lambda = 0.015\text{m}^2 > \lambda_{cr}$, slight differences appear on the local minimum curves.
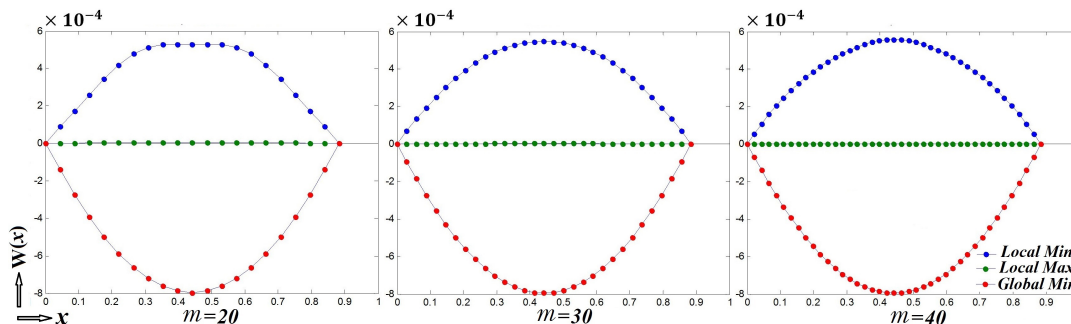
Figure 3.4: *Simply supported beam under a uniformly distributed load with $\lambda = 0.015\text{m}^2$ ($h = 0.05\text{m}$)*

The local minimum solutions with a different number of beam elements at a compressive load $\lambda = 0.005\text{m}^2 > \lambda_{cr}$ look alike, as shown in Figure 3.5. The Gao-Strang gap function for all post-buckled solutions was computed under a uniformly distributed load for a different number of elements with $\lambda = 0.01\text{m}^2$ as reported in Table 3.1.
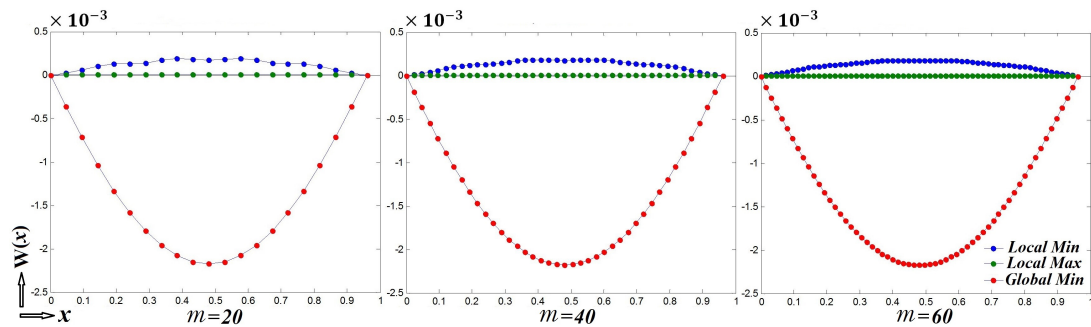
Figure 3.5: *Simply supported beam under a uniformly distributed load with $\lambda = 0.005\text{m}^2$ ($h = 0.05\text{m}$)*

We focus on 40 elements with the same beam length for all the following examples in this section. The deflections of the simply supported beam under a concentrated force with different compressive loads $\lambda > \lambda_{cr}$ are illustrated in Figure 3.6. At $h = 0.1\text{m}$, the critical load of the simply supported beam is $\lambda_{cr} = 0.0078\text{m}^2$. The deflections of this beam under a uniformly distributed load and a concentrated force are summarized in Figures 3.7 and 3.8, respectively. The Gao-Strang gap function for all three post-buckled solutions was computed under a uniformly distributed load and a concentrated force as reported in Tables 3.2 and 3.3, respectively.

Figure 3.6: *Simply supported beam under a concentrated force ($h = 0.05\text{m}$)*
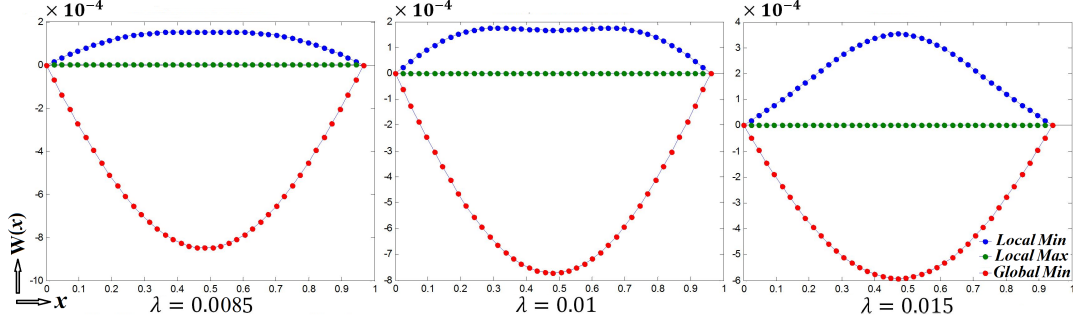
Figure 3.7: *Simply supported beam under a uniformly distributed load ($h = 0.1$m)*
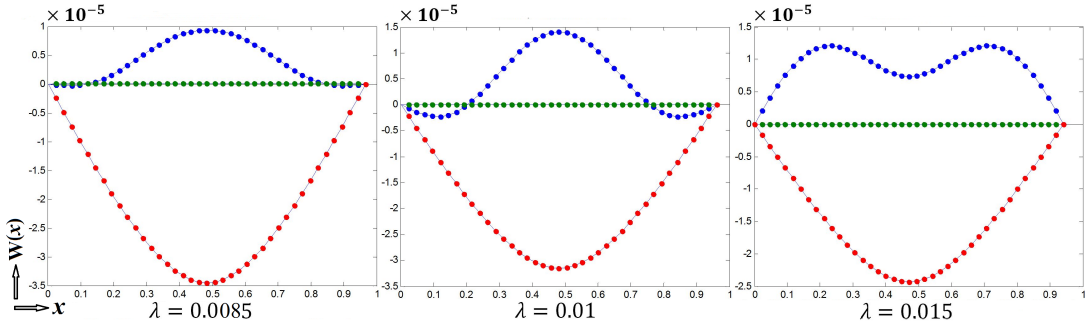
Figure 3.8: *Simply supported beam with a concentrated force ($h = 0.1$m)*

Table 3.1: *Gao-Strang gap function for simply supported beam with different numbers of elements*

Compressive load	No elements m	Gap function under a uniformly distributed load		
		Global Min	Local Min	Local Max
	20	7.63568e-09	-2.15332e-09	-4.16926e-07
$\lambda = 0.01$	40	1.45323e-09	-8.56515e-10	-1.04182e-07
	60	6.10785e-10	-4.93895e-10	-4.62995e-08

3.4.1.2   Doubly/Clamped beam

A clamped beam or doubly/clamped beam model is clamped at both ends as shown in Figure 3.2-b. The boundary conditions are defined as

$$w(0) = w'(0) = w(L) = w'(L) = 0.$$

The Euler buckling load of this beam with $h = 0.05$m is $\lambda_{cr} = 0.0041$m^2. A different number of beam elements are applied with the same conditions and $\lambda = 0.009$m^2.

Table 3.2: *Gao-Strang gap function for simply supported beam under a uniformly distributed load*

Beam height	Compressive loads "λ"	Gap function under a uniformly distributed load		
		Global Min	Local Min	Local Max
$h = 0.05$	0.005	1.38767e-09	-3.90449e-10	-1.04182e-07
	0.01	1.45323e-09	-8.56515e-10	-1.04182e-07
	0.015	1.51964e-09	-1.01164e-09	-1.04182e-07
$h = 0.1$	0.0085	1.66885e-10	-1.48050e-10	-1.30228e-08
	0.01	1.67195e-10	-1.50613e-10	-1.30228e-08
	0.015	1.68227e-10	-1.55455e-10	-1.30228e-08

Table 3.3: *Gao-Strang gap function for simply supported beam under a concentrated load*

Beam height	Compressive loads "λ"	Gap function under a concentrated load		
		Global Min	Local Min	Local Max
$h = 0.05$	0.005	2.72407e-12	-9.56982e-13	-1.89005e-10
	0.01	2.84230e-12	-1.78093e-12	-1.89005e-10
	0.015	2.96381e-12	-2.05556e-12	-1.89005e-10
$h = 0.1$	0.0085	3.28941e-13	-2.95470e-13	-2.36257-11
	0.01	3.29501e-13	-3.00014e-13	-2.36257e-11
	0.015	3.31372e-13	-3.08597e-13	-2.36257e-11

We found that the results looked alike for all three post-buckled solutions as shown in Figure 3.9. The results of the deflections under a uniformly distributed load and a concentrated force for different axial loads $\lambda > \lambda_{cr}$ with $m = 40$ are illustrated in Figures 3.10 and 3.11, respectively.
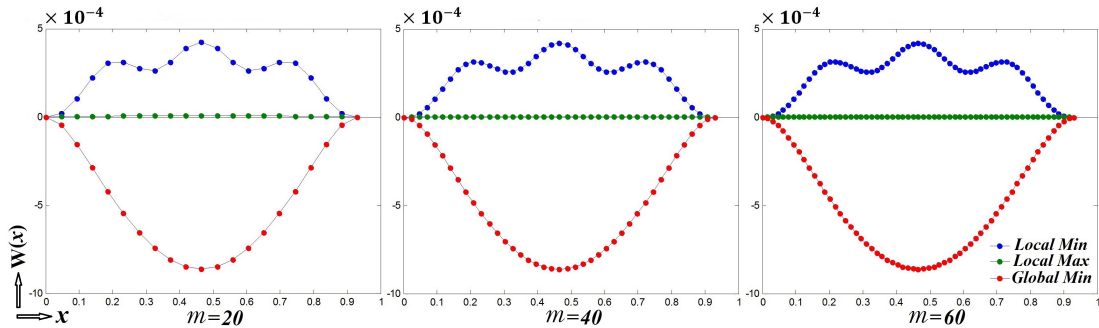
Figure 3.9: *Clamped beam under a uniformly distributed load with $\lambda = 0.009 \text{m}^2$ ($h = 0.05\text{m}$)*
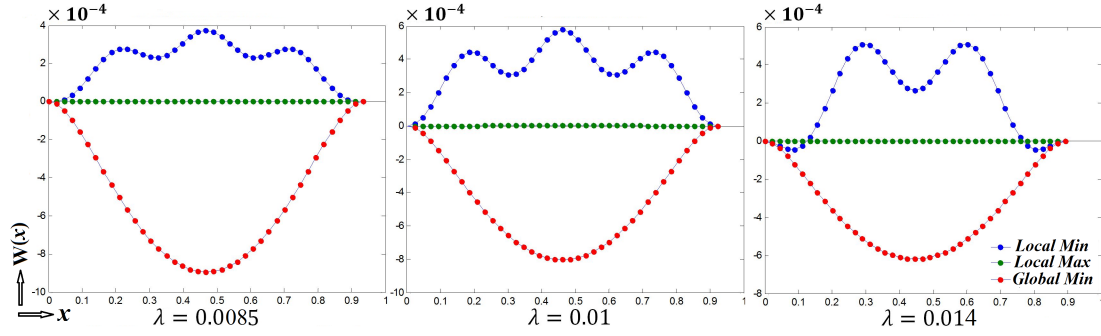
Figure 3.10: *Clamped beam under a uniformly distributed load (h = 0.05m)*
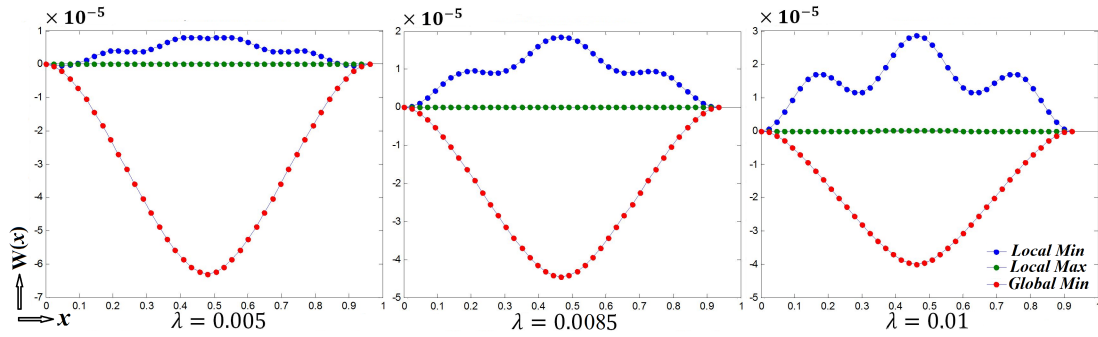
Figure 3.11: *Clamped beam under a concentrated force (h = 0.05m)*

The Gao-Strang gap function for all three post-buckled solutions with different axial loads and beam heights, was computed under a uniformly distributed load and a concentrated force as reported in Tables 3.4 and 3.5, respectively.
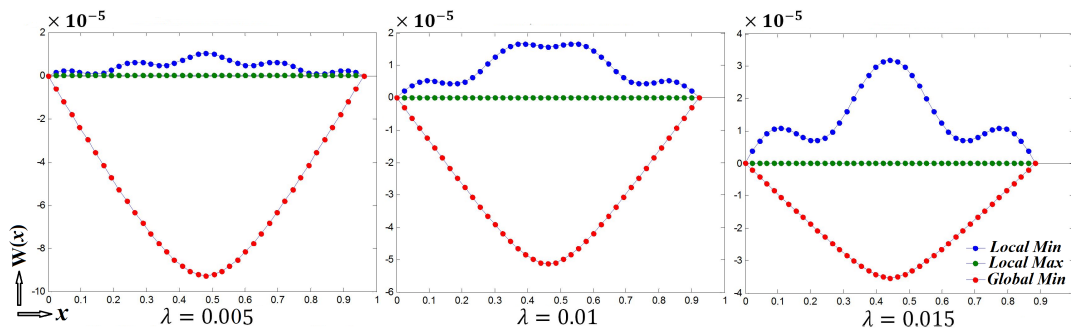
Table 3.4: *Gao-Strang gap function for doubly/clamped beam under a uniformly distributed load*

Beam height	Compressive loads "λ"	Gap function under a uniformly distributed load		
		Global Min	Local Min	Local Max
$h = 0.05$	0.0085	2.09541e-08	-2.01747e-08	-1.04101e-07
	0.009	2.09619e-08	-2.02106e-08	-1.04101e-07
	0.01	2.09768e-08	-2.02717e-08	-1.04101e-07
	0.014	2.10396e-08	-2.04287e-08	-1.04101e-07

Table 3.5: *Gao-Strang gap function for doubly/clamped beam under a concentrated load*

Beam height	Compressive loads "λ"	Gap function under a concentrated load		
		Global Min	Local Min	Local Max
$h = 0.05$	0.005	1.08569e-11	-9.01280e-12	-1.88954e-10
	0.0085	1.09445e-11	-9.72096e-12	-1.88954e-10
	0.01	1.09801e-11	-9.87268e-12	-1.88954e-10

3.5 Large deformation with different dual stress interpolations

According to the triality theory (see Theorem 8) and Theorem 9, canonical double-min duality statement (3.41) holds strongly if $\dim \mathcal{U}_a^h = \dim \mathcal{S}_a^h$. This condition is not verified when we apply PLS mesh, i.e. piecewise-linear stress mesh, on the dual stress field because $\dim \mathcal{U}_a^h = 2(m+1) \neq m+1 = \dim \mathcal{S}_a^h$ (see (3.18) and (3.19)). So, piecewise-quadratic stress (PQS) mesh is more convenient than PLS to verify this theory to obtain the closed dimensions for discretized displacement $\mathbf{w} \in \mathbb{R}^{2(m+1)}$ and discretized stress $\boldsymbol{\sigma} \in \mathbb{R}^{2m+1}$ (where $\boldsymbol{\sigma} \in \mathbb{R}^{m+1}$ with PLS). These two dimensions are still not equal, however, it is possible to make them equal if we use mixed different dual stress interpolations on the elements of the same beam. So, in addition to the PLS mesh and PQS mesh, some mixed meshes of dual stress interpolations are used in this section in order to improve the local unstable buckled configuration solution for a large deformed beam.
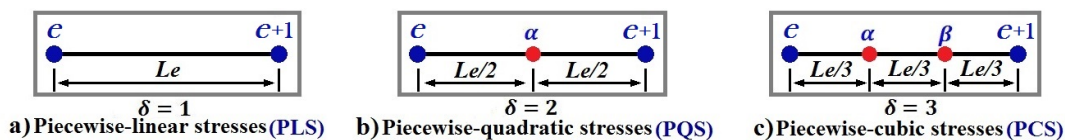
Figure 3.12: *Different dual stress interpolations for the beam element*

Hence, the formulas for the shape functions of the dual stress field, which are based on the PLS ($\delta = 1$), PQS ($\delta = 2$) and piecewise-cubic stresses (PCS, $\delta = 3$), can be expressed as

$$N_\sigma|_{\delta=1} = \frac{1}{2} \begin{bmatrix} 1-\xi \\ 1+\xi \end{bmatrix},$$

$$N_\sigma|_{\delta=2} = \frac{1}{2}\begin{bmatrix} \xi^2 - \xi \\ 1 - \xi^2 \\ \xi^2 + \xi \end{bmatrix},$$

$$N_\sigma|_{\delta=3} = \frac{1}{16}\begin{bmatrix} -1 + \xi + 9\xi^2 - 9\xi^3 \\ 9 - 27\xi - 9\xi^2 + 27\xi^3 \\ 9 + 27\xi - 9\xi^2 - 27\xi^3 \\ -1 - \xi + 9\xi^2 + 9\xi^3 \end{bmatrix},$$

where δ refers to the number of straight lines inside element e, as shown in Figure 3.12. According to the different dual stress interpolations and different values of $\delta = 1, 2, 3$, the symmetric matrix ${G_2}^e(\sigma_e)$ in equation (3.28a) of the gap function $\mathbf{G}(\sigma) \in \mathbb{R}^{2(m+1)} \times \mathbb{R}^{2(m+1)}$ can be formulated as

$${G_2}^e(\sigma_e)\big|_{\delta=1} = \begin{bmatrix} \frac{3(\sigma^e+\sigma^{e+1})}{5Le} & \frac{\sigma^{e+1}}{10} & -g_{11}^e & \frac{\sigma^e}{10} \\ g_{12}^e & L_e(\frac{\sigma^e}{10} + \frac{\sigma^{e+1}}{30}) & -g_{12}^e & -\frac{L_e(\sigma^e+\sigma^{e+1})}{60} \\ -g_{11}^e & -g_{12}^e & g_{11}^e & -g_{14}^e \\ g_{14}^e & g_{24}^e & -g_{14}^e & L_e(\frac{\sigma^e}{30} + \frac{\sigma^{e+1}}{10}) \end{bmatrix},$$

$${G_2}^e(\sigma_e)\big|_{\delta=2} = \begin{bmatrix} \frac{3(\sigma^e+\sigma^{e+1})+18\sigma^\alpha}{35Le} & \frac{2(\sigma^\alpha-\sigma^e)}{35} + \frac{3\sigma^{e+1}}{70} & -g_{11}^e & \frac{2(\sigma^\alpha-\sigma^{e+1})}{35} + \frac{3\sigma^e}{70} \\ g_{12}^e & L_e(\frac{\sigma^e}{14} + \frac{\sigma^{e+1}}{210} + \frac{\sigma^\alpha}{35}) & -g_{12}^e & L_e(\frac{-(\sigma^e+\sigma^{e+1})}{84} - \frac{\sigma^\alpha}{210}) \\ -g_{11}^e & -g_{12}^e & g_{11}^e & -g_{14}^e \\ g_{14}^e & g_{24}^e & -g_{14}^e & L_e(\frac{\sigma^e}{210} + \frac{\sigma^{e+1}}{14} + \frac{\sigma^\alpha}{35}) \end{bmatrix},$$

and,

$${G_2}^e(\sigma_e)\big|_{\delta=3} =$$

$$\begin{bmatrix} \frac{3(\sigma^e+\sigma^{e+1})+81(\sigma^\alpha+\sigma^\beta)}{140L_e} & \frac{\sigma^{e+1}+45\sigma^\beta-9\sigma^e-9\sigma^\alpha}{280} & -g_{11}^e & \frac{\sigma^e+45\sigma^\alpha-9\sigma^{e+1}-9\sigma^\beta}{280} \\ g_{12}^e & \frac{L_e(105\sigma^e+11\sigma^{e+1}+27(3\sigma^\alpha+\sigma^\beta))}{1680} & -g_{12}^e & \frac{-L_e(19(\sigma^{e+1}+\sigma^e)+9(\sigma^\alpha+\sigma^\beta))}{1680} \\ -g_{11}^e & -g_{12}^e & g_{11}^e & -g_{14}^e \\ g_{14}^e & g_{24}^e & -g_{14}^e & \frac{L_e(105\sigma^{e+1}+11\sigma^e+27(3\sigma^\beta+\sigma^\alpha))}{1680} \end{bmatrix},$$

in which $\sigma \in \mathbb{R}^{\delta m+1}$. Also, the positive-definite matrix K_e in equation (3.29a) of the stiffness matrix $\mathbf{K} \in \mathbb{R}^{\delta m+1} \times \mathbb{R}^{\delta m+1}$ can be written as

$$K_e\big|_{\delta=1} = \frac{L_e}{4E\alpha}\begin{bmatrix} 2 & 1 \\ 1 & 2 \end{bmatrix},$$

$$K_e\big|_{\delta=2} = \frac{Le}{20E\alpha} \begin{bmatrix} 4 & 1 & -1 \\ 1 & 4 & 1 \\ -1 & 1 & 4 \end{bmatrix},$$

and,

$$K_e\big|_{\delta=3} = \frac{Le}{E\alpha} \begin{bmatrix} \frac{4}{35} & \frac{99}{1120} & -\frac{9}{280} & \frac{19}{1120} \\ \frac{99}{1120} & \frac{81}{140} & -\frac{81}{1120} & -\frac{9}{280} \\ -\frac{9}{280} & -\frac{81}{1120} & \frac{81}{140} & \frac{99}{1120} \\ \frac{19}{1120} & -\frac{9}{280} & \frac{99}{1120} & \frac{4}{35} \end{bmatrix}.$$

Finally, vector λ_e in equation (3.30a) of $\boldsymbol{\lambda} \in \mathbb{R}^{\delta m+1}$ can be defined as

$$\lambda_e\big|_{\delta=1} = \frac{3\lambda L_e}{4\alpha} \begin{bmatrix} 1 \\ 1 \end{bmatrix},$$

$$\lambda_e\big|_{\delta=2} = \frac{\lambda Le}{4\alpha} \begin{bmatrix} 1 \\ 2 \\ 1 \end{bmatrix},$$

and,

$$\lambda_e\big|_{\delta=3} = \frac{3\lambda Le}{16\alpha} \begin{bmatrix} 1 \\ 3 \\ 3 \\ 1 \end{bmatrix}.$$

According to the boundary conditions of the beam and by designing suitable mixed meshes of different dual stress interpolations, the PD-SDP algorithm in section 3.3 can be used to solve all possible post-buckling problems (3.48), (3.50) and (3.60), in which

$$M^e(\sigma_e)\big|_\delta = \frac{1}{2}G_2^e(\sigma_e)\big|_\delta , \quad \forall\, \delta = 1, 2, 3.$$

3.5.1 Numerical examples with mixed meshes

We present three different types of beams which are controlled by different boundary conditions. Some geometrical data are kept fixed for all computations; $E = 1000Pa$, $v = 0.3$, $L = 1$m, $h = 0.05$m with an odd number of beam elements $m = 51$. The lateral load $q(x)$ is assumed to be either a uniformly distributed load such that $f(x) = (1 - \mu^2)q(x) = 0.08N/\text{m}$ or a concentrated force on the center of the beam in which $f(x) = 0.08N$. Different compressive load λ are considered in our applications.

3.5.1.1 Simply supported beam

According to the boundary conditions of simply supported beams (see Figure 3.2-a), two elements of discretized displacement $w = \{w_e\} \in \mathbb{R}^{2(m+1)}$ should be zero, therefore, the remaining non-zero elements of vector w are $(2m)$. We used three types of dual stress interpolations to construct a mixed mesh of dual stress fields in order to obtain $\dim \mathcal{U}_a^h = \dim \mathcal{S}_a^h$. The PQS is applied for $(m-3)$ beam elements and the PCS is used for only one element on the centre of the beam, while PLS is applied for two elements which are neighboring to the central beam element as shown in "*Mesh-1*" in Figure 3.13. So, we have $dim(\boldsymbol{\sigma}) = dim(\mathbf{w}) = 2m$, and this dimension equals 102 for $m = 51$. The approximate deflections with $\lambda > \lambda_{cr}$ under both uniformly distributed load and concentrated force are shown in Figures 3.14 and 3.15, respectively.
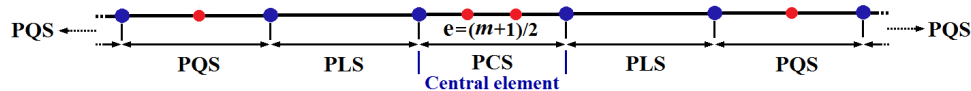
Figure 3.13: **Mesh-1**: *Mixed dual stress interpolations of beam elements*
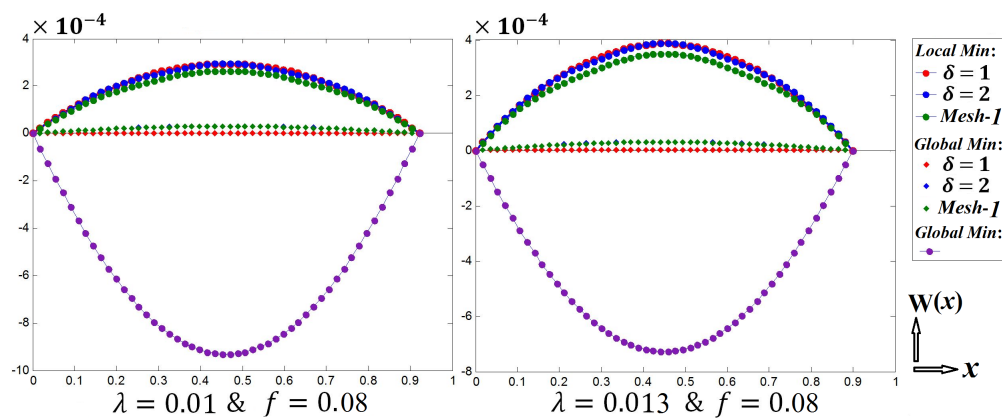
Figure 3.14: *Post-buckling solutions of simply supported beam under uniformly distributed load*

3.5.1.2 Doubly/Clamped beam

The boundary conditions of a doubly/clamped beam (see (3.2-c)) force the first two and the last two elements of discretized displacement w to be zero. Thus, the remaining non-zero elements of the displacement vector are $(2m-2)$. The selected mixed mesh of the dual stress field contains $(m-3)$ of PQS, while PLS can be
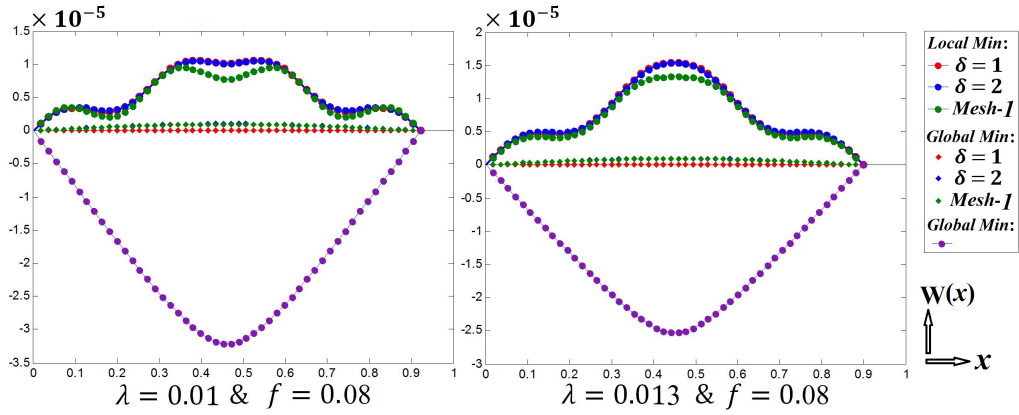
Figure 3.15: *Post-buckling solutions of simply supported beam under a concentrated force*

applied on the three remaining elements of the clamped beam as shown in "*Mesh-2*" in Figure 3.16. For $m = 51$, $dim(\boldsymbol{\sigma}) = dim(\mathbf{w}) = 100$. The approximate deflections for $\lambda > \lambda_{cr}$ under a uniformly distributed load and concentrated force are summarized in Figures 3.17 and 3.18, respectively.
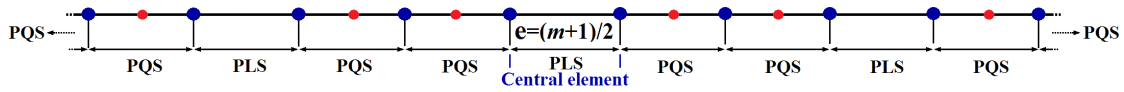
Figure 3.16: **Mesh-2**: *Mixed dual stress interpolations of beam elements*
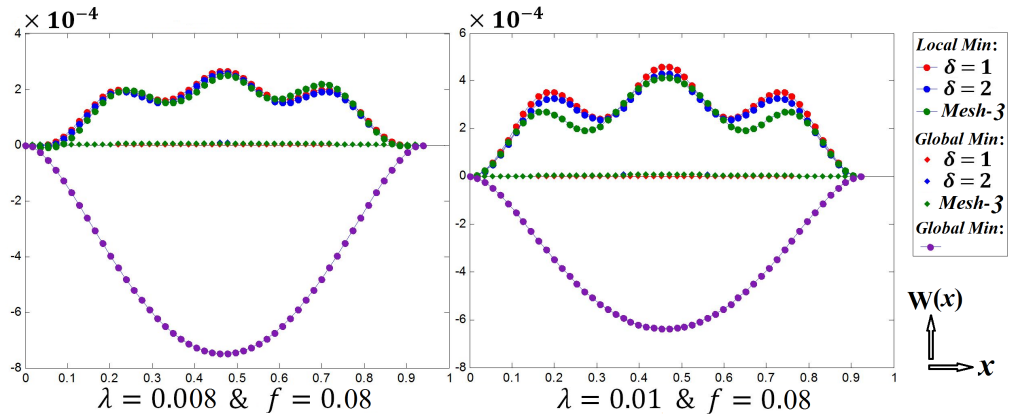
Figure 3.17: *Post-buckling configurations of clamped beam under uniformly distributed load*
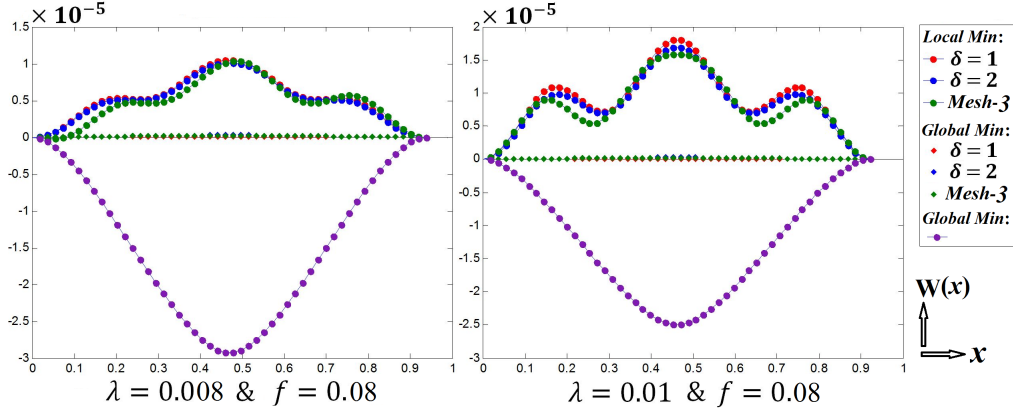
Figure 3.18: *Post-buckling configurations of clamped beam under a concentrated force*

3.5.1.3 Clamped/Simply supported beam

A clamped/simply supported beam is clamped at $x = 0$ and fixed in both directions at $x = L$ as shown in Figure 3.19. According to the boundary conditions

$$w(0) = w'(0) = w(L) = w''(L) = 0,$$

three elements of discretized displacement w should be zero. So, the remaining non-zero elements of w are $(2m-1)$. The " *Mesh-3* " is designed by applying two different dual stress interpolations. $(m-3)$ of beam elements are applied by the PQS, while PLS is applied for two elements which surround the central beam element, as shown in Figure 3.20. Thus, for $m = 51$, the $dim(\boldsymbol{\sigma}) = dim(\mathbf{w}) = 101$. The critical load of this beam is $\lambda_{cr} = 0.0034\text{m}^2$ (see equation (3.6)). The approximate deflections under a uniformly distributed load and concentrated force are summarized in Figures 3.21 and 3.22, respectively.

Figure 3.19: *Clamped/simply supported beam - uniformly distributed load (left), concentrated force (right)*
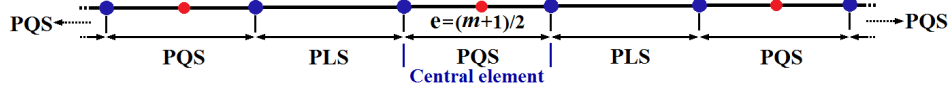
Figure 3.20: **Mesh-3**: *Mixed dual stress interpolations of beam elements*

$$\lambda = 0.008 \ \& \ f = 0.08 \qquad \lambda = 0.012 \ \& \ f = 0.08$$
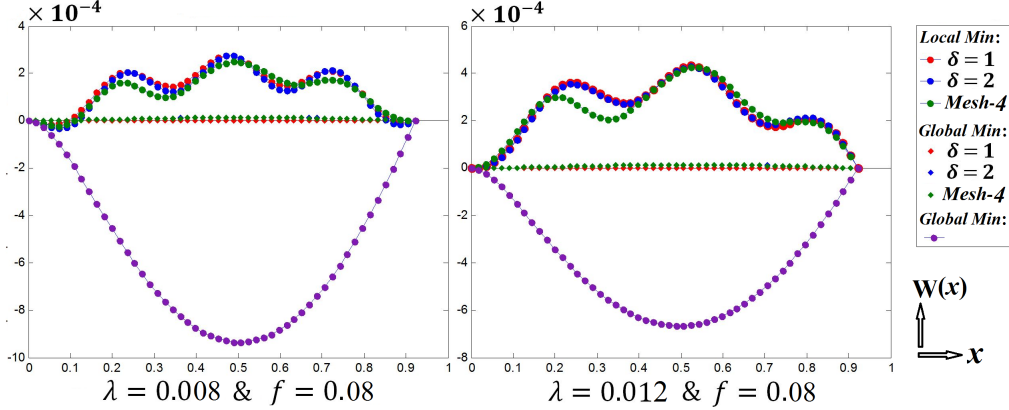
Figure 3.21: *Post-buckling configurations of clamped/simply supported beam under uniformly distributed load*

$$\lambda = 0.008 \ \& \ f = 0.08 \qquad \lambda = 0.012 \ \& \ f = 0.08$$
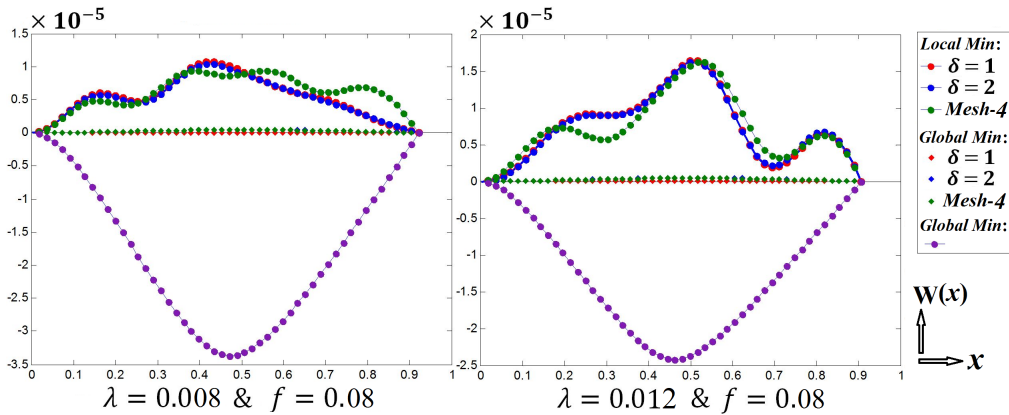
Figure 3.22: *Post-buckling configurations of clamped/simply supported beam under a concentrated force*

3.6   Summary

We have presented a canonical dual finite element method for the post-buckling analysis of a large deformed elastic beam which is governed by a fourth order nonlinear differential equation which was introduced by Gao in 1996. The nonconvexity of the total potential energy $\Pi(w)$ is necessary for the post-buckling phenomenon, but it leads to a fundamental difficulty for traditional numerical methods and algorithms. Based on the canonical duality theory and mixed finite element method,

60

a new primal-dual semi-definite program (PD-SDP) algorithm is proposed, which can be used to solve this challenging nonconvex variational problem to obtain all possible post-buckled solutions. According to the triality theory, the dimensions of the discretized displacement vector and dual stress vector were made equal in some examples by designing suitable mixed meshes of different dual stress interpolations depending on the boundary conditions of the beam. Extensive applications are illustrated for the post-buckled beam with different boundary conditions and external loads. The Gao-Strang gap function is computed for all post-buckled solutions. It is interesting to note that for local and global minima, the value of this gap function is affected by both the number of beam elements and axial loads, but for local maxima, its value is affected mainly by the number of elements. Our results show that the number of post-buckling solutions depends mainly on the external loads. For a given nontrivial $q(x)$, the nonlinear beam can have at most three post-buckled solutions if $\lambda \geq \lambda_{cr}$. Both the global minimizer and local maximizer solutions are very stable. However, the local minimal solution is very sensitive not only to the artificial parameters, such as the size of the finite elements, but also to the natural conditions such as the external loads and boundary conditions.

Chapter 4

Three-Dimensional Topology Optimization

Topology optimization is a mathematical method that optimizes a material structure within a given design space in order to satisfy a given set of loads, boundary conditions, geometry of the design domain, and the amount of material to be used in the final design. The amount of available material is typically distributed into fully solid material and void elements based on the results of the optimization within the structural design domain. Topology optimization is also a powerful tool for optimal design in the multidisciplinary fields of optics, electronics, structural, bio and nano-mechanics. Mathematically speaking, this tool is based on a finite element method such that the coupled variational problems in computational mechanics can be formulated as certain mixed integer nonlinear prograning (MINLP) problems [39]. Due to the integer constraint, traditional theory and methods in continuous optimization cannot be applied for solving topology optimization problems. Therefore, most MINLP problems are considered to be NP-hard in global optimization and computer science [41].

The key feature of the canonical duality theory (CDT) is that by using certain canonical strain measures, general nonconvex/nonsmooth potential variational problems can be equivalently reformulated as a pure (stress-based only) complementary energy variational principle [17]. It was discovered by Gao in 2007 that by simply using a canonical measure $\epsilon(x) = x(x-1) = 0$, the 0-1 integer constraint $x \in \{0, 1\}$ in general nonconvex minimization problems can be equivalently converted to a unified concave maximization problem in continuous space, which can be solved deterministically to obtain a global optimal solution in polynomial time [23]. Therefore, this pure complementary energy principle plays a fundamental role not

only in computational nonlinear mechanics, but also in discrete optimization [27, 29]. Most recently, Gao proved that the topology optimization should be formulated as a bi-level mixed integer nonlinear programming problem (BL-MINLP) [39, 38]. The upper-level optimization of this BL-MINLP is actually equivalent to the well-known Knapsack problem, which can be solved analytically by the CDT [38]. The review articles [27, 28] and the newly published book [41] provide comprehensive reviews and applications of the canonical duality theory in multidisciplinary fields of mathematical modeling, engineering mechanics, nonconvex analysis, global optimization, and computational science.

The main goal of this chapter is to apply the canonical duality theory for solving 3-dimensional benchmark problems in topology optimization. In Section 4.2, we first review Gao's recent work on why topology optimization should be formulated as a bi-level mixed integer nonlinear programming problem. A basic mathematical mistake in topology optimization modeling is explicitly addressed. A canonical penalty-duality method for solving this Knapsack problem is presented in Section 4.3, which is actually the so-called β-perturbation method first proposed in global optimization [29] and recently in topology optimization [39]. Section 4.4 reveals for the first time the unified relation between this canonical penalty-duality method in integer programming and Gao's pure complementary energy principle in nonlinear elasticity. Section 4.5 provides 3-D finite element interpolation and Section 4.6 provides the associated canonical penalty-duality (CPD) algorithm. The volume evolutionary method and computational complexity of this CPD algorithm are discussed. Applications to 3-D benchmark problems are provided in Section 4.7.

4.1 Popular methods in topology optimization

During the past forty years, many approximate methods have been developed for solving topology optimization problems, including the homogenization method [4, 6], density-based method [5], the solid isotropic material with penalization (SIMP) [85, 65, 67], level set approximation [62, 68], evolutionary structural optimization (ESO) [81, 82] and bi-directional evolutionary structural optimization (BESO) [64, 44, 63]. Currently, popular commercial software products used in topology optimization are based on SIMP and ESO/BESO methods [54, 47, 84, 77]. However, these approximate methods cannot mathematically guarantee the global convergence. Also, they usually suffer from having different intrinsic disadvantages, such as slow convergence, the gray scale elements and checkerboards patterns, etc [10, 74, 78].

The popular methods, SIMP and BESO, are applied in our work in Section 4.7 in order to compare them with the current method (CPD).

4.1.1 SIMP method

The SIMP method was originally provided by Bendsøe in 1989 [5], then it was developed independently by Rozvany et al. in 1991 [65]. The process begins with a partially density in all of the elements in the finite element domain. Many iterations are performed to redistribute the dense regions in order to minimize the overall compliance of the output structure. The minimum compliance optimization problem using the SIMP method can be expressed as [46]

$$
\begin{aligned}
(P_{simp}): \quad & \min \quad C = \mathbf{f}^T \mathbf{u} \\
& s.t. \quad \mathbf{K}(\boldsymbol{\rho})\mathbf{u} = \mathbf{f}, \\
& \quad \boldsymbol{\rho}^T \mathbf{v} = V_c, \\
& \quad 0 < \rho_e \le 1, \ \boldsymbol{\rho} = \{\rho_e\},
\end{aligned} \tag{4.1}
$$

where C is the mean compliance, $\mathbf{f}$ and $\mathbf{u}$ are the applied load and displacement vectors, respectively, $V_c > 0$ is the desired volume bound, and $\mathbf{K}(\boldsymbol{\rho})$ is the global stiffness matrix which can be defined as

$$
\mathbf{K}(\boldsymbol{\rho}) = \sum_{e=1}^{n} \rho_e^p \mathbf{K}_e, \tag{4.2}
$$

where $\mathbf{K}_e$ is the elemental stiffness matrix of the solid element and $p > 0$ is a given penalization parameter. This penalization parameter must be carefully selected to ensure more realistic solutions for the stiffness of every element in the structure to avoid results containing regions of intermediate density (i.e. the penalization parameter forces the final solution towards more 0-1 solutions). The most conventional penalization parameter which was selected based on the researchers experience is $p = 3$. However, most elements in the design domain still remain in gray scale, due to the fact that the design variables $\boldsymbol{\rho} = \{\rho_e\}$ are only approximate to 0 or 1. The sensitivity of the target function C is deduced to be [46]

$$
\frac{\partial C}{\partial \rho_e} = -p \, \rho_e^{p-1} \mathbf{u}_e^T \mathbf{K}_e \mathbf{u}_e. \tag{4.3}
$$

Several different methods can be used to solve minimum compliance problem (P_{simp}), such as the optimality criteria methods (OC) [85, 66], the method of moving asymptotes (MMA) [69] and some others. Sigmund presented the following sensitivity filter scheme by modifying elemental sensitivities during every iteration [75, 77] to ensure that the optimal design is mesh independent and checkerboard free,

$$\frac{\partial C}{\partial \rho_e} = \frac{1}{\max(\alpha, \rho_e) \sum_{i=1}^{n} H_{ei}} \sum_{i=1}^{n} H_{ei} \rho_i \frac{\partial C}{\partial \rho_i}, \tag{4.4}$$

where α is a small number to avoid division by zero and H_{ei} is the mesh-independent weight factor given as

$$H_{ei} = r_{\min} - r_{ei}, \quad \{r_{ei} \leq r_{\min}\}, \tag{4.5}$$

where $r_{\min}$ is the filter radius and r_{ei} is the distance between the centres of elements e and i, in which, weight factor H_{ei} is zero outside the circular filter area as shown in Figure 4.1.
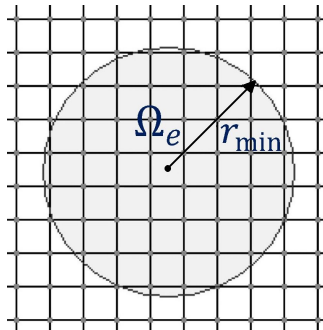
Figure 4.1: *Nodes located inside the circular sub-domain Ω_e for eth element in the filter scheme in the SIMP method*

By introducing material penalization in equation (4.2), the minimum compliance problem (P_{simp}) becomes nonconvex. Thus, it is possible to obtain a local optimum with gray configuration. Rozvany et al. [66] and Sigmund1998 [74] found in their examples that a local optimum may be avoided by applying the continuation method. However, global optimization is unsure even using the continuation method [70] . Sigmund [75] and Sigmund and Torquato [76] introduced in their study a different continuation strategy using a mesh-independency filter. They suggested using a large value for filter radius $r_{\min}$ to ensure a convex solution at the beginning, and then decreasing it gradually until the solution ends up with a 0/1 design.

4.1.2 BESO method

The BESO method was addressed by Yang *et al.* in 1999 [83] for stiffness optimization. They estimated the sensitivity numbers of the void elements through a linear extrapolation of the displacement field after the finite element method. The BESO method allows for not only the removal of solid elements from the structure to eliminate the lowest sensitivity numbers, but also the addition of void elements with the highest sensitivity numbers to the regions until the volume constraint and a convergence criterion are satisfied. The number of removed and added elements in each iteration is controlled by the unrelated parameters, rejection ratio and inclusion ratio, respectively. Querin *et al.* [63] used BESO for a full stress design by applying the von Mises stress criterion, where the elements that have the lowest von Mises stresses are removed and their number in each iteration is determined by the rejection ratio parameter. While the void elements near the highest von Mises stress regions are changed to solid elements and their number is determined by the inclusion ratio parameter. Huang and Xie initially presented a hard-kill scheme in 2007 [44], where the elements are completely removed to create cavities. Then, they introduced further improvements to their BESO algorithm by providing the so-called soft-kill approach to solve compliance problems in the interpolation scheme in 2009 [45, 46]. The removal of an element is realized by switching the relative density from 1 to the lowest value of density ρ instead of a complete deletion.

The minimum compliance optimization problem in the BESO method can be stated as [44, 46]

$$
\begin{aligned}
(P_{beso}): \quad & \min \quad C = \frac{1}{2}\mathbf{f}^T\mathbf{u} \\
& s.t. \quad \mathbf{K}(\boldsymbol{\rho})\mathbf{u} = \mathbf{f}, \\
& \qquad \boldsymbol{\rho}^T\mathbf{v} = V_c, \\
& \qquad \boldsymbol{\rho} \in \{0, 1\}.
\end{aligned}
\tag{4.6}
$$

The sensitivity of the target function C is given by [46]

$$
\frac{\partial C}{\partial \rho_e} = -\frac{1}{2}p\,\rho_e^{p-1}\mathbf{u}_e^T\mathbf{K}_e\mathbf{u}_e.
\tag{4.7}
$$

It was found that the most conventional penalization parameter is $p = 3$ as in SIMP. Problem (P_{beso}) has been used for the topology optimization of a continuum structure [6], but differs from the one used in BESO methods. In general, BESO methods have difficulty dealing with problem (P_{beso}). For example, if the volume is kept constant

to satisfy the volume constraint $\boldsymbol{\rho}^T \mathbf{v} = V_c$, the target function may not converge. The soft-kill BESO makes the algorithm stably convergent towards a solution for minimum compliance problem (P_{beso}).

A mesh-independency filter is activated all over the mesh by averaging the elemental sensitivity number with its neighbouring elements. The sensitivity filter scheme is similar to that introduced by Sigmund and Peterson [74]. To add elements with the highest sensitivity numbers into the design domain, a sensitivity filter scheme is applied to acquire the sensitivity number for the void elements and to smooth the sensitivity number in the prescribed design domain, therefore, BESO is considered a heuristics-based method. For more detail see [46].

Generally speaking, the BESO methods can produce exactly 0-1 solutions, while the SIMP suffers from some key limitations due to the fact that most SIMP solutions are in gray scale which have to be filtered or interpreted physically, a global optimum cannot be guaranteed and checkerboard patterns are problematic. The BESO usually starts from the full design and decreases the volume of the structure iteratively until the prescribed target volume is satisfied. It can produce an analytically exact integer solution without any hard-kill heuristics to obtain a verified global optimal solution. However, removing a small number of design elements may significantly change the performance of the overall structure, particularly in relation to nonlinear problems or in the case of complex constraints [78].

4.2 Mathematical problems for 3-D topology optimization

The minimum total potential energy principle provides a theoretical foundation for all mathematical problems in computational solid mechanics. For general 3-D nonlinear elasticity, the total potential energy has the following standard form [39], (see also (2.1))

$$\Pi(\mathbf{u}, \rho) = \int_\Omega \left(W(\nabla \mathbf{u})\rho + \mathbf{u} \cdot \mathbf{b}\rho \right) d\Omega - \int_{\Gamma_t} \mathbf{u} \cdot \mathbf{t} d\Gamma, \tag{4.8}$$

where the stored energy density $W(\mathbf{F})$ is an *objective function* (see Remark 3) of the deformation gradient $\mathbf{F} = \nabla \mathbf{u}$. In topology optimization, the mass density $\rho : \Omega \to \{0, 1\}$ is the design variable, which takes $\rho(\mathbf{x}) = 1$ at a solid material point $\mathbf{x} \in \Omega$, while $\rho(\mathbf{x}) = 0$ at a void point $\mathbf{x} \in \Omega$. Additionally, it must satisfy the

so-called Knapsack condition:

$$\int_{\Omega} \rho(\mathbf{x}) d\Omega \leq V_c, \tag{4.9}$$

where $V_c > 0$ is a desired volume bound.

By using the finite element method, the whole design domain Ω is meshed with finite elements by dividing them into n disjointed finite elements $\{\Omega_e\}$. In each element, the unknown variables can be numerically written as $\mathbf{u}(\mathbf{x}) = \mathbf{N}(\mathbf{x})\mathbf{u}_e$, $\rho(\mathbf{x}) = \rho_e \in \{0, 1\}$ $\forall \mathbf{x} \in \Omega_e$, where $\mathbf{N}(\mathbf{x})$ is a given interpolation matrix, and $\mathbf{u}_e$ is a nodal displacement vector. Let $\mathcal{U}_a \subset \mathbb{R}^m$ be a kinetically admissible space, in which certain deformation conditions are given, v_e represents the volume of the e-th element Ω_e, and $\mathbf{v} = \{v_e\} \in \mathbb{R}^n$. Then the admissible design space can be discretized as a discrete set

$$\mathcal{Z}_a = \left\{ \boldsymbol{\rho} = \{\rho_e\} \in \mathbb{R}^n \middle| \ \rho_e \in \{0, 1\} \ \forall e = 1, \dots, n, \ \boldsymbol{\rho}^T \mathbf{v} = \sum_{e=1}^{n} \rho_e v_e \leq V_c \right\} \tag{4.10}$$

and on $\mathcal{U}_a \times \mathcal{Z}_a$, the total potential energy functional can be numerically reformulated as a real-valued function

$$\Pi_h(\mathbf{u}, \boldsymbol{\rho}) = C(\boldsymbol{\rho}, \mathbf{u}) - \mathbf{u}^T \mathbf{f}, \tag{4.11}$$

where

$$C(\boldsymbol{\rho}, \mathbf{u}) = \boldsymbol{\rho}^T \mathbf{c}(\mathbf{u}),$$

in which

$$\mathbf{c}(\mathbf{u}) = \left\{ \int_{\Omega_e} [W(\nabla \mathbf{N}(\mathbf{x})\mathbf{u}_e) - \mathbf{b}^T \mathbf{N}(\mathbf{x})\mathbf{u}_e] d\Omega \right\} \in \mathbb{R}^n, \tag{4.12}$$

and

$$\mathbf{f} = \left\{ \int_{\Gamma_t^e} \mathbf{N}(\mathbf{x})^T \mathbf{t}(\mathbf{x}) d\Gamma \right\} \in \mathbb{R}^m.$$

By the facts that the topology optimization is a combination of both variational analysis on a continuous space $\mathcal{U}_a$ and optimal design on a discrete space $\mathcal{Z}_a$, it cannot be simply formulated in a traditional variational form. Instead, a general problem of topology optimization should be proposed as a bi-level programming [38]:

$$(\mathcal{P}_{bl}): \qquad \min\{\Phi(\boldsymbol{\rho}, \mathbf{u}) | \ \boldsymbol{\rho} \in \mathcal{Z}_a, \ \mathbf{u} \in \mathcal{U}_a\}, \tag{4.13}$$

$$\text{s.t.} \ \mathbf{u} \in \arg\min_{\mathbf{v} \in \mathcal{U}_a} \Pi_h(\mathbf{v}, \boldsymbol{\rho}), \tag{4.14}$$

where $\Phi(\boldsymbol{\rho}, \mathbf{u})$ represents the upper-level cost function, $\boldsymbol{\rho} \in \mathcal{Z}_a$ is the upper-level variable. Simillarly, $\Pi_h(\mathbf{u}, \boldsymbol{\rho})$ represents the lower-level cost function and $\mathbf{u} \in \mathcal{U}_a$ is the lower-level variable. The cost function $\Phi(\boldsymbol{\rho}, \mathbf{u})$ depends on both particular problems and numerical methods. It can be $\Phi(\boldsymbol{\rho}^p, \mathbf{u}) = \mathbf{f}^T \mathbf{u} - \mathbf{c}(\mathbf{u})^T \boldsymbol{\rho}^p$ for any given parameter $p \geq 1$, or simply $\Phi(\boldsymbol{\rho}, \mathbf{u}) = -\boldsymbol{\rho}^T \mathbf{c}(\mathbf{u})$.

Since the topology optimization is a design-analysis process, it is reasonable to use the alternative iteration method [38] for solving the challenging topology optimization problem $(\mathcal{P}_{bl})$, i.e.

(i) for a given design variable $\boldsymbol{\rho}_{k-1} \in \mathcal{Z}_a$, solving the lower-level optimization (4.14) for

$$\mathbf{u}_k = \arg\min\{\Pi_h(\mathbf{u}, \boldsymbol{\rho}_{k-1}) | \ \mathbf{u} \in \mathcal{U}_a\} \tag{4.15}$$

(ii) for the given $\mathbf{c}_u = \mathbf{c}(\mathbf{u}_k)$, solve the upper-level optimization problem (4.13) for

$$\boldsymbol{\rho}_k = \arg\min\{\Phi(\boldsymbol{\rho}, \mathbf{u}_k) \mid \boldsymbol{\rho} \in \mathcal{Z}_a\}. \tag{4.16}$$

The upper-level problem (4.16) is actually equivalent to the well-known Knapsack problem in its most simple (linear) form:

$$(\mathcal{P}_u): \ \min\{P_u(\boldsymbol{\rho}) = -\mathbf{c}_u^T \boldsymbol{\rho} \mid \boldsymbol{\rho}^T \mathbf{v} \leq V_c, \ \boldsymbol{\rho} \in \{0,1\}^n\}, \tag{4.17}$$

which makes a perfect sense in topology optimization, i.e. of all elements $\{\Omega_e\}$, one should keep those stored more strain energy. Knapsack problems appear extensively in the multidisciplinary fields of operations research, decision science, and engineering design problems. Due to the integer constraint, even this most simple linear Knapsack problem is listed as one of Karp's 21 NP-complete problems [50]. However, by using the canonical duality theory, this challenging problem can be solved easily to obtain global optimal solution.

For linear elastic structures without the body force, the stored energy C is a quadratic function of $\mathbf{u}$:

$$C(\boldsymbol{\rho}, \mathbf{u}) = \frac{1}{2}\mathbf{u}^T \mathbf{K}(\boldsymbol{\rho})\mathbf{u}, \tag{4.18}$$

where $\mathbf{K}(\boldsymbol{\rho}) = \{\rho_e \mathbf{K}_e\} \in \mathbb{R}^{n \times n}$ is the overall stiffness matrix, obtained by assembling the sub-matrix $\rho_e \mathbf{K}_e$ for each element Ω_e. For any given $\boldsymbol{\rho} \in \mathcal{Z}_a$, the displacement variable can be obtained analytically by solving the linear equilibrium equation $\mathbf{K}(\boldsymbol{\rho})\mathbf{u} = \mathbf{f}$. Thus, the topology optimization for linear elastic structures

can be simply formulated as

$$(\mathcal{P}_{le}): \quad \min\left\{\mathbf{f}^T\mathbf{u} - \frac{1}{2}\mathbf{u}^T\mathbf{K}(\boldsymbol{\rho})\mathbf{u} \mid \mathbf{K}(\boldsymbol{\rho})\mathbf{u} = \mathbf{f}, \ \mathbf{u} \in \mathcal{U}_a, \ \boldsymbol{\rho} \in \varrho_a\right\}. \quad (4.19)$$

4.3 Canonical dual solution to the Knapsack problem

The canonical duality theory for solving general integer programming problems was first proposed by Gao in 2007 [23]. Applications to topology optimization were given recently in [39, 38]. In this work, we present this theory in a different way, i.e. instead of the canonical measure in $\mathbb{R}^{n+1}$, we introduce a canonical measure in $\mathbb{R}^n$:

$$\boldsymbol{\varepsilon} = \Lambda(\boldsymbol{\rho}) = \boldsymbol{\rho} \circ \boldsymbol{\rho} - \boldsymbol{\rho} \in \mathbb{R}^n \quad (4.20)$$

and the associated super-potential

$$\Psi(\boldsymbol{\varepsilon}) = \begin{cases} 0 & \text{if } \boldsymbol{\varepsilon} \in \mathbb{R}^n_- := \{\boldsymbol{\varepsilon} \in \mathbb{R}^n \mid \boldsymbol{\varepsilon} \leq \mathbf{0}\} \\ +\infty & \text{otherwise,} \end{cases} \quad (4.21)$$

such that the integer constraint in the Knapsack problem $(\mathcal{P}_u)$ can be relaxed by the following canonical form

$$\min\left\{\Pi_u(\boldsymbol{\rho}) = \Psi(\Lambda(\boldsymbol{\rho})) - \mathbf{c}_u^T\boldsymbol{\rho} \mid \boldsymbol{\rho}^T\mathbf{v} \leq V_c \ \boldsymbol{\rho} \in \mathbb{R}^n\right\}. \quad (4.22)$$

This is a nonsmooth minimization problem in $\mathbb{R}^n$ with only one linear inequality constraint. The classical Lagrangian for this inequality constrained problem is

$$L(\boldsymbol{\rho}, \tau) = \Psi(\Lambda(\boldsymbol{\rho})) - \mathbf{c}_u^T\boldsymbol{\rho} + \tau(\boldsymbol{\rho}^T\mathbf{v} - V_c), \quad (4.23)$$

and the canonical minimization problem (4.22) is equivalent to the following min-max problem:

$$\min_{\boldsymbol{\rho} \in \mathbb{R}^n} \max_{\tau \in \mathbb{R}} L(\boldsymbol{\rho}, \tau) \ \ s.t. \ \ \tau \geq 0. \quad (4.24)$$

According to the Karush-Kuhn-Tucker theory in inequality constrained optimization, the Lagrange multiplier τ should satisfy the following KKT conditions:

$$\varsigma(\boldsymbol{\rho}^T\mathbf{v} - V_c) = 0, \ \ \varsigma \geq 0, \ \ \boldsymbol{\rho}^T\mathbf{v} - V_c \leq 0. \quad (4.25)$$

The first equality $\varsigma(\boldsymbol{\rho}^T \mathbf{v} - V_c) = 0$ is the so-called *complementarity condition*. It is well-known that to solve the complementarity problems is not an easy task, even for linear complementarity problems [48]. Also, the Lagrange multiplier has to satisfy the constraint qualification $\varsigma \geq 0$. Therefore, the classical Lagrange multiplier theory can be essentially used for linear equality constrained optimization problems [51]. This is one of the main reasons why the canonical duality theory was developed.

By the fact that the super-potential $\Psi(\boldsymbol{\varepsilon})$ is a convex, lower-semi continuous function (l.s.c), its sub-differential is a positive cone $\mathbb{R}^n_+$ [19]:

$$\partial\Psi(\boldsymbol{\varepsilon}) = \begin{cases} \{\boldsymbol{\sigma}\} \in \mathbb{R}^n_+ & \text{if } \boldsymbol{\varepsilon} \leq \mathbf{0} \in \mathbb{R}^n_- \\ \emptyset & \text{otherwise.} \end{cases} \tag{4.26}$$

Using Fenchel transformation, the conjugate function of $\Psi(\boldsymbol{\varepsilon})$ can be uniquely defined as (see [19])

$$\Psi^\sharp(\boldsymbol{\sigma}) = \sup_{\boldsymbol{\varepsilon} \in \mathbb{R}^n}\{\boldsymbol{\varepsilon}^T\boldsymbol{\sigma} - \Psi(\boldsymbol{\varepsilon})\} = \begin{cases} 0 & \text{if } \boldsymbol{\sigma} \in \mathbb{R}^n_+, \\ +\infty & \text{otherwise,} \end{cases} \tag{4.27}$$

which can be viewed as a *super complementary energy* [12]. By the theory of convex analysis, we have the following *canonical duality relations* [23]:

$$\Psi(\boldsymbol{\varepsilon}) + \Psi^\sharp(\boldsymbol{\sigma}) = \boldsymbol{\varepsilon}^T\boldsymbol{\sigma} \quad \Leftrightarrow \quad \boldsymbol{\sigma} \in \partial\Psi(\boldsymbol{\varepsilon}) \quad \Leftrightarrow \quad \boldsymbol{\varepsilon} \in \partial\Psi^\sharp(\boldsymbol{\sigma}). \tag{4.28}$$

By the Fenchel-Young equality

$$\Psi(\boldsymbol{\varepsilon}) = \boldsymbol{\varepsilon}^T\boldsymbol{\sigma} - \Psi^\sharp(\boldsymbol{\sigma}),$$

the Lagrangian $L(\boldsymbol{\rho}, \tau)$ can be written in the following form

$$\Xi(\boldsymbol{\rho}, \boldsymbol{\sigma}, \varsigma) = G_{ap}(\boldsymbol{\rho}, \boldsymbol{\sigma}) - \boldsymbol{\rho}^T\boldsymbol{\sigma} - \Psi^\sharp(\boldsymbol{\sigma}) - \boldsymbol{\rho}^T\mathbf{c}_u + \varsigma(\boldsymbol{\rho}^T\mathbf{v} - V_c). \tag{4.29}$$

This is the Gao-Strang total complementary function for the Knapsack problem, in which

$$G_{ap}(\boldsymbol{\rho}, \boldsymbol{\sigma}) = \boldsymbol{\sigma}^T(\boldsymbol{\rho} \circ \boldsymbol{\rho})$$

is the so-called *complementary gap function*. Clearly, if $\boldsymbol{\sigma} \in \mathbb{R}^n_+$, this gap function is convex and

$$G_{ap}(\boldsymbol{\rho}, \boldsymbol{\sigma}) \geq 0 \ \ \forall \boldsymbol{\rho} \in \mathbb{R}^n.$$

71

Let

$$\mathcal{S}_a^+ = \{\boldsymbol{\zeta} = \{\boldsymbol{\sigma}, \varsigma\} \in \mathbb{R}^{n+1} | \; \boldsymbol{\sigma} > \mathbf{0} \in \mathbb{R}^n, \; \varsigma \geq 0\}. \qquad (4.30)$$

Then on $\mathcal{S}_a$, we have

$$\Xi(\boldsymbol{\rho}, \boldsymbol{\zeta}) = \boldsymbol{\sigma}^T(\boldsymbol{\rho} \circ \boldsymbol{\rho} - \boldsymbol{\rho}) - \boldsymbol{\rho}^T \mathbf{c}_u + \varsigma(\boldsymbol{\rho}^T \mathbf{v} - V_c) \qquad (4.31)$$

and for any given $\boldsymbol{\zeta} \in \mathcal{S}_a^+$, the canonical dual function can be obtained by

$$P_u^d(\boldsymbol{\zeta}) = \min_{\boldsymbol{\rho} \in \mathbb{R}^n} \Xi(\boldsymbol{\rho}, \boldsymbol{\zeta}) = -\frac{1}{4}\boldsymbol{\tau}_u^T(\boldsymbol{\zeta}) \mathbf{G}(\boldsymbol{\sigma})^{-1} \boldsymbol{\tau}_u(\boldsymbol{\zeta}) - \varsigma V_c, \qquad (4.32)$$

where

$$\mathbf{G}(\boldsymbol{\sigma}) = \text{Diag}(\boldsymbol{\sigma}), \quad \boldsymbol{\tau}_u = \boldsymbol{\sigma} + \mathbf{c}_u - \varsigma \mathbf{v}.$$

This canonical dual function is the so-called *pure complementary energy* in nonlinear elasticity, first proposed by Gao in 1999 [17], where $\boldsymbol{\tau}_u$ and $\boldsymbol{\sigma}$ correspond to the first and second Piola-Kirchhoff stresses, respectively. Thus, the canonical dual problem of the Knapsack problem can be proposed in the following

$$(\mathcal{P}_u^d): \quad \max\left\{P_u^d(\boldsymbol{\zeta}) | \; \boldsymbol{\zeta} \in \mathcal{S}_a^+\right\}. \qquad (4.33)$$

Theorem 10 (Canonical Dual Solution for Knapsack Problem [39])
For any given $\mathbf{u}_k \in \mathcal{U}_a$ and $V_c > 0$, if $\bar{\boldsymbol{\zeta}} = (\bar{\boldsymbol{\sigma}}, \bar{\tau}) \in \mathcal{S}_a^+$ is a solution to $(\mathcal{P}_u^d)$, then

$$\bar{\boldsymbol{\rho}} = \frac{1}{2}\mathbf{G}(\bar{\boldsymbol{\sigma}})^{-1}\boldsymbol{\tau}_u(\bar{\boldsymbol{\zeta}}) \qquad (4.34)$$

is a global minimum solution to the Knapsack problem $(\mathcal{P}_u)$ and

$$P_u(\bar{\boldsymbol{\rho}}) = \min_{\boldsymbol{\rho} \in \mathbb{R}^n} P_u(\boldsymbol{\rho}) = \Xi(\bar{\boldsymbol{\rho}}, \bar{\boldsymbol{\zeta}}) = \max_{\boldsymbol{\zeta} \in \mathcal{S}_a^+} P_u^d(\boldsymbol{\zeta}) = P_u^d(\bar{\boldsymbol{\zeta}}). \qquad (4.35)$$

Proof. The following proof was given by Gao recently in [39].

By the convexity of the super-potential $\Psi(\boldsymbol{\varepsilon})$, we have $\Psi^{**}(\boldsymbol{\varepsilon}) = \Psi(\boldsymbol{\varepsilon})$. Thus,

$$L(\boldsymbol{\rho}, \tau) = \sup_{\boldsymbol{\sigma} \in \mathbb{R}^n} \Xi(\boldsymbol{\rho}, \boldsymbol{\sigma}, \tau) \; \forall \boldsymbol{\rho} \in \mathbb{R}^n, \; \tau \in \mathbb{R}. \qquad (4.36)$$

It is easy to show that for any given $\boldsymbol{\rho} \in \mathbb{R}^n$, $\tau \in \mathbb{R}$, the supremum condition is governed by $\Lambda(\boldsymbol{\rho}) \in \partial\Psi^*(\boldsymbol{\sigma})$. By the canonical duality relations given in (4.28), we

have the equivalent relations:

$$\Lambda(\boldsymbol{\rho})^T \boldsymbol{\sigma} = \boldsymbol{\sigma}^T(\boldsymbol{\rho} \circ \boldsymbol{\rho} - \boldsymbol{\rho}) = 0 \quad \Leftrightarrow \quad \boldsymbol{\sigma} \in \mathbb{R}_+^n \quad \Leftrightarrow \quad \Lambda(\boldsymbol{\rho}) = (\boldsymbol{\rho} \circ \boldsymbol{\rho} - \boldsymbol{\rho}) \in \mathbb{R}_-^n. \quad (4.37)$$

This is exactly equivalent to the KKT conditions of the canonical problem for the inequality condition $\Lambda(\boldsymbol{\rho}) \in \mathbb{R}_-^n$. Thus, if $\bar{\boldsymbol{\zeta}} \in \mathcal{S}_a^+$ is a KKT solution to $(\mathcal{P}_u^d)$, then $\bar{\boldsymbol{\sigma}} > \mathbf{0}$ and the complementarity condition in (4.37) leads to

$$\bar{\boldsymbol{\rho}} \circ \bar{\boldsymbol{\rho}} - \bar{\boldsymbol{\rho}} = 0,$$

i.e. $\bar{\boldsymbol{\rho}} \in \{0,1\}^n$. It is easy to prove that for a given $\bar{\boldsymbol{\zeta}}$, equality (4.34) is exactly the criticality condition

$$\nabla_{\boldsymbol{\rho}} \Xi(\bar{\boldsymbol{\rho}}, \bar{\boldsymbol{\zeta}}) = 0.$$

Therefore, vector $\bar{\boldsymbol{\rho}} \in \{0,1\}^n$ defined by (4.34) is a solution to the Knapsack problem $(\mathcal{P}_u)$. According to Gao and Strang [13] the total complementary function $\Xi(\boldsymbol{\rho}, \boldsymbol{\zeta})$ is a saddle function on $\mathbb{R}^n \times \mathcal{S}_a^+$, then

$$\min_{\boldsymbol{\rho} \in \mathbb{R}^n} P_u(\boldsymbol{\rho}) = \min_{\boldsymbol{\rho} \in \mathbb{R}^n} \max_{\boldsymbol{\zeta} \in \mathcal{S}_a^+} \Xi(\boldsymbol{\rho}, \boldsymbol{\zeta}) = \max_{\boldsymbol{\zeta} \in \mathcal{S}_a^+} \min_{\boldsymbol{\rho} \in \mathbb{R}^n} \Xi(\boldsymbol{\rho}, \boldsymbol{\zeta}) = \max_{\boldsymbol{\zeta} \in \mathcal{S}_a^+} P_u^d(\boldsymbol{\zeta}). \quad (4.38)$$

The complementary-dual equality (4.35) can be proved by the canonical duality relations. $\qquad \square$

This theorem shows that the so-called NP-hard Knapsack problem is canonically dual to a concave maximization problem $(\mathcal{P}_u^d)$ in continuous space, which is much easier than the 0-1 programming problem $(\mathcal{P}_u)$ in discrete space. Whence the canonical dual solution $\bar{\boldsymbol{\zeta}}$ is obtained, the solution to the Knapsack problem can be given analytically by (4.34).

4.4 Pure Complementary Energy Principle and Perturbed Solution

Based on Theorem 10, a perturbed solution for the Knapsack problem was recently proposed in [39, 38]. This section demonstrates the relation between this solution with the pure complementary energy principle in nonlinear elasticity discovered by Gao in 1997-1999 [16, 17].

In terms of the deformation

$$\boldsymbol{\chi} = \mathbf{u} + \mathbf{x},$$

the total potential energy variational principle for general large deformation problems can also be written in the following form

$$(\mathcal{P}_\chi): \quad \inf_{\boldsymbol{\chi} \in \mathcal{X}_a} \Pi(\boldsymbol{\chi}) = \int_\Omega [W(\nabla\boldsymbol{\chi}) - \boldsymbol{\chi} \cdot \mathbf{b}]\rho \mathrm{d}\Omega - \int_{\Gamma_t} \boldsymbol{\chi} \cdot \mathbf{t} \mathrm{d}\Gamma, \qquad (4.39)$$

where $\mathcal{X}_a$ is a kinetically admissible deformation space, in which, the boundary condition $\boldsymbol{\chi}(\mathbf{x}) = 0$ is given on Γ_χ. It is well-known that the stored energy $W(\mathbf{F})$ is usually a nonconvex function of the deformation gradient

$$\mathbf{F} = \nabla\boldsymbol{\chi} = \nabla\mathbf{u} + \mathbf{I},$$

in order to model complicated phenomena, such as phase transitions and post-buckling. By the fact that $W(\mathbf{F})$ must be an objective function [61], there exists a real-valued function $\Psi(\mathbf{C})$ such that (see [9])

$$W(\mathbf{F}) = \Psi(\mathbf{F}^T\mathbf{F}).$$

For most reasonable materials (say the St. Venant-Kirchhoff material [34]), the function $\Psi(\mathbf{C})$ is a usually convex function of the Cauchy strain measure $\mathbf{C} = \mathbf{F}^T\mathbf{F}$ such that its complementary energy density can be uniquely defined by the Legendre transformation

$$\Psi^*(\mathbf{S}) = \{\ \mathrm{tr}(\mathbf{C} \cdot \mathbf{S}) - \Psi(\mathbf{C})|\ \mathbf{S} = \nabla\Psi(\mathbf{C})\}. \qquad (4.40)$$

Therefore, a pure complementary energy variational principle was obtained by Gao in 1999 [17, 19]:

Theorem 11 (Pure Complementary Energy Principle for Nonlinear Elasticity [17])
For any given external force field $\mathbf{b}(\mathbf{x})$ *in* Ω *and* $\mathbf{t}(\mathbf{x})$ *on* Γ_t, *if* $\tau(\mathbf{x})$ *is a statically admissible stress field, i.e.*

$$\boldsymbol{\tau} \in \mathcal{T}_a := \{\boldsymbol{\tau}(\mathbf{x}) : \Omega \to \mathbb{R}^{3\times3}|\ -\nabla \cdot \boldsymbol{\tau} = \mathbf{b}\ \forall\mathbf{x} \in \Omega,\ \mathbf{n} \cdot \boldsymbol{\tau} = \mathbf{t}\ \forall\mathbf{x} \in \Gamma_t\}, \quad (4.41)$$

and $\bar{\mathbf{S}}$ *is a critical point of the pure complementary energy*

$$\Pi^d(\mathbf{S}) = -\int_\Omega \left[\frac{1}{4}tr(\boldsymbol{\tau} \cdot \mathbf{S}^{-1} \cdot \boldsymbol{\tau}) + \Psi^*(\mathbf{S})\right]\rho\ \mathrm{d}\Omega, \qquad (4.42)$$

then the deformation field $\bar{\boldsymbol{\chi}}(\mathbf{x})$ defined by

$$\bar{\boldsymbol{\chi}}(\mathbf{x}) = \frac{1}{2} \int_{\mathbf{x}_0}^{\mathbf{x}} \boldsymbol{\tau} \cdot \bar{\mathbf{S}}^{-1} d\mathbf{x} \tag{4.43}$$

along any path from $\mathbf{x}_0 \in \Gamma_\chi$ to $\mathbf{x} \in \Omega$ is a critical point of the total potential energy $\Pi(\boldsymbol{\chi})$ and $\Pi(\bar{\boldsymbol{\chi}}) = \Pi^d(\bar{\mathbf{S}})$. Moreover, if $\bar{\mathbf{S}}(\mathbf{x}) \succ 0 \quad \forall \mathbf{x} \in \Omega$, then $\bar{\boldsymbol{\chi}}$ is a global minimizer of $\Pi(\boldsymbol{\chi})$.

It is easy to prove that the criticality condition $\delta\Pi_\chi^d(\mathbf{S}) = 0$ is governed by the so-called canonical dual algebraic equation [19]:

$$4\mathbf{S} \cdot [\nabla\Psi^*(\mathbf{S})] \cdot \mathbf{S} = \boldsymbol{\tau}^T \cdot \boldsymbol{\tau}. \tag{4.44}$$

For certain materials, this algebraic equation can be solved analytically to obtain all possible solutions [25]. Particularly, for the St Venant-Kirchhoff material, this tensor equation could have at most 27 solutions at each material point $\mathbf{x}$, but only one positive-definite

$$\mathbf{S}(\mathbf{x}) \succ 0 \quad \forall \mathbf{x} \in \Omega, \tag{4.45}$$

which leads to the global minimum solution $\bar{\boldsymbol{\chi}}(\mathbf{x})$ [34]. The pure complementary energy principle solved a well-known open problem in large deformation mechanics and is known as the Gao principle in the literature (see [53]). This principle plays an important role not only in large deformation theory and nonconvex variational analysis, but also in global optimization and computational science. Indeed, Theorem 10 is simply an application of this principle if we consider the quadratic operator $\boldsymbol{\varepsilon}(\boldsymbol{\rho})$ as the Cauchy strain measure $\mathbf{C}(\boldsymbol{\chi})$, then the canonical dual $\boldsymbol{\sigma} \in \partial\Psi(\boldsymbol{\varepsilon})$ corresponds to the second Piola-Kirchhoff stress

$$\mathbf{S} = \nabla\Psi(\mathbf{C}), \tag{4.46}$$

while $\boldsymbol{\tau}_u$ corresponds to the first Piola-Kirchhoff stress $\boldsymbol{\tau}$. By the fact that $\Psi^\sharp(\boldsymbol{\sigma})$ is nonsmooth, the associated canonical dual algebraic equation (4.44) should be governed by the KKT conditions (4.37). In order to solve this problem, a β-perturbation method was proposed in 2010 for solving general integer programming problems [29] and recently for solving the topology optimization problems [39].

According to the canonical duality theory for mathematical modeling [38], the integer constraint $\boldsymbol{\rho} \in \{0, 1\}^n$ in the Knapsack problem $(\mathcal{P}_u)$ is a constitutive condition,

while
$$\boldsymbol{\rho} \cdot \mathbf{v} \leq V_c,$$

is a geometrical constraint. Thus, by using the so-called pan-penalty functions

$$W(\boldsymbol{\rho}) = \begin{cases} 0 & \text{if } \boldsymbol{\rho} \in \{0,1\}^n \\ +\infty & \text{otherwise,} \end{cases} \quad F(\boldsymbol{\rho}) = \begin{cases} \mathbf{c}_u \cdot \boldsymbol{\rho} & \text{if } \boldsymbol{\rho} \cdot \mathbf{v} \leq V_c \\ -\infty & \text{otherwise,} \end{cases} \quad (4.47)$$

the Knapsack problem $(\mathcal{P}_u)$ can be equivalently written in Gao-Strang's unconstrained form [13]:

$$\min \{W(\boldsymbol{\rho}) - F(\boldsymbol{\rho}) | \ \boldsymbol{\rho} \in \mathbb{R}^n\}. \quad (4.48)$$

By introducing a penalty parameter $\beta > 0$ and a Lagrange multiplier $\tau \geq 0$, these two pan-penalty functions can have the following relaxations:

$$W_\beta(\boldsymbol{\rho}) = \beta \|\boldsymbol{\rho} \circ \boldsymbol{\rho} - \boldsymbol{\rho}\|^2, \quad F_\tau(\boldsymbol{\rho}) = \mathbf{c}_u \cdot \boldsymbol{\rho} - \tau(\boldsymbol{\rho} \cdot \mathbf{v} - V_c). \quad (4.49)$$

It is easy to prove that

$$W(\boldsymbol{\rho}) = \lim_{\beta \to \infty} W_\beta(\boldsymbol{\rho}), \quad F(\boldsymbol{\rho}) = \min_{\tau \geq 0} F_\tau(\boldsymbol{\rho}) \ \ \forall \boldsymbol{\rho} \in \mathbb{R}^n. \quad (4.50)$$

Thus, the Knapsack problem can be relaxed by the so-called penalty-duality approach:

$$\min_{\boldsymbol{\rho} \in \mathbb{R}^n} \max_{\tau \geq 0} \{L_\beta(\boldsymbol{\rho}, \tau) = W_\beta(\boldsymbol{\rho}) - \mathbf{c}_u \cdot \boldsymbol{\rho} + \tau(\boldsymbol{\rho} \cdot \mathbf{v} - V_c)\}. \quad (4.51)$$

Since the penalty function $W_\beta(\boldsymbol{\rho})$ is nonconvex, by using the canonical transformation

$$W_\beta(\boldsymbol{\rho}) = \Psi_\beta(\Lambda(\boldsymbol{\rho})),$$

we have

$$\Psi_\beta(\boldsymbol{\varepsilon}) = \beta \|\boldsymbol{\varepsilon}\|^2,$$

which is a convex quadratic function. Its Legendre conjugate is simply

$$\Psi_\beta^*(\boldsymbol{\sigma}) = \frac{1}{4}\beta^{-1}\|\boldsymbol{\sigma}\|^2.$$

Thus, the Gao and Strang total complementary optimization problem for the penalty-

duality approach (4.51) can be given by [39]:

$$\min_{\boldsymbol{\rho}\in\mathbb{R}^n} \max_{\boldsymbol{\zeta}\in\mathcal{S}_a^+} \left\{ \Xi_\beta(\boldsymbol{\rho},\boldsymbol{\zeta}) = (\boldsymbol{\rho}\circ\boldsymbol{\rho}-\boldsymbol{\rho})\cdot\boldsymbol{\sigma} - \frac{1}{4}\beta^{-1}\|\boldsymbol{\sigma}\|^2 - \mathbf{c}_u\cdot\boldsymbol{\rho} + \tau(\boldsymbol{\rho}\cdot\mathbf{v}-V_c) \right\}.$$

(4.52)

For any given $\beta > 0$ and $\boldsymbol{\zeta} = \{\boldsymbol{\sigma},\boldsymbol{\varsigma}\} \in \mathbf{S}_a^+$, a canonical penalty-duality (CPD) function can be obtained as

$$P_\beta^d(\boldsymbol{\zeta}) = \min_{\boldsymbol{\rho}\in\mathbb{R}^n} \Xi_\beta(\boldsymbol{\rho},\boldsymbol{\zeta}) = P_u^d(\boldsymbol{\sigma},\boldsymbol{\varsigma}) - \frac{1}{4}\beta^{-1}\|\boldsymbol{\sigma}\|^2,$$

(4.53)

which is exactly the so-called β-perturbed canonical dual function presented in [39, 38]. It was proved by Theorem 7 in [29] that there exists a $\beta_c > 0$ such that for any given $\beta \geq \beta_c$, both the CPD problem

$$(\mathcal{P}_\beta^d): \quad \max\{P_\beta^d(\boldsymbol{\zeta})| \ \boldsymbol{\zeta} \in \mathcal{S}_a^+\}$$

(4.54)

and the problem $(\mathcal{P}_u^d)$ have the same solution set. Since $\Psi_\beta^*(\boldsymbol{\sigma})$ is a quadratic function, the corresponding canonical dual algebraic equation (4.44) is a coupled cubic algebraic system

$$2\beta^{-1}\sigma_e^3 + \sigma_e^2 = (\tau v_e - c_e)^2, \quad e = 1,\dots,n,$$

(4.55)

$$\sum_{e=1}^n \frac{1}{2}\frac{v_e}{\sigma_e}(\sigma_e - v_e\tau + c_e) - V_c = 0.$$

(4.56)

It was proved in [19, 23] that for any given $\beta > 0$, $\tau \geq 0$ and $\mathbf{c}_u = \{c_e(\mathbf{u}_e)\}$ such that

$$\theta_e = \tau v_e - c_e(\mathbf{u}_e) \neq 0, \ e = 1,\dots,n,$$

the canonical dual algebraic equation (4.55) has a unique positive real solution

$$\sigma_e = \frac{1}{12}\beta[-1 + \phi_e(\tau) + \phi_e^c(\tau)] > 0, \quad e = 1,\dots,n$$

(4.57)

where

$$\phi_e(\varsigma) = \eta^{-1/3}\left[2\theta_e^2 - \eta + 2i\sqrt{\theta_e^2(\eta - \theta_e^2)}\right]^{1/3}, \quad \eta = \frac{\beta^2}{27},$$

and ϕ_e^c is the complex conjugate of ϕ_e, i.e. $\phi_e\phi_e^c = 1$. Thus, a canonical penalty-duality algorithm has been proposed recently for solving general topology optimization problems [39, 38].

4.5   3-D finite element interpolation

For three-dimensional linear elastic structures, we simply use cubic 8-node hexahedral elements $\{\Omega_e\}$, where each element contains 24 degrees of freedom corresponding to the displacements in x-y-z directions (each node has three degrees of freedom), as shown in Figure 4.2. Thus, the displacement interpolation matrix is
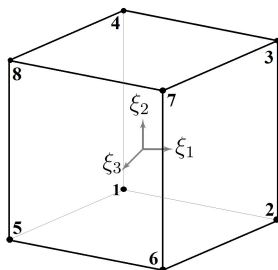
Figure 4.2: *The hexahedron element - eight nodes*

$\mathbf{N} = [\mathrm{N}_1 \;\; \mathrm{N}_2 \;\; ... \;\; \mathrm{N}_8]$ and

$$\mathrm{N}_i = \begin{bmatrix} N_i & 0 & 0 \\ 0 & N_i & 0 \\ 0 & 0 & N_i \end{bmatrix}. \tag{4.58}$$

The shape functions $N_i = N_i(\xi_1, \xi_2, \xi_3)$, $i = 1, ...8$ are derived by

$$N_1 = \frac{1}{8}(1 - \xi_1)(1 - \xi_2)(1 - \xi_3), \qquad N_2 = \frac{1}{8}(1 + \xi_1)(1 - \xi_2)(1 - \xi_3),$$

$$N_3 = \frac{1}{8}(1 + \xi_1)(1 + \xi_2)(1 - \xi_3), \qquad N_4 = \frac{1}{8}(1 - \xi_1)(1 + \xi_2)(1 - \xi_3),$$

$$N_5 = \frac{1}{8}(1 - \xi_1)(1 - \xi_2)(1 + \xi_3), \qquad N_6 = \frac{1}{8}(1 + \xi_1)(1 - \xi_2)(1 + \xi_3),$$

$$N_7 = \frac{1}{8}(1 + \xi_1)(1 + \xi_2)(1 + \xi_3), \qquad N_8 = \frac{1}{8}(1 - \xi_1)(1 + \xi_2)(1 + \xi_3),$$

in which ξ_1, ξ_2 and ξ_3 are the natural coordinates of the ith node. The nodal displacement vector $\mathbf{u}_e$ is given by

$$\mathbf{u}_e^T = [u_1^e \;\; u_2^e \;\; ... \;\; u_8^e],$$

where $u_i^e = (x_i^e, y_i^e, z_i^e) \in \mathbb{R}^3$, $i = 1, ..., 8$ are the displacement components at node i. The components B_i of strain-displacement matrix $\mathbf{B} = [\mathrm{B}_1 \; \mathrm{B}_2 \; ... \; \mathrm{B}_8]$, which relates

to strain ε and nodal displacement $\mathbf{u}_e$ ($\varepsilon = \mathbf{B}\mathbf{u}_e$), are defined as

$$\mathbf{B}_i = \begin{bmatrix} \frac{\partial N_i}{\partial x} & 0 & 0 \\ 0 & \frac{\partial N_i}{\partial y} & 0 \\ 0 & 0 & \frac{\partial N_i}{\partial z} \\ \frac{\partial N_i}{\partial y} & \frac{\partial N_i}{\partial x} & 0 \\ \frac{\partial N_i}{\partial z} & 0 & \frac{\partial N_i}{\partial x} \\ 0 & \frac{\partial N_i}{\partial z} & \frac{\partial N_i}{\partial y} \end{bmatrix}. \tag{4.59}$$

Hooke's law for isotropic materials in constitutive matrix form is given by

$$\mathbf{H} = \frac{E}{(1+\nu)(1-2\nu)} \begin{bmatrix} 1-\nu & \nu & \nu & 0 & 0 & 0 \\ \nu & 1-\nu & \nu & 0 & 0 & 0 \\ \nu & \nu & 1-\nu & 0 & 0 & 0 \\ 0 & 0 & 0 & \frac{1-2\nu}{2} & 0 & 0 \\ 0 & 0 & 0 & 0 & \frac{1-2\nu}{2} & 0 \\ 0 & 0 & 0 & 0 & 0 & \frac{1-2\nu}{2} \end{bmatrix}, \tag{4.60}$$

where E is the Young's modulus and ν is the Poisson's ratio of the isotropic material. The stiffness matrix of the structure in the CPD algorithm is given by

$$\mathbf{K}(\boldsymbol{\rho}) = \sum_{e=1}^{n}(E_{min} + (E - E_{min})\rho_e)\mathbf{K}_e, \tag{4.61}$$

where E_{min} must be small enough (usually let $E_{min} = 10^{-9}$) to avoid singularity in computation and $\mathbf{K}_e$ is defined as

$$\mathbf{K}_e = \int_{-1}^{1} \int_{-1}^{1} \int_{-1}^{1} \mathbf{B}^T \mathbf{H} \mathbf{B} \, d\xi_1 d\xi_2 d\xi_3. \tag{4.62}$$

Substituting the strain-displacement matrix $\mathbf{B}$ and (4.60) into (4.62), the 24×24 element stiffness matrix $\mathbf{K}_e$ for the eight-node quadrilateral element can be stated as

$$\mathbf{K}_e = \frac{1}{(\nu+1)(1-2\nu)} \begin{bmatrix} K_1 & K_2 & K_3 & K_4 \\ K_2^T & K_5 & K_6 & K_3^T \\ K_3^T & K_6 & K_5 & K_2^T \\ K_4 & K_3 & K_2 & K_1 \end{bmatrix}, \tag{4.63}$$

where

$$K_1 = \begin{bmatrix} k_1 & k_2 & k_2 & k_3 & k_5 & k_5 \\ & k_1 & k_2 & k_4 & k_6 & k_7 \\ & & k_1 & k_4 & k_7 & k_6 \\ & & & k_1 & k_8 & k_8 \\ & & & & k_1 & k_2 \\ sym & & & & & k_1 \end{bmatrix}, \qquad K_2 = \begin{bmatrix} k_9 & k_8 & k_{12} & k_6 & k_4 & k_7 \\ k_8 & k_9 & k_{12} & k_5 & k_3 & k_5 \\ k_{10} & k_{10} & k_{13} & k_7 & k_4 & k_6 \\ k_6 & k_5 & k_{11} & k_9 & k_2 & k_{10} \\ k_4 & k_3 & k_5 & k_2 & k_9 & k_{12} \\ k_{11} & k_4 & k_6 & k_{12} & k_{10} & k_{13} \end{bmatrix},$$

$$K_3 = \begin{bmatrix} k_6 & k_7 & k_4 & k_9 & k_{12} & k_8 \\ k_7 & k_6 & k_4 & k_{10} & k_{13} & k_{10} \\ k_5 & k_5 & k_3 & k_8 & k_{12} & k_9 \\ k_9 & k_{10} & k_2 & k_6 & k_{11} & k_5 \\ k_{12} & k_{13} & k_{10} & k_{11} & k_6 & k_4 \\ k_2 & k_{12} & k_9 & k_4 & k_5 & k_3 \end{bmatrix}, \quad K_4 = \begin{bmatrix} k_{14} & k_{11} & k_{11} & k_{13} & k_{10} & k_{10} \\ & k_{14} & k_{11} & k_{12} & k_9 & k_8 \\ & & k_{14} & k_{12} & k_8 & k_9 \\ & & & k_{14} & k_7 & k_7 \\ & & & & k_{14} & k_{11} \\ sym & & & & & k_{14} \end{bmatrix},$$

$$K_5 = \begin{bmatrix} k_1 & k_2 & k_8 & k_3 & k_5 & k_4 \\ & k_1 & k_8 & k_4 & k_6 & k_{11} \\ & & k_1 & k_5 & k_{11} & k_6 \\ & & & k_1 & k_8 & k_2 \\ & & & & k_1 & k_8 \\ sym & & & & & k_1 \end{bmatrix}, \qquad K_6 = \begin{bmatrix} k_{14} & k_{11} & k_7 & k_{13} & k_{10} & k_{12} \\ & k_{14} & k_7 & k_{12} & k_9 & k_2 \\ & & k_{14} & k_{10} & k_2 & k_9 \\ & & & k_{14} & k_7 & k_{11} \\ & & & & k_{14} & k_7 \\ sym & & & & & k_{14} \end{bmatrix},$$

and the $k_j, \; j = 1, ..., 14$, can be formulated as

$$\begin{aligned} k_1 &= -(3\nu - 2)/9, & k_2 &= 1/24, \\ k_3 &= -1/18, & k_4 &= -(4\nu - 1)/24, \\ k_5 &= (4\nu - 1)/24, & k_6 &= 1/36, \\ k_7 &= 1/48, & k_8 &= -1/24, \\ k_9 &= (6\nu - 5)/72, & k_{10} &= -(4\nu - 1)/48, \\ k_{11} &= -1/48, & k_{12} &= (4\nu - 1)/48, \\ k_{13} &= (3\nu - 1)/36, & k_{14} &= (3\nu - 2)/36. \end{aligned}$$

4.6 A CPD Algorithm for Topology Optimization

Based on the canonical duality theory, an evolutionary CPD algorithm[1] for solving the topology optimization problem [39] can be presented in the following.

Canonical Penalty-Duality Algorithm for Topology Optimization (CPD):

1. Initialization:
   Choose a suitable initial volume reduction rate $\mu < 1$.
   Let $\boldsymbol{\rho}^0 = \{1\} \in \mathbb{R}^n$.
   Given an initial value $\tau^0 > 0$.
   Given an initial volume $V_\gamma = \mu V_0$.
   Given a perturbation parameter $\beta > 10$, error allowances ω_1 and ω_2, in which ω_1 is a termination criterion.
   Let $\gamma = 0$

2. Compute
$$\mathbf{u}^0 = \mathbf{K}^{-1}(\boldsymbol{\rho}^0)\mathbf{f}(\boldsymbol{\rho}^0), \quad \mathbf{c}^0 = \mathbf{c}(\mathbf{u}^0) = \mathbf{u}^{0T}\mathbf{K}(\boldsymbol{\rho}^0)\mathbf{u}^0.$$

3. Let $k = 1$.

4. Compute $\boldsymbol{\zeta}_k = \{\boldsymbol{\sigma}^k, \tau^k\}$ by
$$\sigma_e^k = \frac{1}{6}\beta[-1 + \phi_e(\tau^{k-1}) + \phi_e^c(\tau^{k-1})], \quad e = 1, \ldots, n.$$

$$\tau^k = \frac{\sum_{e=1}^n \nu_e(1 + c_e^\gamma/\sigma_e^k) - 2V_\gamma}{\sum_{e=1}^n \nu_e^2/\sigma_e^k}.$$

5. If
$$\Delta = |P_u^d(\boldsymbol{\sigma}^k, \tau^k) - P_u^d(\boldsymbol{\sigma}^{k-1}, \tau^{k-1})| > \omega_1, \tag{4.64}$$
   then let $k = k + 1$, go to Step 4. Otherwise, continue.

6. Compute $\boldsymbol{\rho}^{\gamma+1} = \{\rho_e^{\gamma+1}\}$ and $\mathbf{u}^{\gamma+1}$ by
$$\rho_e^{\gamma+1} = \frac{1}{2}[1 - (\tau^k v_e - c_e^\gamma)/\sigma_e^k], \quad e = 1, \ldots, n.$$

---

[1]This algorithm was called the CDT algorithm in [39]. Since a new CDT algorithm without β perturbation has been developed, this algorithm based on the canonical penalty-duality method should be called CPD algorithm.

$$\mathbf{u}^{\gamma+1} = \mathbf{K}(\boldsymbol{\rho}^{\gamma+1})^{-1}\mathbf{f}(\boldsymbol{\rho}^{\gamma+1}).$$

7. If $|\boldsymbol{\rho}^{\gamma+1} - \boldsymbol{\rho}^{\gamma}| \leq \omega_2$ and $V_\gamma \leq V_c$, then stop. Otherwise, continue.

8. Let $V_{\gamma+1} = \mu V_\gamma$, $\tau^0 = \tau^k$, and $\gamma = \gamma + 1$, go to step 3.

Remark 1 (Volume Reduction Method and Computational Complexity)
This Remark was written by Prof. David Gao. By Theorem 10, we know that for any given desired volume $V_c > 0$, the optimal solution $\bar{\boldsymbol{\rho}}$ can be analytically obtained by (4.34) in terms of its canonical dual solution in continuous space. By the fact that the topology optimization problem $(\mathcal{P}_{bl})$ is a coupled nonconvex minimization, numerical optimization depends sensitively on the the initial volume V_0. If $\mu_c = V_c/V_0 \ll 1$, any given iteration method could lead to unreasonable numerical solutions. In order to resolve this problem, a volume decreasing control parameter $\mu \in (\mu_c, 1)$ was introduced in [39] to produce a volume sequence

$$V_\gamma = \mu V_{\gamma-1}, \ (\gamma = 1, \dots, \gamma_c),$$

such that $V_{\gamma_c} = V_c$ and for any given $V_\gamma \in [V_c, V_0]$, the problem $(\mathcal{P}_{bl})$ is replaced by

$$(\mathcal{P}_{bl})^\gamma : \quad \min \ \left\{ \mathbf{f}^T\mathbf{u} - C_p(\boldsymbol{\rho}, \mathbf{u}) \ | \quad \boldsymbol{\rho} \in \{0,1\}^n, \ \mathbf{v}^T\boldsymbol{\rho} \leq V_\gamma \right\}, \quad (4.65)$$

$$s.t. \quad \mathbf{u}(\boldsymbol{\rho}) = \arg\min\{\Pi_h(\mathbf{v}, \boldsymbol{\rho})| \ \mathbf{v} \in \mathcal{U}_a\}. \quad (4.66)$$

The initial values for solving this γ-th problem are $V_{\gamma-1}, \mathbf{u}_{\gamma-1}, \boldsymbol{\rho}_{\gamma-1}$. Theoretically speaking, for any given sequence $\{V_\gamma\}$ we should have

$$(\mathcal{P}_{bl}) = \lim_{\gamma \to \gamma_c} (\mathcal{P}_{bl})^\gamma. \quad (4.67)$$

Numerically, a different volume sequence $\{V_\gamma\}$ may produce totally different structural topology as long as the alternative iteration is used. This is intrinsic difficulty for all coupled bi-level optimal design problems.

The original idea of this sequential volume decreasing technique is from an evolutionary method for solving optimal shape design problems (see Chapter 7, [19]). It was realized recently that the same idea was used in the ESO and BESO methods. But these two methods are not polynomial-time algorithm. By the facts that there are only two loops in the CPD algorithm, i.e. the γ-loop and the k-loop, and the canonical dual solution is analytically given in the k-loop, the main computing is the $m \times m$ matrix inversion in the γ-loop. The complexity for the Gauss-Jordan elimination is

$O(m^3)$. *Therefore, the CPD is a polynomial-time algorithm.*

4.7 Applications to 3-D benchmark problems

In order to demonstrate the novelty of the CPD algorithm for solving 3-D topology optimization problems, our numerical results are compared with the two popular methods, BESO and SIMP. The algorithm for the soft-kill BESO was applied according to [47]. A modified SIMP algorithm was used according to [54]. The parameters used in BESO and SIMP are: the minimum radius $r_{\min} = 1.5$, the evolutionary rate $er = 0.05$ and the penalization power $p = 3$. Young's modulus and Poisson's ratio of the material are taken as $E = 1$ and $\nu = 0.3$, respectively. The initial value for τ used in CPD is $\tau^0 = 1$. We take the design domain $V_0 = 1$, the initial design variable $\boldsymbol{\rho}^0 = \{1\}$ for both CPD and BESO algorithms. All computations are performed by a computer with a Processor Intel Core I7-4790, CPU 3.60GHz and memory 16.0 GB.

4.7.1 Cantilever beam problems

For this benchmark problem, we present results based on three types of mesh resolutions with two types of loading conditions. All the Matlab codes, CPD, BESO and SIMP, for the cantilever beam problems are given in Appendix A.

4.7.1.1 Uniformly distributed load with $60 \times 20 \times 4$ meshes.

First, let us consider a cantilever beam with a uniformly distributed load at the right end as illustrated in Figure 4.3. The target volume and termination criterion
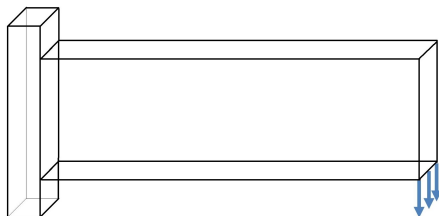
Figure 4.3: *Cantilever beam with uniformly distributed load in the right end*

for CPD, BESO and SIMP are selected as $V_c = 0.3$ and $\omega_1 = 10^{-6}$, respectively. For both CPD and BESO methods, we take the volume evolution rate $\mu = 0.89$, and the

perturbation parameter for CPD is $\beta = 4000$. The results are reported in Table 4.1[2].

Table 4.1: *Structures produced by CPD, BESO and SIMP for cantilever beam (60 × 20 × 4)*

Method	Details	Structure
CPD	$C = 1973.028$ $It. = 23$ Time= 27.1204	
BESO	$C = 1771.3694$ $It. = 154$ Time= 2392.9594	
SIMP	$C = 2416.6333$ $It. = 200$ Time= 98.7545	
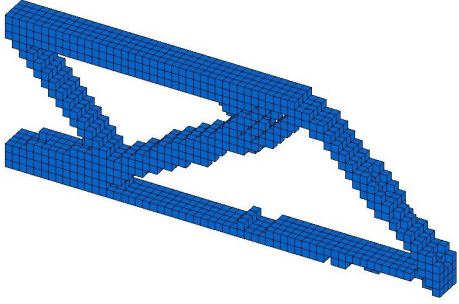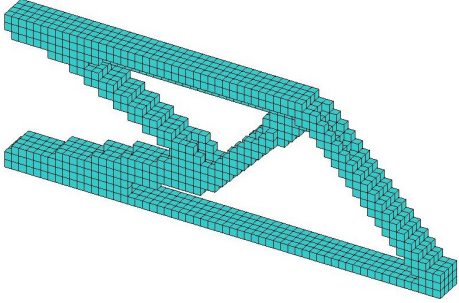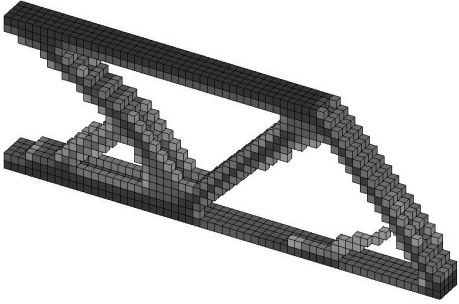
Figure 4.4 shows the convergence of compliances produced by all the three methods. It can be seen that the SIMP provides an upper bound approach since this method is based on the minimization of the compliance, i.e. the problem (P). This problem violates the minimum total potential energy principle, the SIMP converges in a strange way, i.e. the structures produced by the SIMP at the beginning are bro-

---

[2]The so-called compliance in this section is actually a doubled strain energy, i.e. $c = 2C(\boldsymbol{\rho}, \mathbf{u})$ as used in [54].

ken until $It. = 15$ (see Figure 4.4), which is physically unreasonable. Dually, both the CPD and BESO provide lower bound approaches. It is reasonable to believe that the main idea of the BESO is similar to the Knapsack problem, i.e. at each volume iteration, to eliminate elements which stored less strain energy by simply using a comparison method. By the fact that the same volume evolutionary rate μ is adopted, the results obtained by the CPD and BESO are very close to each other (see also Figure 4.5). However, the CPD is almost 100 times faster than the BESO method since the BESO is not a polynomial-time algorithm.
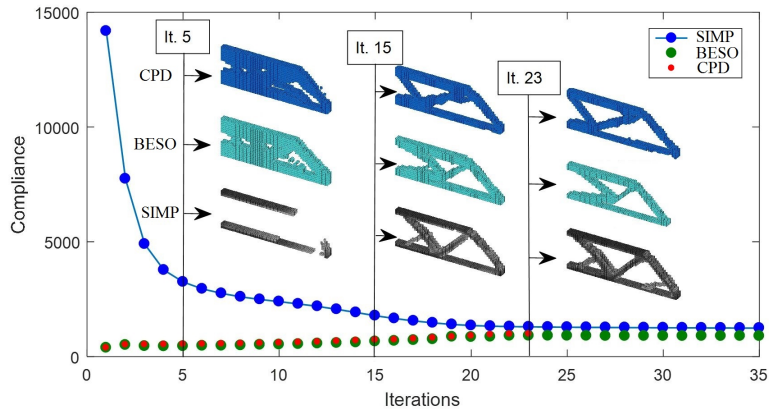
Figure 4.4: *Convergence of the compliances produced by CPD, BESO and SIMP*
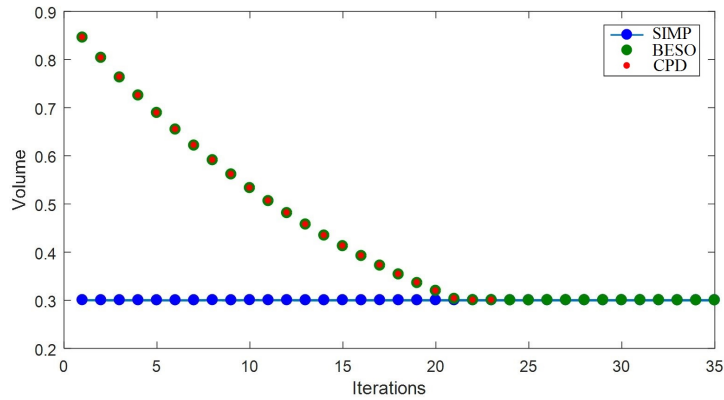
Figure 4.5: *Comparison of volume variations for CPD, BESO and SIMP*

The optimal structures produced by the CPD with $\omega_1 = 10^{-16}$ and with different values of μ and β are summarized in Table 4.2. Also, the target compliances during the iterations for all CPD examples are reported in Figure 4.6 with different values of μ and β. The results show that the CPD algorithm sensitively depends on the

volume evolution parameter μ, but not the penalty parameter β. A comparison of the volume evolutions of CPD and BESO is given in Figure 4.7, which shows as expected that the BESO method also sensitively depends on the volume evolutionary rate μ. For a fixed $\beta = 4000$, the convergence of the CPD is more stable and faster than the BESO. The C-Iteration curve for BESO jumps for every given μ, which could be the so-called "chaotic convergence curves" addressed by G. I. N. Rozvany in [67].
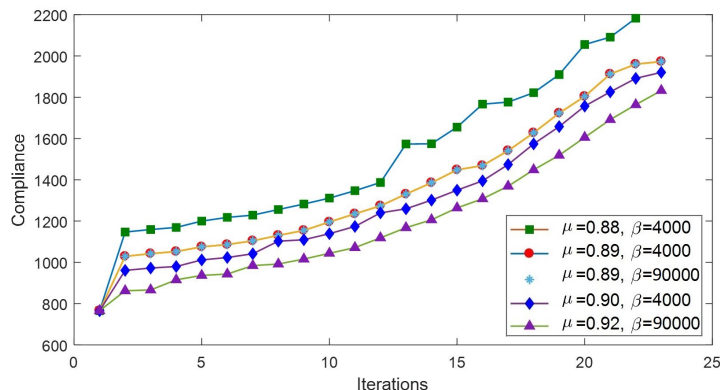
Figure 4.6: *Convergence tests for CPD method at different values of μ and β*

4.7.1.2 Uniformly distributed load with $120 \times 50 \times 8$ mesh resolution

Now let us consider the same loaded beam as shown in Figure 4.3 but with a finer mesh resolution of $120 \times 50 \times 8$. In this example the target volume fraction and termination criterion for all procedures are assumed to be $V_c = 0.3$ and $\omega_1 = 10^{-6}$, respectively. The initial volume reduction rate for both CPD and BESO is $\mu = 0.935$. The perturbation parameter for CPD is $\beta = 7000$. The optimal topologies produced by the CPD, BESO and SIMP methods are reported in Table 4.3. It can be seen that the CPD is about five times faster than the SIMP and almost 100 times faster than the BESO method.

If we choose $\omega_1 = 0.001$, the computing times (iterations) for CPD, BESO and SIMP are 0.97 (24), 24.67 (44) and 4.3 (1000) hours, respectively. Actually, the SIMP failed to reach the given precision. If we increase $\omega_1 = 0.01$, the SIMP takes 3.14 hours with 742 iterations to satisfy the given precision. Our numerical results show that the CPD method can produce very good results with much less computing time. For a given very small $\omega_1 = 10^{-16}$, Table 4.4 shows the effects of the parameters of μ, β and V_c on the computing time of the CPD method.
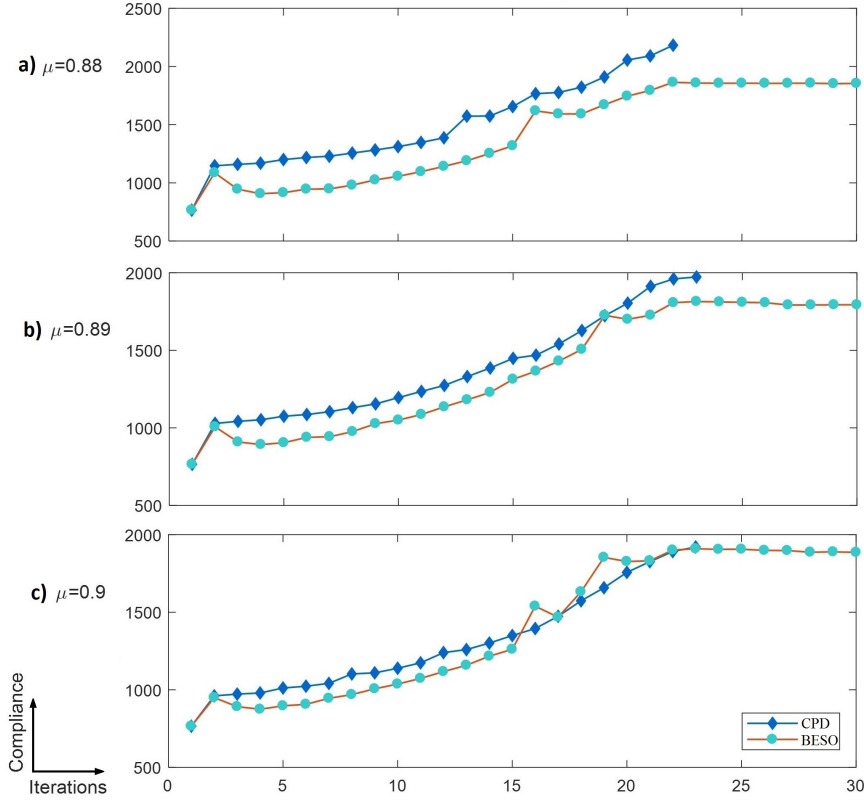
Figure 4.7: *Convergence test for CPD and BESO with different μ.*

4.7.1.3 Beam with a central load and $40 \times 20 \times 20$ meshes

In this example, the beam is subjected to a central load at its right end (see Figure 4.8). We let $V_c = 0.095$, $\omega_1 = 0.001$, $\beta = 7000$ and $\mu = 0.888$. The topology
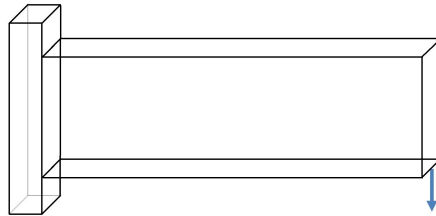
Figure 4.8: *Design domain for a cantilever beam with a central load in the right end*

optimized structures produced by CPD, SIMP and BESO methods are summarized in Table 4.5. Compared with the SIMP method, we can see that by using only 20% of the computing time, the CPD can produce a global optimal solution, which is better than that produced by the BESO, but with only 8% of computing time. We

Table 4.2: *Optimal structures produced by CPD with different values of μ and β*

Details	Structure	Details	Structure
$\mu = 0.88$ $\beta = 4000$ $C = 2182.78$ $It. = 22$ Time=29.44		$\mu = 0.89$ $\beta = 90000$ $C = 1973.02$ $It. = 23$ Time=30.69	
$\mu = 0.9$ $\beta = 4000$ $C = 1920.68$ $It. = 23$ Time=30.87		$\mu = 0.92$ $\beta = 90000$ $C = 1832.59$ $It. = 23$ Time=33.73	
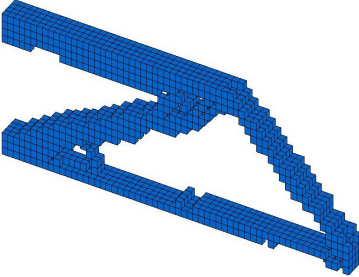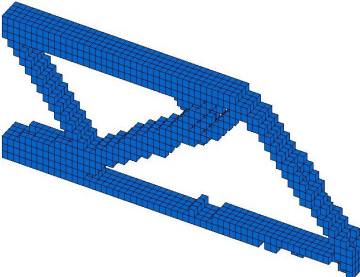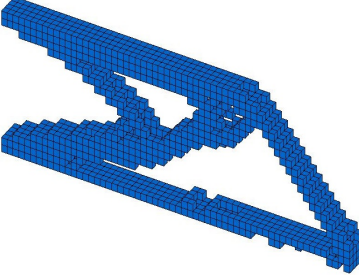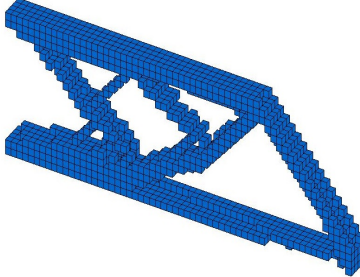
should point out that for the given $\omega_1 = 0.001$, the SIMP method failed to converge in 1000 iterations (the so-called "change" $\Delta = 0.0061 > \omega_1$).

4.7.2 MBB beam

The second benchmark problem is the 3-D Messerschmitt-Bölkow-Blohm (MBB) beam. Two examples with different loading and boundary conditions are given.

4.7.2.1 Example 1

The MBB beam design for this example is illustrated in Figure 4.9. In this example, we use $40 \times 20 \times 20$ mesh resolution, $V_c = 0.1$ and $\omega_1 = 0.001$. The initial volume reduction rate and perturbation parameter are $\mu = 0.89$ and $\beta = 5000$, respectively.

Table 4.6 summarizes the optimal topologies by using CPD, BESO and SIMP methods. Compared with the BESO method, it can again be seen that the CPD produces a mechanically sound structure and takes only 12.6% of the computing time. Also, the SIMP method failed to converge for this example and the result presented in Table 4.6 is only the output of the 1000th iteration when $\Delta = 0.039 > \omega_1$.

Table 4.3: *Topology optimization for a cantilever beam ($120 \times 50 \times 8$)*

Method	Details	Structure
CPD	$C = 1644.0886$ $It. = 24$ Time=3611.23	
BESO	$C = 1605.1102$ $It. = 200$ Time=342751.96	
SIMP	$C = 1835.4106$ $It. = 1000$ Time=15041.06	
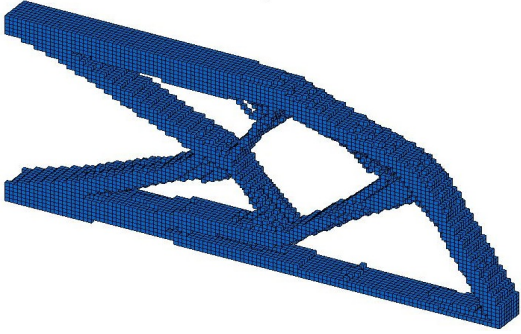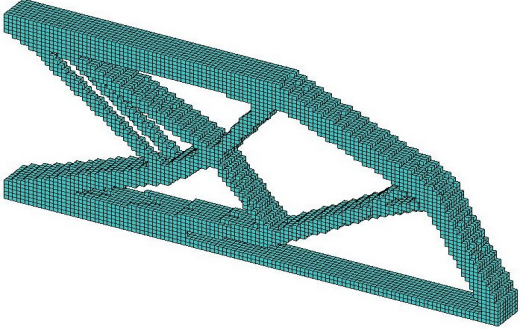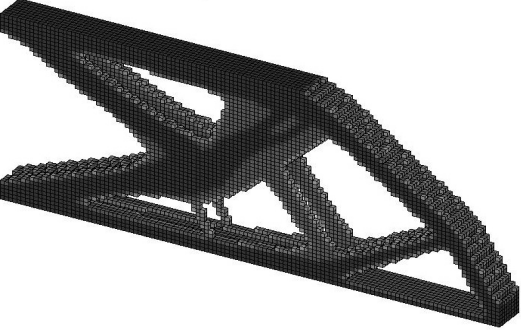
4.7.2.2 Example 2

In this example, the MBB beam is supported horizontally on its four bottom corners under a central load, as shown in Figure 4.10. The mesh resolution is $60 \times 10 \times 10$, the target volume is $V_c = 0.155$. The initial volume reduction rate and perturbation parameter are defined as $\mu = 0.943$ and $\beta = 7250$, respectively.

Table 4.4: *Effects of μ, β and V_c to the final results by CPD method ($\omega_1 = 10^{-16}$)*

$\mu = 0.935$, $\beta = 3000$ $V_c = 0.3$, $C = 1632.959$ *It.* =25, Time=3022.029	$\mu = 0.935$, $\beta = 7000$ $V_c = 0.18$, $C = 2669.980$ *It.* =34, Time=5040.6647
$\mu = 0.98$, $\beta = 7000$ $V_c = 0.3$, $C = 1635.922$ *It.* =25, Time=3531.3235	$\mu = 0.98$, $\beta = 7000$ $V_c = 0.18$, $C = 2892.914$ *It.* =35, Time=4853.3776
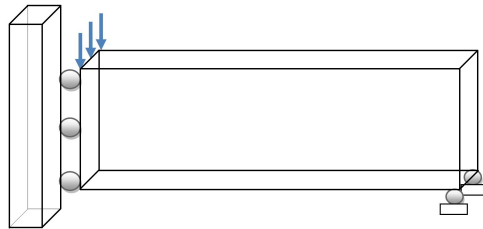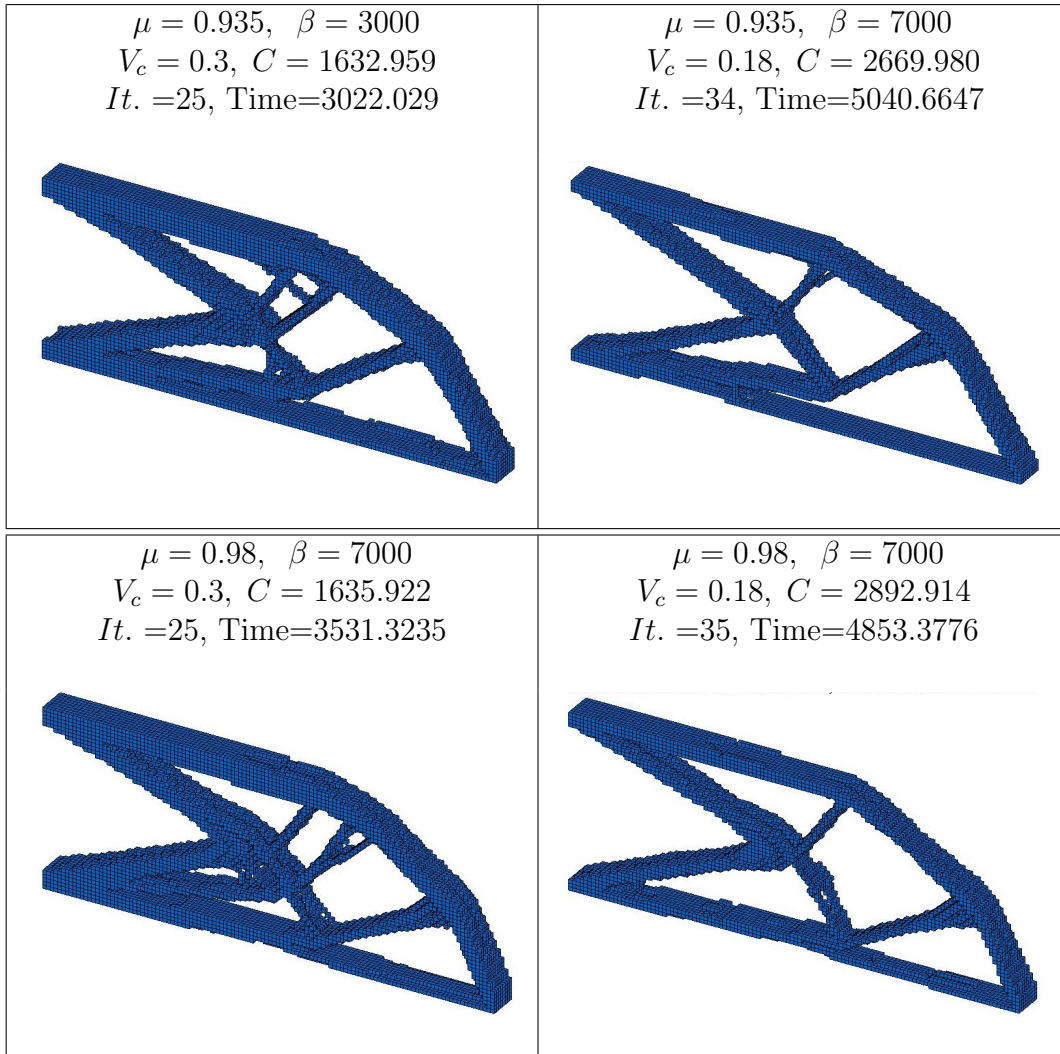
Figure 4.9: *MBB beam with uniformly distributed central load*

The topology optimized structures produced by the CPD, BESO and SIMP with $\omega_1 = 10^{-5}$ are reported in Table 4.7. Once again, it can be seen that without using any artificial techniques, the CPD produces a mechanically sound integer density

Table 4.5: *Topologies of the cantilever beam with a central load on the right end*

CPD: $C = 20.564$, $It. = 45$, Time=959.7215

BESO: $C = 20.1533$, $It. = 53$, Time=11461.128

SIMP: $C = 25.7285$, $It. = 1000$, Time=4788.4762
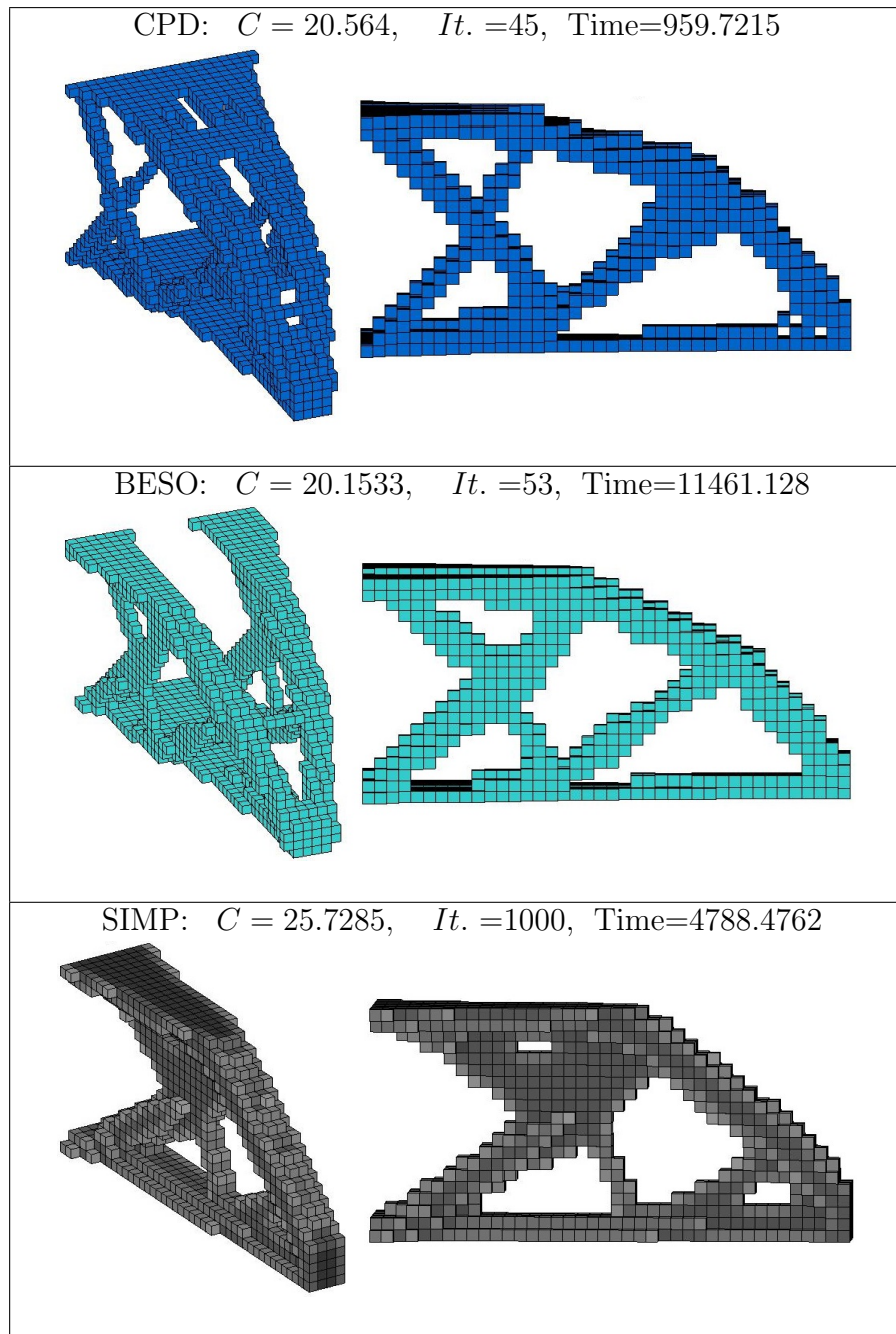
distribution but the computing time is only 3.3% of that used by the BESO.

Table 4.6: *Results for a 3-D MBB beam with a uniformly distributed load*

CPD: $C = 7662.5989$, $It.=46$, Time=1249.1267

BESO: $C = 7745.955$, $It. =55$, Time=9899.0921

SIMP: $C = 12434.8629$, $It. =1000$, Time=5801.0065
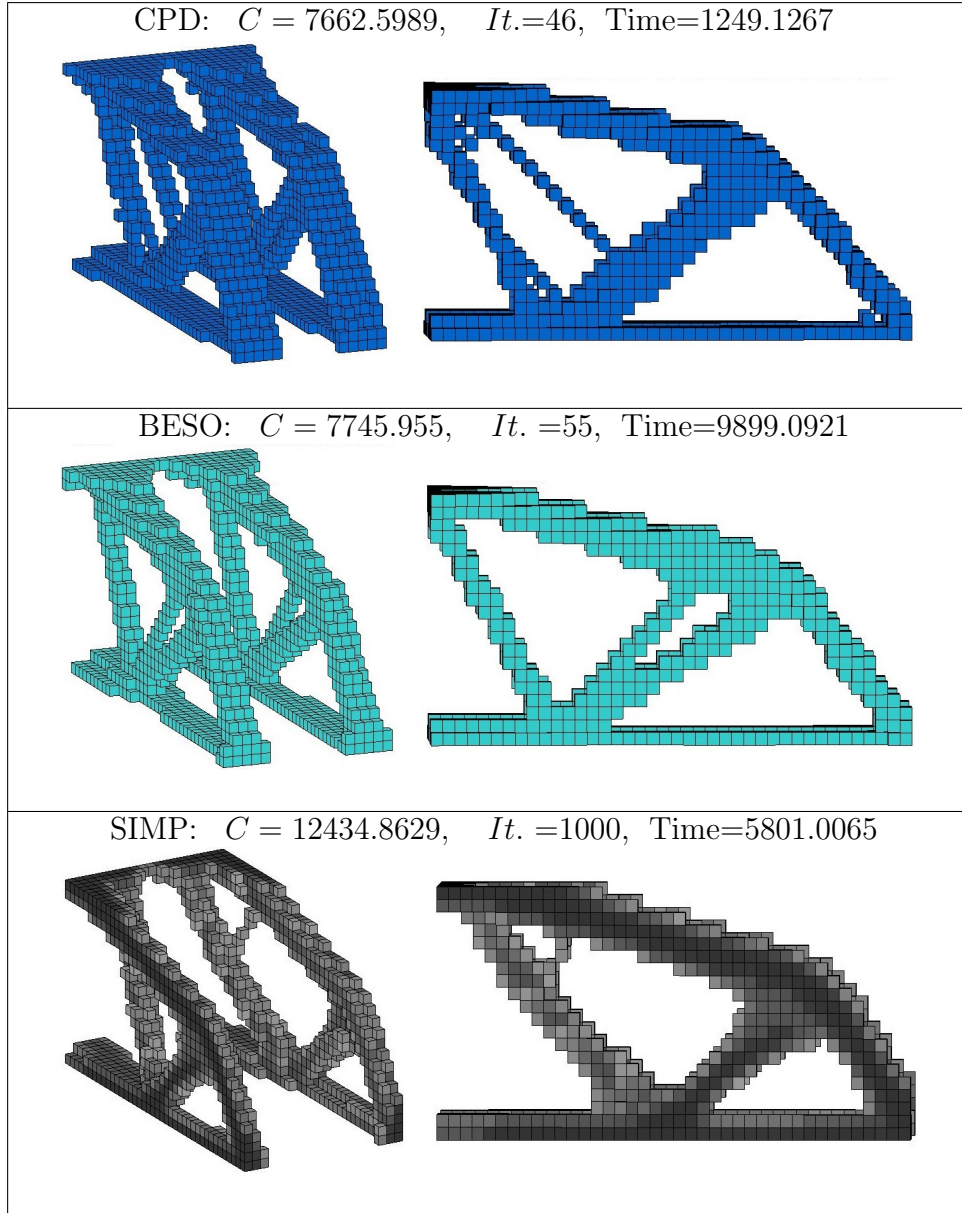
4.7.3 Cantilever beam with a given hole

In real-world applications, the desired structures are usually subjected to certain design constraints such that some elements are required to be either solid or void. Now let us consider a cantilever beam with a given hole, as illustrated in Figure 4.11. We use mesh resolution $70 \times 30 \times 6$ and parameters $V_c = 0.5$, $\beta = 7000$, $\mu = 0.94$ and $\omega_1 = 0.001$.

The optimal topologies produced by CPD, BESO, and SIMP are summarized in
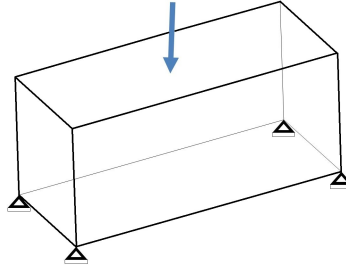
Figure 4.10: *3-D MBB beam with a central load*
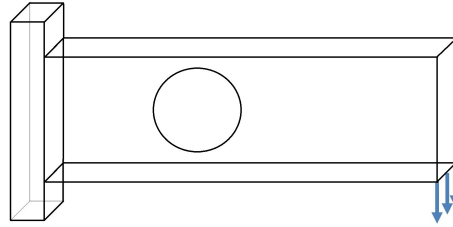
Figure 4.11: *Design domain for a cantilever beam with a given hole*

Table 4.8. The results show clearly that the CPD method is significantly faster than both BESO and SIMP. Again, the SIMP failed to converge in 1000 iterations and the "Change" $\Delta = 0.011 > \omega_1$ at the last iteration.

4.7.4   3-D wheel problem

The 3-D wheel design problem is constrained by a planar joint on the corners with a downward point load in the center of the bottom, as shown in Figure 4.12. The mesh resolution for this problem is $40 \times 20 \times 40$. The target volume is $V_c = 0.2$ and the parameters used are $\beta = 150$, $\mu = 0.94$ and $\omega_1 = 10^{-5}$. The optimal topologies produced by CPD, BESO and SIMP are reported in Table 4.9. It can be seen that the CPD takes only about 18% and 32% of the computing time of BESO and SIMP, respectively. Once again, the SIMP failed to converge in 1000 iterations and the "Change" $\Delta = 0.0006 > \omega_1$ at the last iteration.

For a given very small termination criterion $\omega_1 = 10^{-16}$ and for mesh resolution $30 \times 20 \times 30$, Table 4.10 shows thr effects of the parameters μ and V_c on the topology optimized results of CPD. Clearly, for a fixed $\mu = 0.88$, If we decrease the target volume fraction V_c, the number of iterations increases and many solid elements disappear, as shown in the first two columns of Table 4.10. It can also be seen that, if the same target volume fraction $V_c = 0.1$ is adopted, a slight difference appears on

Table 4.7: *Structures for 3-D MBB beam with a central load*

Method	Details	Structure
CPD	$C = 19.5313$ $It. \quad = \quad 37$ Time=48.2646	
BESO	$C = 20.1132$ $It. \qquad =57$ Time=1458.488	
SIMP	$C = 41.4099$ $It. \qquad =95$ Time=366.4988	
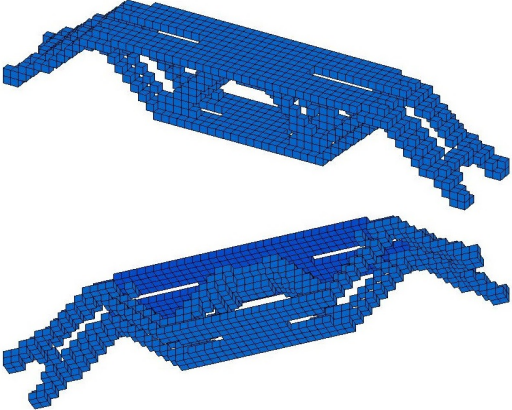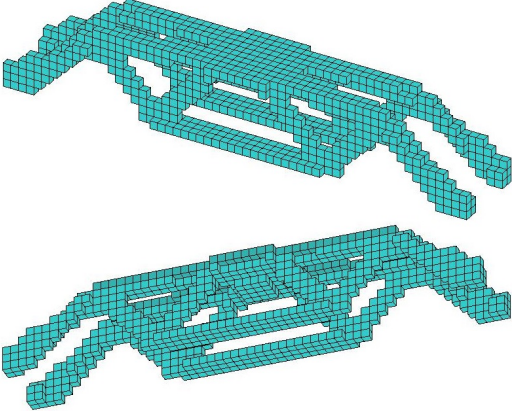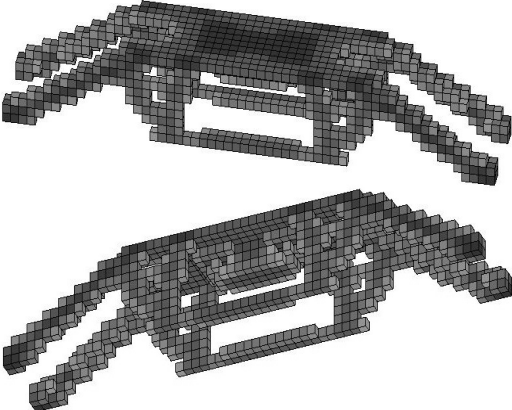
Table 4.8: *Topology optimized structures for a cantilever beam with a given hole*

CPD: $C = 910.0918$, $It.. = 14$,   Time=74.61

BESO: $C = 916.3248$, $It. = 21$,   Time=1669.5059

SIMP: $C = 997.1556$, $It. = 1000$,   Time=1932.7697
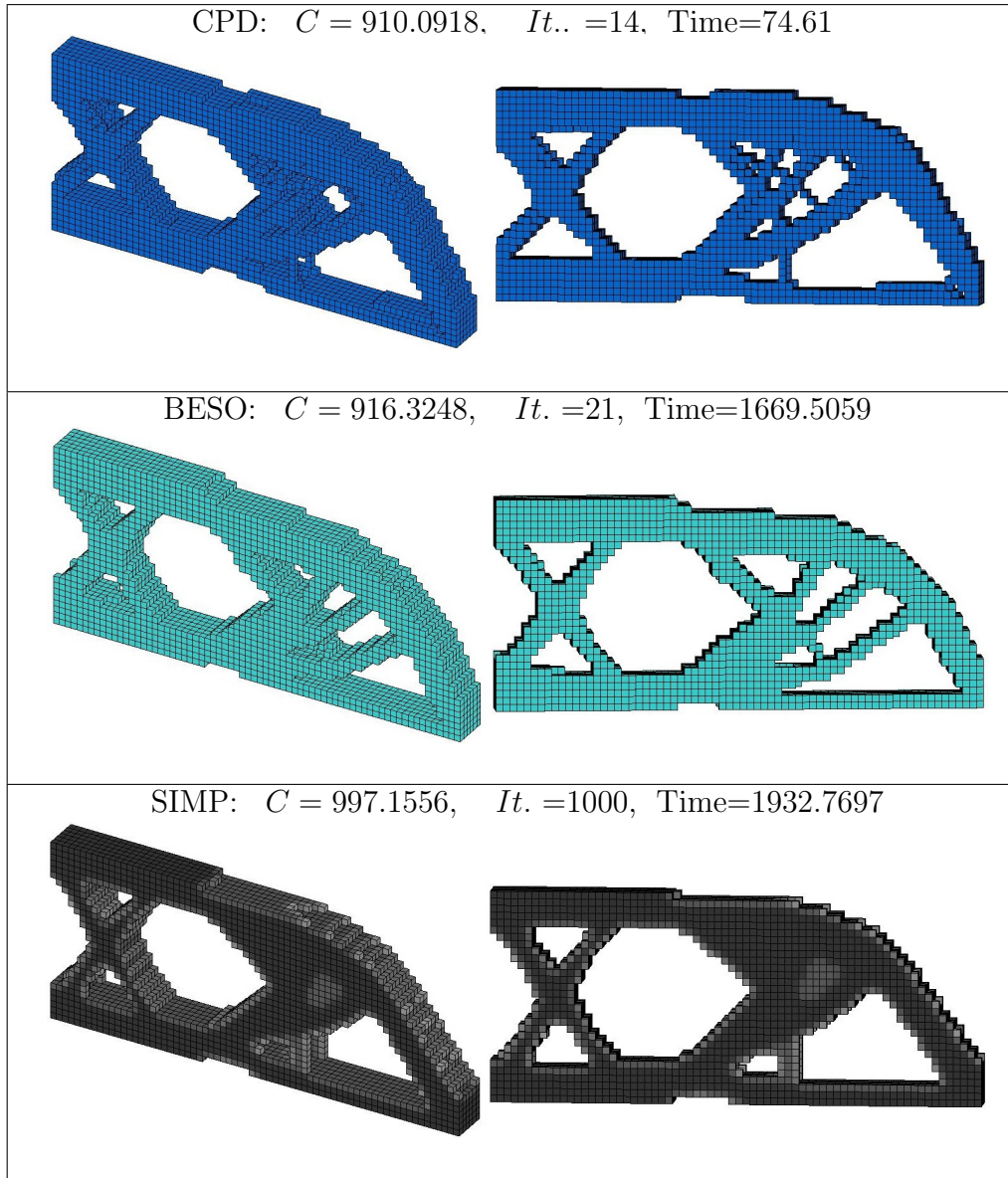
the 3-D wheel design when the parameter μ is changed from 0.88 to 0.92. The results show that, the latest value of μ makes the body more solid as shown in the last two columns of Table 4.10, that means the global optimal solution of CPD algorithm depends sensitively on the evolutionary rate $\mu \in [\mu_c, 1)$.
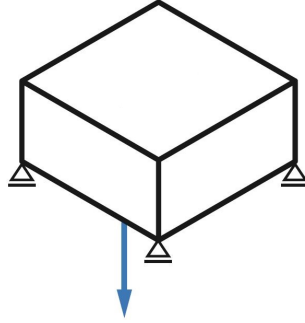
Figure 4.12: *3-D wheel problem*

Table 4.9: *Topology optimized results for a 3-D wheel problem (40 × 20 × 40) for CPD (left), BESO (middle), and SIMP (right)*

$C = 3.6164,\ It.\ =32$ Time=6716.1433	$C = 3.6135,\ It.\ =66$ Time=37417.5089	$C = 3.7943,\ It.\ =1000$ Time=20574.8348

4.8   Summary

We have presented a novel canonical penalty-duality (CPD) method for solving challenging topology optimization problems. The relation between the CPD method for solving 0-1 integer programming problems and the pure complementary energy principle in nonlinear elasticity is revealed for the first time. Applications are demonstrated by 3-D linear elastic structural topology optimization problems. By the fact that the integer density distribution is obtained analytically, it should be considered as the global optimal solution at each volume iteration. Generally speaking, the so-called compliance produced by the CPD is higher than those by BESO for most of the tested problems except for the MBB beam and the cantilever beam with a given hole. A possible reason for this is that certain artificial techniques such as the so-called soft-kill, filter and sensitivity are used by the BESO method. The follow-

96

Table 4.10: *Topology optimized results for CPD for the 3-D wheel problem (30 × 20 × 30) with two different views*

$\mu = 0.88$, $V_c = 0.06$ $C = 5.7296$, *It.* $=55$ Time=2324.0445	$\mu = 0.88$, $V_c = 0.1$ $C = 4.2936$, *It.* $=44$ Time=1888.6451	$\mu = 0.92$, $V_c = 0.1$ $C = 4.3048$, *It.* $=45$ Time=1823.7826
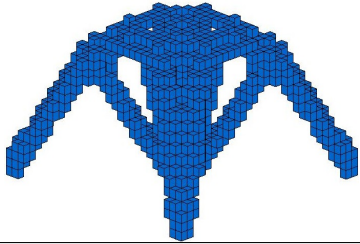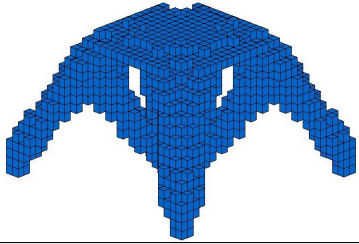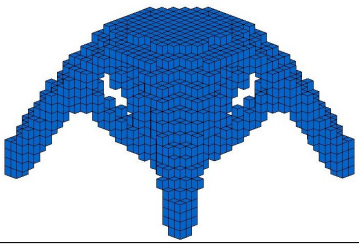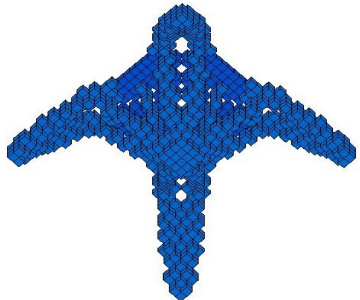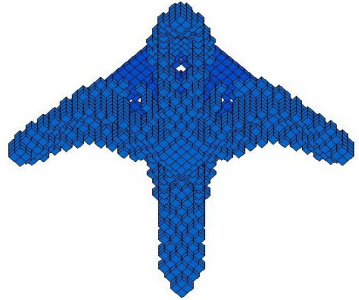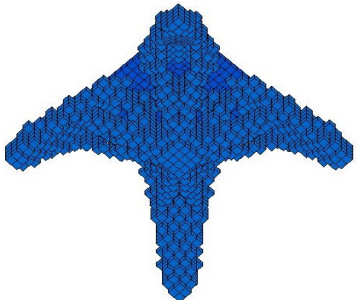
ing remarks are important for understanding these popular methods and conceptual mistakes in topology optimization.

Remark 2 (On Penalty-Duality, SIMP, and BESO Methods)

This Remark was written by Prof. David Gao. It is well-known that the Lagrange multiplier method can be used essentially for solving convex problem with equality constraints. The Lagrange multiplier must be a solution to the Lagrangian dual problem (see the Lagrange Multiplier's Law in [19], page 36). For an inequality constraint, the Lagrange multiplier must satisfy the KKT conditions. The penalty method can be used for solving problems with both equality and inequality constraints, but the iteration method must be used. By the fact that the penalty parameter is hard to control during the iterations and in principle, needs to be large enough for the penalty function to be truly effective, which on the other hand, may cause numerical instabilities, the penalty method was becoming disreputable after the augmented Lagrange multiplier method was proposed in 1970 and 1980s. The augmented Lagrange multiplier method is simply the combination of the Lagrange multiplier method and the penalty method, which has been actively studied for more than 40 years. But this method can be used mainly for solving linearly constrained problems since any simple nonlinear

97

constraint could lead to a nonconvex minimization problem [51].

For example, let us consider the Knapsack problem $(\mathcal{P}_u)$. As we know by using the canonical measure

$$\Lambda(\boldsymbol{\rho}) = \boldsymbol{\rho} \circ \boldsymbol{\rho} - \boldsymbol{\rho},$$

the 0-1 integer constraint $\boldsymbol{\rho} \in \{0,1\}^n$ can be equivalently written in equality

$$\boldsymbol{\rho} \circ \boldsymbol{\rho} - \boldsymbol{\rho} = \mathbf{0}.$$

Even for this most simple quadratic nonlinear equality constraint, its penalty function

$$W_\beta = \beta\|\boldsymbol{\rho} \circ \boldsymbol{\rho} - \boldsymbol{\rho}\|^2,$$

is a nonconvex function. In order to solve this nonconvex optimization problem, the canonical duality theory has to be used as discussed in Section 4.4. The idea for this penalty-duality method was originally from Gao's PhD thesis [11]. By Theorem 10, the canonical dual variable $\boldsymbol{\sigma}$ is exactly the Lagrange multiplier to the canonical equality constraint

$$\boldsymbol{\varepsilon} = \Lambda(\boldsymbol{\rho}) = \boldsymbol{\rho} \circ \boldsymbol{\rho} - \boldsymbol{\rho} = \mathbf{0},$$

the penalty parameter β is theoretically not necessary for the canonical duality approach. But, by this parameter, the canonical dual solution can be analytically and uniquely obtained. By Theorem 7 in [29], there exists a $\beta_c > 0$ such that for any given $\beta \geq \beta_c$, this analytical solution solves the canonical dual problem $(\mathcal{P}_u^d)$, therefore, parameter β is not arbitrary and no iteration is needed for solving the β-perturbed canonical dual problem $(\mathcal{P}_\beta^d)$.

The SIMP problem (P_{simp}) in (4.1) can be formulated as a box constrained minimization problem:

$$(P_{sp}): \quad \min\left\{\frac{1}{2}\mathbf{u}^T\mathbf{K}(\boldsymbol{\rho}^p)\mathbf{u} \mid \mathbf{K}(\boldsymbol{\rho}^p)\mathbf{u} = \mathbf{f}, \ \mathbf{u} \in \mathcal{U}_a, \ \boldsymbol{\rho} \in \mathcal{Z}_b\right\}, \qquad (4.68)$$

and

$$\mathcal{Z}_b = \{\boldsymbol{\rho} \in \mathbb{R}^n \mid \boldsymbol{\rho}^T\mathbf{v} \leq V_c, \ \boldsymbol{\rho} \in (0,1]^n\}.$$

By the fact that $\boldsymbol{\rho}^p = \boldsymbol{\rho} \ \forall p \in \mathbb{R}, \ \forall \boldsymbol{\rho} \in \{0,1\}^n$, the problem (P_{sp}) is obtained from (P_s) by artificially replacing the integer constraint $\boldsymbol{\rho} \in \{0,1\}^n$ in $\mathcal{Z}_a$ with the box constraint $\boldsymbol{\rho} \in (0,1]^n$. Therefore, the SIMP is not a mathematically correct penalty method for solving the integer constrained problem (P_s) and p is not a correct penalty

parameter. The alternative iteration cannot be used for solving (P_{sp}) and the target function must be written in term of $\boldsymbol{\rho}$ only, i.e.

$$P_c(\boldsymbol{\rho}^p) = \frac{1}{2}\mathbf{f}^T[\mathbf{K}(\boldsymbol{\rho}^p)]^{-1}\mathbf{f},$$

which is not a coercive function and, for any given $p > 1$, its extrema are usually located on the boundary of $\mathcal{Z}_b$ (see [38]). Therefore, unless some artificial techniques are adopted, any mathematically correct approximations to (P_{sp}) cannot produce reasonable solutions to either (P_c) or (P_s). Indeed, from all the examples presented above, the SIMP produces only gray-scaled topology, and from Figure 4.4 we can see clearly that during the first 15 iterations, the structures produced by SIMP are broken, which are both mathematically and physically unacceptable. Also, the so-called magic number $p = 3$ works only for certain homogeneous material/structures. For general composite structures, the global min of $P_c(\boldsymbol{\rho}^3)$ cannot be integers [38].

The BESO problem (P_{beso}) in (4.6), as formulated in [44] is posed in the form of minimization of mean compliance, i.e. problem (P). Since the alternative iteration is adopted by BESO, this alternative iteration leads to an anti-Knapsack problem, the BESO should theoretically produce only a trivial solution at each volume evolution. However, a comparison method is used to determine whether an element needs to be added to or removed from the structure, which is actually a direct method for solving the Knapsack problem $(\mathcal{P}_u)$. This is the reason why the numerical results obtained by BESO are similar to that by CPD. But, the direct method is not a polynomial-time algorithm. Due to the combinatorial complexity, this popular method is computationally expensive and be used only for small sized problems. This is the very reason that the Knapsack problem was considered as NP-complete for all existing direct approaches.

Remark 3 (On Compliance, Objectivity, and Modeling in Engineering Optimization)
This Remark was written by Prof. David Gao. By Wikipedia (see $\mathtt{https://en.}$ $\mathtt{wikipedia.org/wiki/Stiffness}$), the concept of "compliance" in mechanical science is defined as the inverse of stiffness, i.e. if the stiffness of an elastic bar is k, then the compliance should be $c = 1/k$, which is also called the flexibility. In 3-D linear elasticity, the stiffness is the Hooke tensor $\mathbf{K}$, which is associated with the strain energy

$$W(\boldsymbol{\varepsilon}) = \frac{1}{2}\boldsymbol{\varepsilon} : \mathbf{K} : \boldsymbol{\varepsilon},$$

while the compliance is $\mathbf{C} = \mathbf{K}^{-1}$, which is associated with the complementary energy

$$W^*(\boldsymbol{\sigma}) = \frac{1}{2}\boldsymbol{\sigma} : \mathbf{K}^{-1} : \boldsymbol{\sigma}.$$

However, in the topology optimization literature, the linear function

$$F(\mathbf{u}) = \mathbf{u}^T\mathbf{f},$$

is called the compliance. Mathematically speaking, the inner product $\mathbf{u}^T\mathbf{f}$ is a scalar, while the compliance $\mathbf{C}$ is a matrix; physically, the scaler-valued function $F(\mathbf{u})$ represents the external (or input) energy, while the compliance matrix $\mathbf{C}$ depends on the material of structure, which is related to the internal energy $W^*(\boldsymbol{\sigma})$. Therefore, they are two very different concepts, and erroneously using these interchangeably could lead to serious confusions in multidisciplinary research[3] Also, the well-defined stiffness and compliance are mainly for linear elasticity. For nonlinear elasticity or plasticity, the strain energy is nonlinear and the complementary energy cannot be explicitly defined. For nonconvex $W(\boldsymbol{\varepsilon})$, the complementary energy is not unique. In these cases, even if stiffness can be defined by the Hessian matrix $\mathbf{K}(\boldsymbol{\varepsilon}) = \nabla^2 W(\boldsymbol{\varepsilon})$, the compliance $\mathbf{C}$ cannot be well-defined since $\mathbf{K}(\boldsymbol{\varepsilon})$ could be singular even for the so-called G-quasiconvex materials [40].

Objectivity is a central concept in our daily life, related to reality and truth. According to Wikipedia, objectivity in philosophy means the state or quality of being true even outside a subject's individual biases, interpretations, feelings, and imaginings[4]. In science, objectivity is often attributed to the property of scientific measurement, as the accuracy of a measurement can be tested independently from the individual scientist who first reports it[5]. In continuum mechanics, it is well-known that a real-valued function $W(\boldsymbol{\varepsilon})$ is called objective if and only if $W(\boldsymbol{\varepsilon}) = W(\mathbf{R}\boldsymbol{\varepsilon})$ for any given rotation tensor $\mathbf{R} \in \mathrm{SO}(3)$, i.e. $W(\boldsymbol{\varepsilon})$ must be an invariant under rigid rotation, (see [9], and Chapter 6 [19]). The duality relation $\boldsymbol{\varepsilon}^* = \nabla W(\boldsymbol{\varepsilon})$ is called the constitutive law, which is independent of any particularly given problem. Clearly, any linear function is not objective. The objectivity lays a foundation for mathematical modeling. In order to emphasize its importance, the objectivity is also called the principle of

---

[3] The strain energy is also called the compliance in topology optimization and (P_c) is a correct model for topology optimization. The general problem $(\mathcal{P}_{bl})$ was originally formulated as a minimum total potential energy so that using $\mathbf{f} = \mathbf{K}(\boldsymbol{\rho})\bar{\mathbf{u}}$, $\min\{\Pi_h(\bar{\mathbf{u}}, \boldsymbol{\rho})| \ \boldsymbol{\rho} \in \mathcal{Z}_a\} = \min\{-\frac{1}{2}\mathbf{c}(\mathbf{u})\boldsymbol{\rho}^T| \ \boldsymbol{\rho} \in \mathcal{Z}_a\}$ is a Knapsack problem [39].

[4] https://en.wikipedia.org/wiki/Objectivity_(philosophy)

[5] https://en.wikipedia.org/wiki/Objectivity_(science)

frame-indifference in continuum physics [80].

Unfortunately, this fundamentally important concept has been mistakenly used in the optimization literature with other functions, such as the target, cost, energy, and utility functions, etc[6]. As a result, the general optimization problem has been proposed as

$$\min f(x), \quad s.t. \ g(x) \le 0, \tag{4.69}$$

and the arbitrarily given $f(x)$ is called the objective function[7], which is also allowed to be a linear function. Clearly, this general problem is artificial. Without detailed information on the functions $f(x)$ and $g(x)$, it is impossible to have a powerful theory and method for solving this artificially given problem. It turns out that many nonconvex/nonsmooth optimization problems are considered to be NP-hard.

In linguistics, a grammatically correct sentence should be composed by at least three components: subject, object and a predicate. Based on this rule and the canonical duality principle [19], a unified mathematical problem for multi-scale complex systems was proposed by Gao in [35]:

$$(\mathcal{P}_g): \quad \min\{\Pi(\mathbf{u}) = W(\mathbf{Du}) - F(\mathbf{u})| \ \mathbf{u} \in \mathcal{U}_c\}, \tag{4.70}$$

where $W(\boldsymbol{\varepsilon}) : \mathcal{E}_a \to \mathbb{R}$ is an objective function such that the internal duality relation

$$\boldsymbol{\varepsilon}^* = \nabla W(\boldsymbol{\varepsilon}),$$

is governed by the constitutive law, its domain $\mathcal{E}_a$ contains only physical constraints (such as the incompressibility and plastic yield conditions [12]), which depends on mathematical modeling; $F(\mathbf{u}) : \mathcal{U}_a \to \mathbb{R}$ is a subjective function such that the external duality relation

$$\mathbf{u}^* = \nabla F(\mathbf{u}) = \mathbf{f},$$

is a given input (or source), its domain $\mathcal{U}_a$ contains only geometrical constraints (such as boundary and initial conditions), which depends on each given problem; $\mathbf{D} : \mathcal{U}_a \to \mathcal{E}_a$ is a linear operator which links the two spaces $\mathcal{U}_a$ and $\mathcal{E}_a$ with different physical scales; the feasible space is defined by $\mathcal{U}_c = \{\mathbf{u} \in \mathcal{U}_a| \ \mathbf{Du} \in \mathcal{E}_a\}$. The predicate in $(\mathcal{P}_g)$ is the operator "$-$" and the difference $\Pi(\mathbf{u})$ is called the target function in general problems. The object and subject are in balance only at the

---

[6] `http://en.wikipedia.org/wiki/Mathematical_optimization`

[7] This terminology is used mainly in English literature. The function $f(x)$ is correctly called the target function in Chinese and Japanese literature.

optimal states.

The unified form $(\mathcal{P}_g)$ covers general constrained nonconvex/nonsmooth/discrete variational and optimization problems in multi-scale complex systems [41, 26]. Since the input $\mathbf{f}$ does not depend on the output $\mathbf{u}$, the subjective function $F(\mathbf{u})$ must be linear. Dually, the objective function $W(\boldsymbol{\varepsilon})$ must be nonlinear such that there exists an objective measure $\boldsymbol{\xi} = \Lambda(\mathbf{u})$ and a convex function $\Psi(\boldsymbol{\xi})$, hence the canonical transformation $W(\mathbf{Du}) = \Psi(\Lambda(\mathbf{u}))$ holds for most real-world systems. This is the reason why the canonical duality theory was naturally developed and can be used to solve general challenging problems in multidisciplinary fields. However, since objectivity has been misused in the optimization community, this theory was mistakenly challenged by M.D. Voisei and C. Zălinescu (cf. [41]). By oppositely choosing linear functions for $W(\boldsymbol{\varepsilon})$ and nonlinear functions for $F(\mathbf{u})$, they produced a list of "count-examples" and concluded: "a correction of this theory is impossible without falling into trivial". The conceptual mistakes in their challenges revealed at least two important truths:

1. *there exists a huge gap between optimization and mechanics;*

2. *incorrectly using the well-defined concepts can lead to absurd arguments.*

Interested readers are recommended to read recent paper [36] for further discussion.

For continuous systems, the necessary optimality condition for the general problem $(\mathcal{P}_g)$ leads to an abstract equilibrium equation

$$\mathbf{D}^*\partial_{\boldsymbol{\varepsilon}}W(\mathbf{Du}) = \mathbf{f}. \tag{4.71}$$

It is linear if the objective function $W(\boldsymbol{\varepsilon})$ is a quadratic. This abstract equation includes almost all the well-known equilibrium problems in textbooks from partial differential equations in mathematical physics to algebraic systems in numerical analysis and optimization [79]. In mathematical economics, if the output $\mathbf{u} \in \mathcal{U}_a \subset \mathbb{R}^n$ represents the product of a manufacturing company, the input $\mathbf{f}$ can be considered as the market price of $\mathbf{u}$, then the subjective function $F(\mathbf{u}) = \mathbf{u}^T\mathbf{f}$ in this example is the total income of the company. The products are produced by workers $\boldsymbol{\varepsilon} = \mathbf{Du}$ and $\mathbf{D} \in \mathbb{R}^{m \times n}$ is a cooperation matrix. The workers are paid by salary $\boldsymbol{\varepsilon}^* = \nabla W(\boldsymbol{\varepsilon})$ and the objective function $W(\boldsymbol{\varepsilon})$ is the total cost. Thus, the optimization problem $(\mathcal{P}_g)$ is to minimize the total loss $\Pi(\mathbf{u})$ under certain given constraints in $\mathcal{U}_c$. A comprehensive review on modeling, problems and NP-hardness in multi-scale optimization is given in [42].

In summary, the theoretical results presented in this chapter show that the canonical duality theory is indeed an important methodological theory not only for solving the most challenging topology optimization problems, but also for correctly understanding and modeling multi-scale problems in complex systems. The numerical results verified that the CPD method can produce a mechanically sound optimal topology, and it is much more powerful than the popular SIMP and BESO methods. Specific conclusions are as follows:

1. The mathematical model for general topology optimization should be formulated as a bi-level mixed integer nonlinear programming problem $(\mathcal{P}_{bl})$. This model works for both linearly and nonlinearly deformed elasto-plastic structures.

2. The alternative iteration is allowed for solving $(\mathcal{P}_{bl})$, which leads to a Knapsack problem for linear elastic structures. The CPD is a polynomial-time algorithm, which can solve $(\mathcal{P}_{bl})$ to obtain a global optimal solution at each volume iteration.

3. The pure complementary energy principle is a special application of the canonical duality theory in nonlinear elasticity. This principle plays an important role not only in nonconvex analysis and computational mechanics, but also in topology optimization, especially for large deformed structures.

4. Unless a magic method is proposed, the volume evolution is necessary for solving $(\mathcal{P}_{bl})$ if $\mu_c = V_c/V_0 \ll 1$. But the global optimal solution depends sensitively on the evolutionary rate $\mu \in [\mu_c, 1)$.

5. The compliance minimization problem (P) should be written in the form of (P_c) instead of the minimum strain energy form (P_s). The problem (P_c) is actually a single-level reduction of $(\mathcal{P}_{bl})$ for linear elasticity. An alternative iteration for solving (P_s) leads to an anti-Knapsack problem.

6. The SIMP method is not a mathematically correct penalty method for solving either (P) or (P_c). Even if the magic number $p = 3$ works for certain material/structures, this method cannot produce correct integer solutions.

7. Although the BESO algorithm is posed in the form of minimization of mean compliance, it is actually a direct method for solving a Knapsack problem at each volume reduction. For small-scale problems, BESO can produce reasonable results much better than SIMP. But it is time consuming for large-scale

topology optimization problems since the direct method is not a polynomial-time algorithm.

Chapter 5

Conclusions and future work

5.1   Conclusions

A detailed study of a large deformation problem in 2-D structure is presented. The extremality condition is a fundamentally difficult problem in nonconvex mechanics and global optimization, therefore, none of the traditional convexity methods can be used for solving a large class of nonconvex minimization problems in finite deformation theory. Canonical duality theory provides a potentially useful methodology for solving this challenging problem. Besides the canonical duality theory, the mixed finite element method is applied in two separate fields, displacement and dual stress fields, in order to compute the global minimizer of the total potential energy problem. Numerical applications are illustrated with different structural designs and different external loads. We found that the gap function of the present problem is strictly positive, and therefore, our results are the unique solutions.

Moreover, the canonical dual finite element method for the post-buckling analysis of a large deformation elastic beam which is governed by a fourth order non-linear differential equation is introduced. The Gao-Strang total complementary energy associated with this model is a nonconvex functional. Combining the Gao-Strang total complementary energy and the proposed formula of pure complementary energy with the triality theory, a canonical duality algorithm is investigated. A new primal-dual semi-definite program algorithm is applied to solve this challenging nonconvex variational problem and to obtain all possible post-buckled solutions. The triality theory is verified by using different types of dual stress interpolations to get the closed dimensions between the discretized displacement and discretized stress. The numerical results show that the global minimum of the total potential energy is a

stable buckled configuration, while the local extrema present unstable deformation states and the solutions to unstable buckled states are very sensitive not only to the artificial parameters, such as the size of the finite elements, but also to the natural conditions, such as the external loads and boundary conditions.

Finally, we presented a novel canonical penalty-duality (CPD) method to solve the challenging 3-dimensional benchmark problems in topology optimization. The relation between the CPD method for solving 0-1 integer programming problems and the pure complementary energy principle in nonlinear elasticity is discussed. Our theoretical results show that the pure complementary energy principle plays an important role, not only for large deformation theory and nonconvex variational analysis, but also in solving challenging problems in computational mechanics and mixed integer nonlinear programming. Applications are demonstrated by 3-D linear elastic structural topology optimization problems and show that the CPD can provide mechanically sound optimal design with much less computing time and fewer iterations compared with the most widely used topology optimization procedures, SIMP and BESO. Moreover, the CPD method has a convergent solution even if the termination criterion is very small. Additionally, mathematical mistakes and computational complexity in topology optimization modeling and popular methods are discussed in detail for the first time.

5.2 Future work

The canonical duality theory is particularly useful for studying nonconvex, nonsmooth, nonconservative large deformed dynamical systems [21]. Therefore, future work includes investigating the CPD method for solving general topology optimization problems of large deformed elasto-plastic structures subjected to dynamical loads. The main open problems include the optimal parameter μ in order to ensure a fast convergence rate with optimal results, the existence and uniqueness of the global optimization solution for a given design domain V_c. The computations of the powerful CDT method can be applied not only to structural designs but also in other fields of the sciences. The author would like to investigate the possible applications of this method, including heat conduction and reduction problems which can be easily applied in 3-D design domain due to the fact that the number of degrees freedom per node is only one rather than three as in structural designs. Another interesting problem for future study relates to finding analytical solutions for the elasto-plasticity of beams by applying the canonical duality theory.

Bibliography

[1] Ahn, J., Kuttler, K. L., & Shillor, M. (2012). Dynamic contact of two Gao beams, *Electronic Journal of Differential Equations*, 194, 1-42.

[2] Andrews, K.T., Dumont, Y., M'Bengue, M. F., Purcell, J., & Shillor, M. (2012). Analysis and simulations of a nonlinear elastic dynamic beam, *Z. Angew. Math. Phys*, 63, 1005-1019.

[3] Bajer, C.I., Dyniewicz, B., & Shillor, M. (2018). A Gao beam subjected to a moving inertial point load, *Math. Mech. Solids*, 23(3), 461-472.

[4] Bendsφe, M.P., & Kikuchi, N. (1988). Generating optimal topologies in structural design using a homogenization method, *Computer Methods in Applied Mechanics and Engineering*, 71(2), 197-224.

[5] Bendsøe, M.P. (1989). Optimal shape design as a material distribution problem, *Struct Optim*, 1, 193-202.

[6] Bendsφe, M. P., & Sigmund, O. (2003). *Topological optimization: theory, methods and applications*, Berlin, Springer.

[7] Chen Y., & Gao, D.Y. (2016). Global solutions to nonconvex optimization of 4th-order polynomial and log-sum-exp functions, *J. Global Optimization*, 64(3), 417-431.

[8] Cai, K., Gao, D.Y., & Qin, Q.H. (2014). Post-buckling solutions of hyper-elastic beam by canonical dual finite element method, *Mathematics and Mechanics of Solids*, 19(6), 659-671.

[9] Ciarlet, P.G. (2013). *Linear and Nonlinear Functional Analysis with Applications,* SIAM, Philadelphia.

[10] Díaz, A., & Sigmund, O. (1995). Checkerboard patterns in layout optimization. *Structural Optimization*, 10(1), 40-45.

[11] Gao, D.Y. (1986). *On Complementary-Dual Principles in Elastoplastic Systems and Pan-Penalty Finite Element Method*, PhD Thesis, Tsinghua University.

[12] Gao, D.Y. (1988). Panpenalty finite element programming for limit analysis, *Computers & Structures*, 28, 749-755.

[13] Gao, D.Y., & Strang, G. (1989). Geometric nonlinearity: potential energy, complementary energy and the gap function, *Quarterly of Applied Mathematics*, 47(3), 487-504.

[14] Gao, D.Y. (1996). Canonical duality: Complementary finite-element method for finite deformation nonsmooth mechanics, *Journal of Engineering Mathematics,* 30, 339-353.

[15] Gao, D.Y. (1996). Nonlinear elastic beam theory with application in contact problems and variational approaches, *Mechanics Research Communications* 23(1), 11-17.

[16] Gao, D.Y. (1997). Dual extremum principles in finite deformation theory with applications to post-buckling analysis of extended nonlinear beam model, *Applied Mechanics Review*, 50, S64-S71.

[17] Gao, D.Y. (1999). Pure complementary energy principle and triality theory in finite elasticity, *Mechanics Research Communications*, 26, 31-37.

[18] Gao, D.Y. (1999). General analytic solutions and complementary variational principles for large deformation nonsmooth mechanics, *Meccanica*, 34, 169-198.

[19] Gao, D.Y. (2000). *Duality Principles in Nonconvex Systems: Theory, Methods and Applications*, Springer, London/New York/Boston.

[20] Gao, D.Y. (2000). Canonical dual transformation method and generalized triality theory in nonsmooth global optimization, in *J. Global Optimization*, 17, 127-160.

[21] Gao, D.Y. (2001). Complementarity, polarity and triality in nonsmooth, nonconvex and nonconservative Hamilton systems, *Philosophical Transactions of the Royal Society: Mathematical, Physical and Engineering Sciences*, 359, 2347-2367.

[22] Gao, D.Y. (2003). Perfect duality theory and complete set of solutions to a class of global optimization, *Opt.* 52 (4-5), 467-493.

[23] Gao, D.Y. (2007). Solutions and optimality criteria to box constrained nonconvex minimization problems. *Journal of Industrial & Management Optimization*, 3(2), 293-304.

[24] Gao, D.Y., & Ogden, R.W. (2008). Closed-form solutions, extremality and non-smoothness criteria in a large deformation elasticity problem, in *Zeitschrift fur angewandte Mathematik und Physik,* 59, 498-517.

[25] Gao, D.Y., & Ogden, R.W. (2008). Multiple solutions to nonconvex variational problems with implications for phase transitions and numerical computation, in *Quarterly Journal of Mechanics and Applied Mathematics*, 61(4), 497-522.

[26] Gao, D.Y., & Yu, H.F. (2008). Multi-scale modelling and canonical dual finite element method in phase transitions of solids, *Int. J. Solids Struct.* 45, 3660-3673.

[27] Gao, D.Y. (2009). Canonical duality theory: unified understanding and generalized solutions for global optimization. *Comput. & Chem. Eng.* 33, 1964-1972.

[28] Gao, D.Y., & Sherali, H.D. (2009). Canonical duality: Connection between nonconvex mechanics and global optimization, in *Advances in Appl. Mathematics and Global Optimization, Springer*, 249-316.

[29] Gao, D.Y., & Ruan, N. (2010). Solutions to quadratic minimization problems with box and integer constraints. *J. Glob. Optim.*, 47, 463-484.

[30] Gao, D.Y., Ruan, N., & Pardalos, P. (2010). Canonical dual solutions to sum of fourth-order polynomials minimization problems with applications to sensor network localization, *Springer Optimization and Its Applications*, 61, 37-54.

[31] Gao, D.Y., & Wu, C.Z. (2012). On the triality theory for a quartic polynomial optimization problem, *J. Ind. Manag. Optim.*, 8(1), 229-242.

[32] Gao, D.Y., Ruan, N., & Latorre, V. (2016). *Advances of Canonical Duality-Triality Theory*, Springer.

[33] Gao, D.Y. (2016). Analytical solutions to general anti-plane shear problems in finite elasticity, *Continuum Mech. Thermodyn.*, 28, 175-194.

[34] Gao, D.Y., & Hajilarov, E. (2016). On analytic solutions to 3-d finite deformation problems governed by St Venant-Kirchhoff material. in *Canonical Duality*

Theory: Unified Methodology for Multidisciplinary Studies, DY Gao, V. Latorre and N. Ruan (Eds). Springer.

[35] Gao, D.Y. (2016). On unified modeling, theory, and method for solving multi-scale global optimization problems, *Numerical Computations: Theory And Algorithms,* (Eds) Y. D. Sergeyev, D. E. Kvasov and M. S. Mukhametzhanov, AIP Conference Proceedings 1776, 020005.

[36] Gao, D.Y. (2016). On unified modeling, canonical duality-triality theory, challenges and breakthrough in optimization, `https://arxiv.org/abs/1605.05534` .

[37] Gao, D.Y., Ruan, N. & Latorre, V. (2017). Canonical duality-triality theory: Bridge between nonconvex analysis/mechanics and global optimization in complex systems, in *Canonical Duality Theory: Unified Methodology for Multidisciplinary Study*, Spriner, New York, 1-48.

[38] Gao, D.Y. (2018). On Topology Optimization and Canonical Duality Solution, *Comput. Meth. Appl. Mech. Engrg.*, 341, 249-277.

[39] Gao, D.Y. (2017). Canonical Duality Theory for Topology Optimization, *Canonical Duality-Triality: Unified Theory and Methodology for Multidisciplinary Study*, D.Y. Gao, N. Ruan and V. Latorre (Eds). Springer, New York, pp.263-276.

[40] Gao, D.Y. (2017). Analytical solution to large deformation problems governed by generalized neo-Hookean model, *Canonical Duality Theory: Unified Methodology for Multidisciplinary Studies*, DY Gao, V. Latorre and N. Ruan (Eds). Springer, pp.49-68.

[41] Gao, D.Y., Latorre, V., & Ruan, N. (2017). *Canonical Duality Theory: Unified Methodology for Multidisciplinary Study*, Spriner, New York.

[42] Gao, D.Y. (2018). Canonical duality-triality: Unified understanding modeling, problems, and NP-hardness in multi-scale optimization. *Emerging Trends in Applied Mathematics and High-Performance Computing*, V.K. Singh, D.Y. Gao and A. Fisher (Eds), Springer, New York.

[43] Gärtner, B., & Matousek, J. (2012). *Approximation Algorithms and Semidefinite Programming*, Springer, London, New York.

[44] Huang, X., & Xie, Y.M. (2007). Convergent and mesh-independent solutions for the bi-directional evolutionary structural optimization method. *Finite Elements in Analysis and Design*, 43(14), 1039-1049.

[45] Huang, X., & Xie, Y.M. (2009). Bi-Directional Evolutionary Topology Optimization of Continuum Structures with One or Multiple Materials. *Computational Mechanics*, 43, 393-401.

[46] Huang, X., & Xie, Y.M. (2009). *Evolutionary Topology Optimization of Continuum Structures: Methods and Applications*, Wiley, Melbourne.

[47] Huang, R., & Huang, X. (2011). Matlab implementation of 3D topology optimization using BESO. *Incorporating Sustainable Practice in Mechanics of Structures and Materials*, 813-818.

[48] Isac, G. (1992). *Complementarity Problems.* Springer, New York.

[49] Kuttlera, K.L., Li, J., & Shillor, M. (2015). Existence for dynamic contact of a stochastic viscoelastic Gao Beam, *Nonlinear Analysis: Real World Applications*, 22, 568-580.

[50] Karp, R. (1972). Reducibility among combinatorial problems. In: Miller, R.E., Thatcher, J.W. (Eds) *Complexity of Computer Computations*, pp. 85-103. Plenum Press, New York.

[51] Latorre, V., & Gao, D.Y. (2016). Canonical duality for solving general nonconvex constrained problems. *Optimization Letters*, 10(8), 1763-1779.

[52] Levere, K.M. (2014). An inverse problem for the nonlinear Gao beam, *Int. J. Applied Nonlinear Science*, 1(2), 122-135.

[53] Li, S.F., & Gupta, A. (2006). On dual configurational forces, *Journal of Elasticity,* 84, 13-31.

[54] Liu, K., & Tovar, A. (2014). An efficient 3D topology optimization code written in Matlab. *Struct Multidisc Optim*, 50, 1175-1196.

[55] Machalová, J., & Netuka, H. (2015). Optimal control of system governed by the Gao beam equation, *AIMS Proceedings of Dynamical Systems, Differential Equations and Applications*, 783-792.

[56] Machalová, J., & Netuka, H. (2015). Solution of contact problems for nonlinear Gao beam and obstacle, *Journal of Applied Mathematics*, 1-12.

[57] Machalová, J., & Netuka, H. (2017). Control variational method approach to bending and contact problems for Gao beam, *Applications of Mathematics*, 62(6), 661-677.

[58] Machalová, J., & Netuka, H. (2018). Solution of contact problems for Gao beam and elastic foundation, *Math. Mech. Solids*, 23(3), 473-488.

[59] Morales-Silva, D., & Gao, D.Y. (2013). Complete solutions and triality theory to a nonconvex optimization problem with double-well potential in R^n, in *Numer. Algebra Contr. Optim.*, 3(2), 271-282.

[60] Morales, D.M., & Gao, D.Y. (2015). Canonical duality theory and triality for solving general nonconstrained global optimization problems, *Mathematics and Mechanics of Complex Systems*, 3(2), 139-161.

[61] Marsden, J.E., & Hughes, T.J.R. (1983). *Mathematical Foundations of Elasticity,* Prentice-Hall, 1983.

[62] Osher, S., & Sethian, J.A. (1988). Fronts propagating with curvature-dependent speed: algorithms based on HamiltonJacobi formulations. *Journal of Computational Physics*, 79(1), 12-49.

[63] Querin, O.M., Young V., Steven, G.P., & Xie, Y.M. (2000). Computational Efficiency and validation of bi-directional evolutionary structural optimization. *Comput Methods Applied Mechanical Engineering,* 189(2), 559-573.

[64] Querin, O.M., & Steven, G.P. (2000). Evolutionary Structural optimization using an additive algorithm. *Finite Element in Analysis and Design,* 34(3-4), 291-308.

[65] Rozvany, G.I.N., Zhou, M., & Birker, T. (1992). Generalized shape optimization without homogenization. *Structural Optimization,* 4(3), 250-252.

[66] Rozvany, G.I.N., & Zhou, M. (1994). *Optimality criteria methods for large structural systems.* In: H. Adeli (ed.) Advances in Design Optimization Chapman and Hall, London.

[67] Rozvany, G.I.N. (2009). A critical review of established methods of structural topology optimization. *Structural and Multidisciplinary Optimization,* 37(3), 217-237.

[68] Sethian, J.A. (1999). Level set methods and fast marching methods: evolving interfaces in computation algeometry, fluid mechanics, computer version and material science. *Cambridge, UK: Cambridge University Press*, 12-49.

[69] Svanberg, K. (1987). The method of moving asymptotes - a new method for structural optimization. *Int. J. Numer. Meth. Engrg.*, 24, 359-73.

[70] Stolpe, M., & Svanberg, K. (2001). On the trajectories of penalization methods for topology optimization. *Struct. Multidisc. Optim.*, 21, 128-139.

[71] Santos, H.A.F.A., & Gao, D.Y. (2012). Canonical dual finite element method for solving post-buckling problems of a large deformation elastic beam, *International Journal of Non-Linear Mechanics*, 47, 240-247.

[72] Stephen, B., & Lieven, V. (2004). *Convex Optimization* (1st ed.). Cambridge University Press.

[73] Sturm, J.F. (1999). Using SeDuMi 1.02, a MATLAB toolbox for optimization over symmetric cones, *Optimization Methods and Software*, 11, 625-653.

[74] Sigmund, O., & Petersson, J. (1998). Numerical instabilities in topology optimization: A survey on procedures dealing with checkerboards, mesh-dependencies and local minima. *Structural Optimization*, 16(1), 68-75.

[75] Sigmund, O. (1997). On the design of compliant mechanisms using topology optimization. *Mech. Struct. Mach.*, 25, 495-526.

[76] Sigmund, O., & Torquato, S. (1997). Design of materials with extreme thermal expansion using a three-phase topology optimization method. *J. Mech. Phys. Solids*, 45, 1037-1067.

[77] Sigmund, O. (2001). A 99 line topology optimization code written in matlab. *Struct Multidiscip Optim,* 21(2), 120-127.

[78] Sigmund O., & Maute K. (2013). Topology optimization approaches: a comparative review. *Structural and Multidisciplinary Optimization*, 48(6), 1031-1055.

[79] Strang, G. (1986). *Introduction to Applied Mathematics*, Wellesley-Cambridge Press.

[80] Truesdell, C.A. & Noll, W. (1992). *The Non-Linear Field Theories of Mechanics*, Second Edition, 591 pages. Springer-Verlag, Berlin-Heidelberg-New York.

[81] Xie, Y.M., & Steven, G.P. (1993). A simple evolutionary procedure for structural optimization. *Comput Struct,* 49(5), 885-896.

[82] Xie, Y.M., & Steven, G.P. (1997). *Evolutionary structural optimization*, Springer, London.

[83] Yang, X.Y., Xie, Y.M., Steven, G.P., & Querin, Q. M. (1999). Bidirectional evolutionary method for stiffness optimization, *AIAA Journal*, 37, 1483-1488.

[84] Zuo, Z.H., & Xie, Y.M. (2015). A simple and compact Python code for complex 3D topology optimization. *Advances in Engineering Software*, 85, 1-11.

[85] Zhou, M., & Rozvany, G.I.N. (1991). The COC algorithm, Part II: Topological geometrical and generalized shape optimization. *Computer Methods in Applied Mechanics and Engineering,* 89(1), 309-336.

Appendices

Appendix A

Matlab codes for solving 3D topology optimization problems

According to the Section 4.7.1 in Chapter 4, we present three MATLAB codes for CPD, BESO and SIMP methods in order to compare the results of the present method CPD with the results of the popular methods, BESO and SIMP. These codes are for a cantilever beam problem which is subjected to a uniformly distributed load in the right end, as shown in examples 4.7.1.1 and 4.7.1.2.

We can also easily obtain the codes for the other structures that are described in the other examples of Section 4.7, by changing some lines in the present codes in accordance with their boundary conditions and loading conditions. Some elements are required to be either solid or void depending on their design, such as in a cantilever beam with a given hole, as in Section 4.7.3.

A.1   Matlab Code for the CPD method

We present in this section a Matlab code "CPD3D" for solving 3D topology optimization problems. It is created based on the canonical penalty-duality (CPD) algorithm which is explained in Section 4.6. The CPD3D code is developed according to the Matlab CDT code for 2D structures which was presented by Prof. M. Li [39]. The CPD algorithm is specified by lines 75-97. The main program is called by the following Matlab input line

$$\text{CPD3D(nelx,nely,nelz,volfrac,mu,beta)},$$

where "nelx", "nely" and "nelz" represent the number of elements along x, y, and z directions, "volfrac" is the target volume fraction, "mu" is the volume evolution rate and "beta" is the perturbation parameter.

```matlab
1  % Canonical Penalty−Duality Algorithm for 3D Topology
       Optimization .. By Elaf J. Ali (2017) , Federation University
       Australia
2  function CPD3D( nelx , nely , nelz , volfrac ,mu, beta )
3  FigHandle = figure ( 'Position', [600 , 90 , 800 , 350]) ;
4  tic ;              % stopwatch timer
5  % USER−DEFINED LOOP PARAMETERS
6  maxloop = 200;     % Maximum number of iterations
7  tolx = 1e−16;      % Terminarion criterion
8  displayflag = 0;   % Display structure flag
9  % USER−DEFINED MATERIAL PROPERTIES
10  E0 = 1;           % Young 's modulus of solid material
11  Emin = 1e−9;      % Young 's modulus of void−like material
12  nu = 0.3;         % Poisson 's ratio
13  tau=1;
14  Err=2e−16;
15  er= 0.05;
16  % USER−DEFINED LOAD DOFs
17  [ il , jl , kl ] = meshgrid ( nelx , 0, 0: nelz ) ;  % Coordinates
18  loadnid = kl ∗( nelx+1)∗( nely+1)+il ∗( nely+1)+(nely+1−jl ) ;%Node IDs
19  loaddof = 3∗loadnid (:) − 1;     %DOFs
20  % USER−DEFINED SUPPORT FIXED DOFs
21  [ iif , jf , kf ] = meshgrid (0,0: nely ,0: nelz ) ;  % Coordinates
22  fixednid = kf ∗( nelx+1)∗( nely+1)+iif ∗( nely+1)+(nely+1−jf ) ; %Node
       IDs
23  fixeddof = [3∗ fixednid (:) ; 3∗ fixednid (:) −1; 3∗ fixednid (:) −2];%
       DOFs
24  % PREPARE FINITE ELEMENT ANALYSIS
25  nele = nelx ∗ nely ∗ nelz ;
26  ndof = 3∗( nelx+1)∗( nely+1)∗( nelz+1);
27  F = sparse ( loaddof ,1,−1, ndof ,1) ;
28  U = zeros ( ndof ,1) ;
29  freedofs = setdiff (1: ndof , fixeddof ) ;
30  KE = lk_H8 (nu) ;
31  nodegrd = reshape (1:( nely+1)∗( nelx+1) , nely+1,nelx+1) ;
32  nodeids = reshape ( nodegrd (1: end −1,1: end−1) , nely ∗ nelx ,1) ;
33  nodeidz = 0:( nely+1)∗( nelx+1):( nelz −1)∗( nely+1)∗( nelx+1) ;
34  nodeids = repmat ( nodeids , size ( nodeidz ))+repmat ( nodeidz , size (
       nodeids )) ;
```

117

```matlab
35  edofVec = 3*nodeids(:)+1;
36  edofMat = repmat(edofVec,1,24)+ repmat([0 1 2 3*nely + [3 4 5 0 1
        2] -3 -2 -1 ...
37      3*(nely+1)*(nelx+1)+[0 1 2 3*nely + [3 4 5 0 1 2] -3 -2 -1]],
          nele,1);
38  iK = reshape(kron(edofMat,ones(24,1))',24*24*nele,1);
39  jK = reshape(kron(edofMat,ones(1,24))',24*24*nele,1);
40  % INITIALIZE ITERATION
41  loop = 0;
42  change = 1;
43  a = ones(nely,nelx,nelz);
44  xPhys = ones(nely,nelx,nelz);
45  while change > tolx && loop < maxloop
46          loop = loop + 1;
47          mu = max(volfrac,mu*(1-er));
48  % FE-ANALYSIS
49          sK = reshape(KE(:)*(Emin+(E0-Emin)*xPhys(:)'),24*24*nele,1)
               ;
50          K = sparse(iK,jK,sK);
51  %    K = (K+K')/2;
52          U(freedofs,:) = K(freedofs,freedofs)\F(freedofs,:);
53  % OBJECTIVE FUNCTION AND SENSITIVITY ANALYSIS
54          ce = reshape(sum((U(edofMat)*KE).*U(edofMat),2),[nely,nelx,
               nelz]);
55          c = sum(sum(sum((Emin+(E0-Emin)*xPhys).*ce)));
56  % DUAL METHOD
57          CM=xPhys*E0.*ce;
58          [rho_new,tau]=CPDAlgorithm(CM,a,mu,Err,tau,beta);
59          change = max(abs(rho_new(:)-xPhys(:)));
60          xPhys = rho_new;
61  % PRINT RESULTS
62          fprintf(' It.:%5i Obj.:%11.4f Vol.:%7.3f ch.:%7.3f\n',loop,
               c,mean(xPhys(:)),change);
63          % PLOT DENSITIES
64          if displayflag, clf; display_3D(xPhys); end
65          clf; display_3D(xPhys);
66  end
67  Time=toc;
68  clf; display_3D(xPhys);
```

118

```matlab
69   title ([ 'CPD3D' ,' v.f.=' ,num2str (( volfrac )) ,' \mu=' ,num2str ((mu) )
        ,...
70   ' \beta=' ,num2str (beta ) ,' nx=' ,num2str ( nelx ) ,' ny=' ,num2str ( nely
        ) ,...
71   ' nz=' ,num2str ( abs ( nelz )) , ' c=' ,num2str ( c ) , ' It.=' ,num2str (
        loop ) ,...
72   ' Time=' ,num2str (Time) , ' tolx= ' ,num2str ( tolx ) ]) ;
73   end
74   % === Canonical Penalty−Duality Algorithm ===
75   function [rho , tau]=CPDAlgorithm (CM, a ,mu, Err , tau , beta )
76   [ nely , nelx , nelz ]= size (CM) ;
77   NE=nelx ∗ nely ∗ nelz ;
78   vp=mu∗NE;
79   pd0=1000;
80   dpd=1000;
81   k=0;
82   while dpd>Err
83       k=k+1;
84       eta=beta ˆ2/27;
85       theta=(tau∗a − CM) .ˆ2;
86       phi=eta ˆ(−1/3)∗(2∗theta−eta+2∗(theta .∗( theta−eta )) .ˆ0.5)
            .ˆ(1/3) ;
87       sg=1/6∗beta∗(−1+2∗real ( phi )) ;
88       tau= (sum(sum(sum(a .∗(1+CM./ sg ) ) ) )−2∗vp)/sum(sum(sum(a .ˆ2./
            sg ) ) ) ;
89       mc=sg+CM−tau∗a ;
90       dc =0.5∗( sg .∗ sg )/ beta ;
91       pd=sum(sum(sum(0.25∗mc .ˆ2./ sg+dc ) ) )−tau∗vp ;
92       dpd=abs (pd−pd0) ;
93       pd0=pd ;
94   end
95   rho=1/2∗(1−(tau∗a−CM) ./ sg ) ;   % compute the density
96   rho=real (( rho >0.01)) ;
97   end
98   % === GENERATE ELEMENT STIFFNESS MATRIX ===
99   function [KE] = lk_H8 (nu)
100  A = [32 6 −8 6 −6 4 3 −6 −10 3 −3 −3 −4 −8;
101      −48 0 0 −24 24 0 0 0 12 −12 0 12 12 12];
102  k = 1/144∗A' ∗[1; nu ];
```

```
103  K1 = [ k ( 1 )  k ( 2 )  k ( 2 )  k ( 3 )  k ( 5 )  k ( 5 ) ;
104        k ( 2 )  k ( 1 )  k ( 2 )  k ( 4 )  k ( 6 )  k ( 7 ) ;
105        k ( 2 )  k ( 2 )  k ( 1 )  k ( 4 )  k ( 7 )  k ( 6 ) ;
106        k ( 3 )  k ( 4 )  k ( 4 )  k ( 1 )  k ( 8 )  k ( 8 ) ;
107        k ( 5 )  k ( 6 )  k ( 7 )  k ( 8 )  k ( 1 )  k ( 2 ) ;
108        k ( 5 )  k ( 7 )  k ( 6 )  k ( 8 )  k ( 2 )  k ( 1 ) ] ;
109  K2 = [ k ( 9 )   k ( 8 )   k ( 1 2 )  k ( 6 )   k ( 4 )   k ( 7 ) ;
110        k ( 8 )   k ( 9 )   k ( 1 2 )  k ( 5 )   k ( 3 )   k ( 5 ) ;
111        k ( 1 0 )  k ( 1 0 )  k ( 1 3 )  k ( 7 )   k ( 4 )   k ( 6 ) ;
112        k ( 6 )   k ( 5 )   k ( 1 1 )  k ( 9 )   k ( 2 )   k ( 1 0 ) ;
113        k ( 4 )   k ( 3 )   k ( 5 )   k ( 2 )   k ( 9 )   k ( 1 2 )
114        k ( 1 1 )  k ( 4 )   k ( 6 )   k ( 1 2 )  k ( 1 0 )  k ( 1 3 ) ] ;
115  K3 = [ k ( 6 )   k ( 7 )   k ( 4 )   k ( 9 )   k ( 1 2 )  k ( 8 ) ;
116        k ( 7 )   k ( 6 )   k ( 4 )   k ( 1 0 )  k ( 1 3 )  k ( 1 0 ) ;
117        k ( 5 )   k ( 5 )   k ( 3 )   k ( 8 )   k ( 1 2 )  k ( 9 ) ;
118        k ( 9 )   k ( 1 0 )  k ( 2 )   k ( 6 )   k ( 1 1 )  k ( 5 ) ;
119        k ( 1 2 )  k ( 1 3 )  k ( 1 0 )  k ( 1 1 )  k ( 6 )   k ( 4 ) ;
120        k ( 2 )   k ( 1 2 )  k ( 9 )   k ( 4 )   k ( 5 )   k ( 3 ) ] ;
121  K4 = [ k ( 1 4 )  k ( 1 1 )  k ( 1 1 )  k ( 1 3 )  k ( 1 0 )  k ( 1 0 ) ;
122        k ( 1 1 )  k ( 1 4 )  k ( 1 1 )  k ( 1 2 )  k ( 9 )   k ( 8 ) ;
123        k ( 1 1 )  k ( 1 1 )  k ( 1 4 )  k ( 1 2 )  k ( 8 )   k ( 9 ) ;
124        k ( 1 3 )  k ( 1 2 )  k ( 1 2 )  k ( 1 4 )  k ( 7 )   k ( 7 ) ;
125        k ( 1 0 )  k ( 9 )   k ( 8 )   k ( 7 )   k ( 1 4 )  k ( 1 1 ) ;
126        k ( 1 0 )  k ( 8 )   k ( 9 )   k ( 7 )   k ( 1 1 )  k ( 1 4 ) ] ;
127  K5 = [ k ( 1 )  k ( 2 )   k ( 8 )   k ( 3 )  k ( 5 )   k ( 4 ) ;
128        k ( 2 )  k ( 1 )   k ( 8 )   k ( 4 )  k ( 6 )   k ( 1 1 ) ;
129        k ( 8 )  k ( 8 )   k ( 1 )   k ( 5 )  k ( 1 1 )  k ( 6 ) ;
130        k ( 3 )  k ( 4 )   k ( 5 )   k ( 1 )  k ( 8 )   k ( 2 ) ;
131        k ( 5 )  k ( 6 )   k ( 1 1 )  k ( 8 )  k ( 1 )   k ( 8 ) ;
132        k ( 4 )  k ( 1 1 )  k ( 6 )   k ( 2 )  k ( 8 )   k ( 1 ) ] ;
133  K6 = [ k ( 1 4 )  k ( 1 1 )  k ( 7 )   k ( 1 3 )  k ( 1 0 )  k ( 1 2 ) ;
134        k ( 1 1 )  k ( 1 4 )  k ( 7 )   k ( 1 2 )  k ( 9 )   k ( 2 ) ;
135        k ( 7 )   k ( 7 )   k ( 1 4 )  k ( 1 0 )  k ( 2 )   k ( 9 ) ;
136        k ( 1 3 )  k ( 1 2 )  k ( 1 0 )  k ( 1 4 )  k ( 7 )   k ( 1 1 ) ;
137        k ( 1 0 )  k ( 9 )   k ( 2 )   k ( 7 )   k ( 1 4 )  k ( 7 ) ;
138        k ( 1 2 )  k ( 2 )   k ( 9 )   k ( 1 1 )  k ( 7 )   k ( 1 4 ) ] ;
139  KE =  1 / ( ( nu+1 ) * ( 1 - 2 * nu ) ) * . . .
140        [  K1   K2   K3   K4 ;
141        K2'   K5   K6   K3' ;
```

```matlab
142        K3'  K6   K5'  K2';
143        K4   K3   K2   K1'];
144  end
145  % === DISPLAY 3D TOPOLOGY (ISO−VIEW) ===
146  function display_3D(rho)
147  [nely,nelx,nelz] = size(rho);
148  hx = 1; hy = 1; hz = 1;        % User−defined unit element size
149  face = [1 2 3 4; 2 6 7 3; 4 3 7 8; 1 5 8 4; 1 2 6 5; 5 6 7 8];
150  set(gcf,'Name','ISO display','NumberTitle','off');
151  for k = 1:nelz
152      z = (k−1)*hz;
153      for i = 1:nelx
154          x = (i−1)*hx;
155          for j = 1:nely
156              y = nely*hy − (j−1)*hy;
157              if (rho(j,i,k) > 0.5) %User−defined display density
                      threshold
158                  vert = [x y z; x y−hx z; x+hx y−hx z; x+hx y z;x
                          y z+hx;x y−hx z+hx; x+hx y−hx z+hx;x+hx y z+hx
                          ];
159                  vert(:,[2 3]) = vert(:,[3 2]); vert(:,2,:) = −
                          vert(:,2,:);
160                  patch('Faces',face,'Vertices',vert,'FaceColor',
                          [0.0,0.4*(rho(j,i,k)),0.8]);
161                  hold on;
162              end
163          end
164      end
165  end
166  axis equal; axis tight; axis off; box on; view([30,30]); pause(1e
      −6);
167  end
```

A.2 Matlab Code for the BESO method

We present in this section a Matlab code "BESO3D" for solving 3D topology optimization problems by using the soft-kill BESO method. This code is based on [47].

```matlab
1  % == This code was written by Elaf J Ali(2017),according to the
        paper: (Matlab implementation of 3D topology optimization
        using BESO, by Huang, R., and Huang, X., 2011).
2  % The soft-kill BESO algorithm- Cantilever beam problem
3  function BESO3D( nelx , nely , nelz , volfrac , er ,mu,  rmin )
4  tic ;
5  FigHandle = figure ('Position', [600, 90, 800, 350]);
6  maxloop=200;
7  E0 = 1;              % Young's modulus of solid material
8  Emin = 1e-9;         % Young's modulus of void-like material
9  tolx = 1e-6 ;        % Terminarion criterion
10 % INITIALIZE
11 xPhys = ones ( nelx , nely , nelz );
12 vol=mu;
13 loop = 0; change = 1.; penal = 3.;
14 displayflag = 0;
15 % START iTH ITERATION
16 while change > tolx  && loop < maxloop
17   loop = loop + 1;
18   vol = max( vol*(1-er) , volfrac );
19   if loop >1; olddc = dc; end
20 % FE-ANALYSIS
21   [U]=FE( nelx , nely , nelz , xPhys , penal );
22 % OBJECTIVE FUNCTION AND SENSITIVITY ANALYSIS
23   [KE] = lk ;
24   c ( loop ) = 0.;
25 for  elz = 1: nelz
26    for  ely = 1: nely
27       for  elx = 1: nelx
28           n1 = ( nelx+1)*( nelz+1)*( ely-1)+(elx-1)*( nelz+1) +elz ;
29           n2 = ( nelx+1)*( nelz+1)*( ely-1)+(elx )*( nelz+1)+elz ;
30           n4 = ( nelx+1)*( nelz+1)*( ely )+(elx-1)*( nelz+1)+elz ;
31           n3 = ( nelx+1)*( nelz+1)*( ely )+(elx )*( nelz+1)+elz ;
32           Ue = U ( [...
33                 3*n1-2; 3*n1-1; 3*n1 ;...
34                 3*n2-2; 3*n2-1; 3*n2 ;...
35                 3*n3-2; 3*n3-1; 3*n3 ;...
36                 3*n4-2; 3*n4-1; 3*n4 ;...
37                 3*n1+1; 3*n1+2; 3*n1+3;...
```

122

```matlab
38                      3*n2+1; 3*n2+2; 3*n2+3;...
39                      3*n3+1; 3*n3+2; 3*n3+3;...
40                      3*n4+1; 3*n4+2; 3*n4+3],1);
41
42              c(loop)=c(loop)+ xPhys(elx,ely,elz)^penal*(E0-Emin)*Ue'*
                    KE*Ue;
43              dc(elx,ely,elz)=xPhys(elx,ely,elz)^(penal-1)*(E0-Emin)*
                    Ue'*KE*Ue;
44        end
45      end
46  end
47  % FILTERING OF SENSITIVITIES
48  [dc]     = check(nelx,nely,nelz,rmin,dc);
49  % STABLIZATION OF EVOLUTIONARY PROCESS
50  if loop > 1; dc = (dc+olddc)/2.; end
51  % BESO DESIGN UPDATE
52  [xPhys] = ADDDEL(nelx,nely,nelz,vol,dc,xPhys);
53  % PRINT RESULTS
54  if loop>10
55  change=abs(sum(c(loop-9:loop-5))-sum(c(loop-4:loop)))/sum(c(loop
        -4:loop));
56  end
57  fprintf(' It.:%5i Obj.:%11.4f Vol.:%7.3f ch.:%7.3f\n',loop,c(loop
        ),mean(xPhys(:)),change);
58      if displayflag, clf; display_3D(xPhys); end
59      clf; display_3D(xPhys)
60  end
61  Time=toc;
62  clf; display_3D(xPhys);
63
64  title([ 'BESO',' v.f.= ',num2str((volfrac)) ,...
65          ' nx= ',num2str(nelx),' ny= ',num2str(nely) ,...
66          ' nz= ',num2str(abs(nelz)),' \mu= ',num2str(mu) ,...
67          ' c=',num2str(c(loop)),' It.= ',num2str(loop) ,...
68          ' Time= ',num2str(Time), ' tolx= ',num2str(tolx)]);
69  end
70  % === OPTIMALITY CRITERIA UPDATE ===
71  function [xPhys]=ADDDEL(nelx,nely,nelz,volfra,dc,xPhys)
72  l1 = min(min(min(dc))); l2 = max(max(max(dc)));
```

```matlab
73  while ((l2-l1)/l2 > 1.0e-5)
74     th = (l1+l2)/2.0;
75     xPhys = max(0.001,sign(dc-th));
76     if sum(sum(sum(xPhys)))-volfra*(nelx*nely*nelz) > 0
77         l1 = th;
78     else
79         l2 = th;
80     end
81  end
82  end
83  % === MESH-INDEPENDENCY FILTER ===
84  function [dcf]=check(nelx,nely,nelz,rmin,dc)
85  dcf=zeros(nelx,nely,nelz);
86  for i = 1:nelx
87      for j = 1:nely
88          for n = 1:nelz
89              sum=0.0;
90              for k = max(i-floor(rmin),1):min(i+floor(rmin),nelx)
91                  for l = max(j-floor(rmin),1):min(j+floor(rmin),nely)
92                      for m = max(n-floor(rmin),1):min(n+floor(rmin),nelz)
93                          fac = rmin-sqrt((i-k)^2+(j-l)^2+(n-m)^2);
94                          sum = sum+max(0,fac);
95                          dcf(i,j,n) = dcf(i,j,n) + max(0,fac)*dc(k,l,m);
96                      end
97                  end
98              end
99              dcf(i,j,n) = dcf(i,j,n)/sum;
100         end
101     end
102 end
103 end
104 % === FE-ANALYSIS ===
105 function [U]=FE(nelx,nely,nelz,xPhys,penal)
106 [KE] = lk;
107 a=3*(nelx+1)*(nely+1)*(nelz+1);
108 K = sparse(a, a);
```

```matlab
109  F = sparse(a,1);
110  U = zeros(a,1);
111  for elz = 1:nelz
112      for ely = 1:nely
113          for elx = 1:nelx
114      n1 = (nelx+1)*(nelz+1)*(ely-1)+(elx-1)*(nelz+1) +elz;
115      n2 = (nelx+1)*(nelz+1)*(ely-1)+(elx)*(nelz+1)+elz;
116      n4 = (nelx+1)*(nelz+1)*(ely)+(elx-1)*(nelz+1)+elz;
117      n3 = (nelx+1)*(nelz+1)*(ely)+(elx)*(nelz+1)+elz;
118      edof = [...
119              3*n1-2; 3*n1-1; 3*n1;...
120              3*n2-2; 3*n2-1; 3*n2;...
121              3*n3-2; 3*n3-1; 3*n3;...
122              3*n4-2; 3*n4-1; 3*n4;...
123              3*n1+1; 3*n1+2; 3*n1+3;...
124              3*n2+1; 3*n2+2; 3*n2+3;...
125              3*n3+1; 3*n3+2; 3*n3+3;...
126              3*n4+1; 3*n4+2; 3*n4+3];
127
128      K(edof,edof) = K(edof,edof) + xPhys(elx,ely,elz)^penal*KE;
129          end
130      end
131  end
132  % DEFINE LOADS AND SUPPORTS
133  % USER-DEFINED LOAD DOFs
134  [il,jl,kl]= meshgrid(nelx, 0, 0:nelz);
135  loadnid= jl*(nelx+1)*(nelz+1)+il*(nelz+1)+(nelz+1-kl);%Node IDs
136  loaddof= 3*loadnid(:) - 1;                % DOFs
137  % USER-DEFINED SUPPORT FIXED DOFs
138  [iif,jf,kf] = meshgrid(0,0:nely,0:nelz);
139  fixednid= jf*(nelx+1)*(nelz+1)+iif*(nelz+1)+(nelz+1-kf);
140  fixeddof= [3*fixednid(:);3*fixednid(:)-1;3*fixednid(:)-2];
141  % PREPARE FINITE ELEMENT ANALYSIS
142  ndof = 3*(nelx+1)*(nelz+1)*(nely+1);
143  F = sparse(loaddof,1,-1,ndof,1);
144  U = zeros(ndof,1);
145  freedofs = setdiff(1:ndof,fixeddof);
146  % SOLVING
147  U(freedofs,:) = K(freedofs,freedofs) \ F(freedofs,:);
```

```
148  U( fixeddof ,:)= 0;
149  end
150  % === ELEMENT STIFFNESS MATRIX ===
151  function [KE] = lk
152  nu = 0.3;
153  A = [32 6 -8 6 -6 4 3 -6 -10 3 -3 -3 -4 -8;
154      -48 0 0 -24 24 0 0 0 12 -12 0 12 12 12];
155  k = 1/144*A'*[1; nu];
156  K1 = [k(1) k(2) k(2) k(3) k(5) k(5);
157      k(2) k(1) k(2) k(4) k(6) k(7);
158      k(2) k(2) k(1) k(4) k(7) k(6);
159      k(3) k(4) k(4) k(1) k(8) k(8);
160      k(5) k(6) k(7) k(8) k(1) k(2);
161      k(5) k(7) k(6) k(8) k(2) k(1)];
162  K2 = [k(9)  k(8)  k(12) k(6)  k(4)  k(7);
163      k(8)  k(9)  k(12) k(5)  k(3)  k(5);
164      k(10) k(10) k(13) k(7)  k(4)  k(6);
165      k(6)  k(5)  k(11) k(9)  k(2)  k(10);
166      k(4)  k(3)  k(5)  k(2)  k(9)  k(12)
167      k(11) k(4)  k(6)  k(12) k(10) k(13)];
168  K3 = [k(6)  k(7)  k(4)  k(9)  k(12) k(8);
169      k(7)  k(6)  k(4)  k(10) k(13) k(10);
170      k(5)  k(5)  k(3)  k(8)  k(12) k(9);
171      k(9)  k(10) k(2)  k(6)  k(11) k(5);
172      k(12) k(13) k(10) k(11) k(6)  k(4);
173      k(2)  k(12) k(9)  k(4)  k(5)  k(3)];
174  K4 = [k(14) k(11) k(11) k(13) k(10) k(10);
175      k(11) k(14) k(11) k(12) k(9)  k(8);
176      k(11) k(11) k(14) k(12) k(8)  k(9);
177      k(13) k(12) k(12) k(14) k(7)  k(7);
178      k(10) k(9)  k(8)  k(7)  k(14) k(11);
179      k(10) k(8)  k(9)  k(7)  k(11) k(14)];
180  K5 = [k(1) k(2)  k(8)  k(3) k(5)  k(4);
181      k(2) k(1)  k(8)  k(4) k(6)  k(11);
182      k(8) k(8)  k(1)  k(5) k(11) k(6);
183      k(3) k(4)  k(5)  k(1) k(8)  k(2);
184      k(5) k(6)  k(11) k(8) k(1)  k(8);
185      k(4) k(11) k(6)  k(2) k(8)  k(1)];
186  K6 = [k(14) k(11) k(7)  k(13) k(10) k(12);
```

126

```matlab
187        k(11) k(14) k(7)  k(12) k(9)  k(2);
188        k(7)   k(7)  k(14) k(10) k(2)   k(9);
189        k(13) k(12) k(10) k(14) k(7)   k(11);
190        k(10) k(9)  k(2)   k(7)   k(14) k(7);
191        k(12) k(2)  k(9)   k(11) k(7)   k(14)];
192  KE = 1/((nu+1)*(1-2*nu)) *...
193        [ K1   K2   K3   K4;
194        K2'  K5   K6   K3';
195        K3'  K6   K5'  K2';
196        K4   K3   K2   K1'];
197  end
198  % === DISPLAY 3D TOPOLOGY (ISO-VIEW) ===
199  function display_3D(rho)
200  [nelx,nely,nelz] = size(rho);
201  hx = 1; hy = 1; hz = 1;
202  face = [1 2 3 4; 2 6 7 3; 4 3 7 8; 1 5 8 4; 1 2 6 5; 5 6 7 8];
203  set(gcf,'Name','ISO display','NumberTitle','off');
204  for k = 1:nely
205      z = (k-1)*hz;
206      for i = 1:nelz
207          y = (i-1)*hy;
208          for j = 1: nelx
209              x = (j-1)*hx -nelx*hx;
210              if (rho(j,k,i) ==1)
211                  vert = [x y z;  x-hy y z;  x-hy y+hy z;  x y+hy z
                          ; x y z+hy; x-hy y z+hy;  x-hy y+hy z+hy; x y+
                          hy z+hy];
212                  patch('Faces',face,'Vertices',vert,'FaceColor'
                          ,[0.2,0.8*(rho(j,k,i)),0.8]);
213                  hold on;
214              end
215          end
216      end
217  end
218  axis equal; axis tight; axis off; box on; view([30,30]); pause(1e
      -6);
219  end
```

A.3 Matlab Code for the SIMP method

This section presents the Matlab top3d code for solving 3D topology optimization problems by using SIMP method. This code was written by K Liu and A Tovar in 2013 [54].

```matlab
% === This code was written by K Liu and A Tovar (AN 169 LINE 3D
    TOPOLOGY OPITMIZATION CODE, 2013)
% SIMP method - Cantilever beam problem
function top3d(nelx,nely,nelz,volfrac,penal,rmin)
tic;
FigHandle = figure('Position', [600, 90, 800, 350]);
% USER-DEFINED LOOP PARAMETERS
maxloop = 200;     % Maximum number of iterations
tolx = 1e-6;       % Terminarion criterion
displayflag = 0;   % Display structure flag
% USER-DEFINED MATERIAL PROPERTIES
E0 = 1;            % Young's modulus of solid material
Emin = 1e-9;       % Young's modulus of void-like material
nu = 0.3;          % Poisson's ratio
% USER-DEFINED LOAD DOFs
[il,jl,kl]= meshgrid(nelx, 0, 0:nelz);
loadnid= kl*(nelx+1)*(nely+1)+il*(nely+1)+(nely+1-jl); % Node IDs
loaddof= 3*loadnid(:) - 1;          % DOFs
% USER-DEFINED SUPPORT FIXED DOFs
[iif,jf,kf] = meshgrid(0,0:nely,0:nelz);  % Coordinates
fixednid= kf*(nelx+1)*(nely+1)+iif*(nely+1)+(nely+1-jf);  % Node
    IDs
fixeddof= [3*fixednid(:);3*fixednid(:)-1;3*fixednid(:)-2];% DOFs
% PREPARE FINITE ELEMENT ANALYSIS
nele = nelx*nely*nelz;
ndof = 3*(nelx+1)*(nely+1)*(nelz+1);
F = sparse(loaddof,1,-1,ndof,1);
U = zeros(ndof,1);
freedofs = setdiff(1:ndof,fixeddof);
KE = lk_H8(nu);
nodegrd= reshape(1:(nely+1)*(nelx+1),nely+1,nelx+1);
nodeids= reshape(nodegrd(1:end-1,1:end-1),nely*nelx,1);
nodeidz= 0:(nely+1)*(nelx+1):(nelz-1)*(nely+1)*(nelx+1);
nodeids= repmat(nodeids,size(nodeidz))+repmat(nodeidz,size(
    nodeids));
```

```matlab
33  edofVec= 3*nodeids(:)+1;
34  edofMat= repmat(edofVec,1,24)+ repmat([0 1 2 3*nely + [3 4 5 0 1
        2] −3 −2 −1 ...
35        3*(nely+1)*(nelx+1)+[0 1 2 3*nely + [3 4 5 0 1 2] −3 −2 −1]],
            nele,1);
36  iK = reshape(kron(edofMat,ones(24,1))',24*24*nele,1);
37  jK = reshape(kron(edofMat,ones(1,24))',24*24*nele,1);
38  % PREPARE FILTER
39  iH = ones(nele*(2*(ceil(rmin)−1)+1)^2,1);
40  jH = ones(size(iH));
41  sH = zeros(size(iH));
42  k = 0;
43  for k1 = 1:nelz
44      for i1 = 1:nelx
45          for j1 = 1:nely
46              e1 = (k1−1)*nelx*nely + (i1−1)*nely+j1;
47              for k2 = max(k1−(ceil(rmin)−1),1):min(k1+(ceil(rmin)
                    −1),nelz)
48                  for i2 = max(i1−(ceil(rmin)−1),1):min(i1+(ceil(
                        rmin)−1),nelx)
49                      for j2 = max(j1−(ceil(rmin)−1),1):min(j1+(
                            ceil(rmin)−1),nely)
50                          e2 = (k2−1)*nelx*nely + (i2−1)*nely+j2;
51                          k = k+1;
52                          iH(k) = e1;
53                          jH(k) = e2;
54                          sH(k) = max(0,rmin−sqrt((i1−i2)^2+(j1−j2)
                                ^2+(k1−k2)^2));
55                      end
56                  end
57              end
58          end
59      end
60  end
61  H = sparse(iH,jH,sH);
62  Hs = sum(H,2);
63  % INITIALIZE ITERATION
64  x = repmat(volfrac,[nely,nelx,nelz]);
65  xPhys = x;
```

```matlab
66  loop = 0;
67  change = 1;
68  % START ITERATION
69  while change > tolx && loop < maxloop
70      loop = loop+1;
71      % FE-ANALYSIS
72      sK=reshape(KE(:)*(Emin+xPhys(:)'.^penal*(E0-Emin)),24*24*nele
            ,1);
73      K =sparse(iK,jK,sK); K = (K+K')/2;
74      U(freedofs,:) = K(freedofs,freedofs)\F(freedofs,:);
75      % OBJECTIVE FUNCTION AND SENSITIVITY ANALYSIS
76      ce = reshape(sum((U(edofMat)*KE).*U(edofMat),2),[nely,nelx,
            nelz]);
77      c = sum(sum(sum((Emin+xPhys.^penal*(E0-Emin)).*ce)));
78      dc = -penal*(E0-Emin)*xPhys.^(penal-1).*ce;
79      dv = ones(nely,nelx,nelz);
80  %       FILTERING AND MODIFICATION OF SENSITIVITIES
81      dc(:) = H*(dc(:)./Hs);
82      dv(:) = H*(dv(:)./Hs);
83      % OPTIMALITY CRITERIA UPDATE
84      l1 = 0; l2 = 1e9; move = 0.2;
85      while (l2-l1)/(l1+l2) > 1e-3
86          lmid=0.5*(l2+l1);
87          xnew=max(0,max(x-move,min(1,min(x+move,x.* sqrt(-dc./dv/
                lmid)))));
88          xPhys(:)=(H*xnew(:))./Hs;
89          if sum(xPhys(:))> volfrac*nele, l1 = lmid; else l2 = lmid;
                end
90      end
91      change = max(abs(xnew(:)-x(:)));
92      x = xnew;
93      % PRINT RESULTS
94      fprintf(' It.:%5i Obj.:%11.4f Vol.:%7.3f ch.:%7.3f\n', loop,c
            ,mean(xPhys(:)),change);
95      % PLOT DENSITIES
96      if displayflag, clf; display_3D(xPhys); end
97      clf; display_3D(xPhys);
98  end
99  Time=toc;
```

```matlab
100   clf; display_3D(xPhys);
101   title(['SIMP3D ',' .. volfrac= ',num2str((volfrac)),...
102       ' nelx= ',num2str(nelx),' nely= ',num2str(abs(nely)),...
103       ' nelz= ',num2str(abs(nelz)),'.. c= ',num2str(c),...
104       '.. It.= ',num2str(loop),'.. Time= ',num2str(Time),...
105       ' tolx= ',num2str(tolx)]);
106   end
107   % === GENERATE ELEMENT STIFFNESS MATRIX ===
108   function [KE] = lk_H8(nu)
109   A = [32 6 -8 6 -6 4 3 -6 -10 3 -3 -3 -4 -8;
110       -48 0 0 -24 24 0 0 0 12 -12 0 12 12 12];
111   k = 1/144*A'*[1; nu];
112   K1 = [k(1) k(2) k(2) k(3) k(5) k(5);
113       k(2) k(1) k(2) k(4) k(6) k(7);
114       k(2) k(2) k(1) k(4) k(7) k(6);
115       k(3) k(4) k(4) k(1) k(8) k(8);
116       k(5) k(6) k(7) k(8) k(1) k(2);
117       k(5) k(7) k(6) k(8) k(2) k(1)];
118   K2 = [k(9)  k(8)  k(12) k(6)  k(4)  k(7);
119       k(8)  k(9)  k(12) k(5)  k(3)  k(5);
120       k(10) k(10) k(13) k(7)  k(4)  k(6);
121       k(6)  k(5)  k(11) k(9)  k(2)  k(10);
122       k(4)  k(3)  k(5)  k(2)  k(9)  k(12)
123       k(11) k(4)  k(6)  k(12) k(10) k(13)];
124   K3 = [k(6)  k(7)  k(4)  k(9)  k(12) k(8);
125       k(7)  k(6)  k(4)  k(10) k(13) k(10);
126       k(5)  k(5)  k(3)  k(8)  k(12) k(9);
127       k(9)  k(10) k(2)  k(6)  k(11) k(5);
128       k(12) k(13) k(10) k(11) k(6)  k(4);
129       k(2)  k(12) k(9)  k(4)  k(5)  k(3)];
130   K4 = [k(14) k(11) k(11) k(13) k(10) k(10);
131       k(11) k(14) k(11) k(12) k(9)  k(8);
132       k(11) k(11) k(14) k(12) k(8)  k(9);
133       k(13) k(12) k(12) k(14) k(7)  k(7);
134       k(10) k(9)  k(8)  k(7)  k(14) k(11);
135       k(10) k(8)  k(9)  k(7)  k(11) k(14)];
136   K5 = [k(1) k(2)  k(8)  k(3) k(5)  k(4);
137       k(2) k(1)  k(8)  k(4) k(6)  k(11);
138       k(8) k(8)  k(1)  k(5) k(11) k(6);
```

```matlab
139        k(3)  k(4)   k(5)   k(1) k(8)   k(2);
140        k(5)  k(6)   k(11) k(8) k(1)   k(8);
141        k(4) k(11) k(6)   k(2) k(8)   k(1)];
142  K6 = [k(14) k(11) k(7)   k(13) k(10) k(12);
143        k(11) k(14) k(7)   k(12) k(9)   k(2);
144        k(7)   k(7)   k(14) k(10) k(2)   k(9);
145        k(13) k(12) k(10) k(14) k(7)   k(11);
146        k(10) k(9)   k(2)   k(7)   k(14) k(7);
147        k(12) k(2)   k(9)   k(11) k(7)   k(14)];
148  KE = 1/((nu+1)*(1-2*nu))*...
149        [ K1   K2   K3   K4;
150        K2'   K5   K6   K3';
151        K3'  K6   K5'  K2';
152        K4   K3   K2   K1'];
153  end
154  % === DISPLAY 3D TOPOLOGY (ISO-VIEW) ===
155  function display_3D(rho)
156  [nely,nelx,nelz] = size(rho);
157  hx = 1; hy = 1; hz = 1;    % User-defined unit element size
158  face = [1 2 3 4; 2 6 7 3; 4 3 7 8; 1 5 8 4; 1 2 6 5; 5 6 7 8];
159  set(gcf,'Name','ISO display','NumberTitle','off');
160  for k = 1:nelz
161     z = (k-1)*hz;
162     for i = 1:nelx
163          x = (i-1)*hx;
164          for j = 1:nely
165              y = nely*hy -(j-1)*hy;
166              if (rho(j,i,k)>0.5)%User-defined display density
                      threshold
167                  vert = [x y z; x y-hx z; x+hx y-hx z; x+hx y z;  ...
168                      x y z+hx;x y-hx z+hx; x+hx y-hx z+hx;x+hx y z+hx
                          ];
169                  vert(:,[2 3])=vert(:,[3 2]);vert(:,2,:)= -vert
                          (:,2,:);
170                  patch('Faces',face,'Vertices',vert,'FaceColor'
                          ,[0.2+0.8*(1-rho(j,i,k)),0.2+0.8*(1-rho(j,i,k))
                          ,0.2+0.8*(1-rho(j,i,k))]);
171                  hold on;
172              end
```

132

```
173            end
174        end
175    end
176    axis equal; axis tight; axis off; box on; view([30,30]); pause(1e-6);
177    end
```